THE RADIATION CHEMISTRY AND PHOTOCHEMISTRY OF ETHYL BROMIDE IN THE GAS PHASE

By

ARTHUR JESSE FRANK

A DISSERTATION PRESENTED TO THE GRADUATE COUNCIL OF THE UNIVERSITY OF FLORIDA IN PARTIAL FULFILLMENT OF THE REQUIREMENTS FOR THE DEGREE OF DOCTOR OF PHILOSOPHY

UNIVERSITY OF FLORIDA

1975

The author is proud to dedicate this dissertation to his wife, Abbey, who has come on strong during the low moments of this work and has also shared in all of the highlights of it.

ACKNOWLEDGMENTS

The author wishes to express his sincere appreciation to Dr. R. J. Hanrahan who first suggested this research project and who has always been willing to take the time to offer his advice and encouragement throughout this work. Thanks are also extended to Drs. M. L. Muga and P. M. Achey for their interest in this project.

Special appreciation is given to Dr. J. E. Fanning and A. R. Ravishankara for their friendship and assistance, especially during the final stages of this work. Again, thanks are due to T. Hsieh for his assistance. The author also wishes to acknowledge the many hours that A. Wendt spent doing the programming that produced the Gould plots found in the dissertation. He is also grateful to Alexis VanDenAbell who gallantly volunteered her time to type portions of the first draft.

Thanks are also due to Nancy McDavid for typing the final manuscript.

Finally he is especially grateful to his wife, Abbey, for her unfailing encouragement and understanding that has made this work possible.

TABLE OF CONTENTS

TABLE OF CONTENTS (continued)

TABLE OF CONTENTS (continued)

LIST OF TABLES

LIST OF TABLES (continued)

LIST OF FIGURES

LIST OF FIGURES (continued)

LIST OF FIGURES (continued)

Abstract of Dissertation Presented to the Graduate Council
of the University of Florida in Partial Fulfillment of the Requirements
for the Degree of Doctor of Philosophy

THE RADIATION CHEMISTRY AND PHOTOCHEMISTRY OF ETHYL BROMIDE IN THE GAS PHASE

By

Arthur Jesse Frank

March, 1975

Chairman: Dr. R. J. Hanrahan
Major Department: Chemistry

The primary and secondary decomposition modes of gamma irradiated ethyl bromide in the gas phase at room temperature have been investigated. Supplementary information on the system has been derived from a parallel study of the 253.7 nm photolysis and the high pressure mass spectrometry.

The G values and quantum yields of the major and minor products both in the absence and in the presence of oxygen are reported. In both the photolysis and radiolysis several products exhibit a well-defined induction period. For the oxygen-free system in the dose range from 1.0×10^{20} e.v./gram to 1.5×10^{20} e.v./gram the major radiolytic products and their respective G values are hydrogen bromide, 3.89; hydrogen, 1.39; ethane, 2.70; ethylene, 2.17; acetylene, 0.31; methane, 0.0831; methyl bromide, 0.080; vinyl bromide, 0.32; 1,1-dibromoethane, 0.88 and 1,2-dibromoethane, 0.12. In the photolysis of the pure system between 60 and 90 seconds at an absorbed light intensity of 7.7×10^{15} quanta/sec, the major photolytic

products and their respective quantum yields are hydrogen bromide, 0.26; ethane, 0.40; ethylene, 0.028; methane, 0.00052; methyl bromide, 0.00091; vinyl bromide, 0.009; 1,1-dibromoethane, 0.102 and 1,2-dibromoethane, 0.0092.

Carbon-halogen bond rupture is the major primary event in each system. There is also substantial evidence for HBr elimination. In addition, all secondary processes in the photolysis apparently occur in the radiolysis as well.

A numerical integration method capable of handling steady state assumptions has been used to calculate the product distribution based on the proposed photolysis mechanism. The predicted and experimental product distributions are found to be in reasonable agreement.

A comparison has been made of the radiation chemistry of ethyl bromide with that of ethyl chloride and ethyl iodide which have already been studied. The product distributions of the three systems differ substantially. The C_2 dihalogenated compounds in the ethyl bromide system are produced in a substantially larger amount than in either ethyl chloride or ethyl iodide. Differences in the chemical kinetics of the three systems are explained primarily on the basis of energetic arguments.

I. INTRODUCTION

A. Foreword

The investigation of the gamma radiolysis of ethyl bromide in the gas phase was undertaken to study the primary and secondary processes leading to its decomposition. Parallel studies of the 253.7 nm photolysis and high pressure mass spectrometry of the system provided supplementary information on the decomposition mechanism. In both the radiolysis and photolysis, oxygen was added to identify free radical intermediates and to determine their contribution to the observed stable products.

An additional goal of this investigation was to compare the radiation chemistry of ethyl bromide with that of other ethyl halides since the chloride and the iodide systems have already been studied.

No extensive work on the gas phase radiolysis or the room temperature photolysis of ethyl bromide is reported in the literature. A survey of other investigations relevant to the present work follows in Sec. I-B.

B. Review of Previous Work

Roof and Daniels (1) investigated the 313 nm photolysis of acetaldehyde and ethyl bromide at about 310°C. Progress of the reaction was followed by pressure measurements and by end-product analysis of CO from acetyaldehyde and C_2H_4 from ethyl bromide. The authors reported that the decomposition of ethyl bromide gave rise to free radicals which sensitized the decomposition of acetaldehyde.

$$C_2H_5Br \longrightarrow C_2H_5\cdot + Br\cdot \qquad 1$$

Friedman, Bernstein and Gunning (2) studied the gas phase photolysis of ethyl bromide in the presence of mercury and a ten-fold excess of cyclopentane to measure the C^{13} isotope effect. Over the temperature range measured (30 to 250°C) the isotope effect, as determined mass spectrometrically, was constant. The cyclopentane and mercury eliminated the back reaction involving ethyl radicals and bromine atoms.

$$C_2H_5\cdot + C_5H_{10} \longrightarrow C_2H_6 + C_5H_9\cdot \qquad 2$$

$$Hg + Br\cdot \longrightarrow 1/2Hg_2Br_2 \qquad 3$$

Ethane was formed with a quantum yield of nearly unity over the entire temperature range investigated; only a small amount of ethylene was detected. These results suggested that in the spectral band of their lamp, 210 to 260 nm, the major primary event was C-Br bond scission.

Barker and Maccoll (3) photolyzed ethyl bromide in the gas phase with 253.7 nm radiation between 150 and 300°C. The progress of the reaction was monitored continuously by pressure measurements and checked by HBr titration. The following observations were noted:

(1) The pressure-time plots exhibited well-defined induction periods.

(2) Small amounts of the free radical scavenger propene inhibited the reaction and prolonged the induction period.

(3) Added hydrogen bromide accelerated the reaction rate.

(4) Above 500 torr the kinetic equation was first order in ethyl bromide with an overall activation energy of 10.5 kcal/mol.

(5) Also above 500 torr and at 293°C the quantum yield for the reaction was quite large, about 500.

(6) Below 50 torr the rate equation became second order.

(7) The stoichiometry of the overall reaction corresponded to

$$C_2H_5Br \longrightarrow C_2H_4 + HBr \qquad 4$$

A radical chain mechanism was proposed to account for these observations.

$$h\nu + C_2H_5Br \longrightarrow C_2H_5\cdot + Br\cdot \qquad 5$$

$$Br\cdot + C_2H_5Br \longrightarrow HBr + C_2H_4Br\cdot \qquad 6$$

$$C_2H_4Br\cdot \longrightarrow C_2H_4 + Br\cdot \qquad 7$$

$$C_2H_4Br^{\cdot} + Br^{\cdot} \longrightarrow \text{Chain-ending} \qquad 8$$

$$C_2H_5^{\cdot} + Br^{\cdot} \longrightarrow \text{Chain-ending} \qquad 9$$

$$Br^{\cdot} + Br^{\cdot} + M \longrightarrow \text{Chain-ending} \qquad 10$$

$$Br^{\cdot} + \text{Wall} \longrightarrow \text{Chain-ending} \qquad 11$$

Steps 5, 6, 7 and 11 lead to the low pressure second order kinetic equation and steps 5, 6, 7 and, for instance, 8 satisfied the first order kinetic equation.

From pyrolysis studies, Semenov (4) postulated that the radical formed in step 6 can take one of two forms:

$$Br^{\cdot} + C_2H_5Br \longrightarrow HBr + {}^{\cdot}CH_2CH_2Br \qquad 6a$$

$$Br^{\cdot} + C_2H_5Br \longrightarrow HBr + CH_3\dot{C}HBr \qquad 6b$$

Reaction 6a was estimated to be 3 kcal/mol more exoergic than reaction 6b. Only the radical ${}^{\cdot}CH_2CH_2Br$ can decay to C_2H_4 and $Br^{\cdot}$ in a unimolecular process and so propagate the chain. In contrast, the radical $CH_3\dot{C}HBr$ is relatively inert to unimolecular decay and can only recombine or react as in step 12.

$$CH_3\dot{C}HBr + CH_3CH_2Br \longrightarrow CH_3CH_2Br + {}^{\cdot}CH_2CH_2Br \qquad 12$$

Benson and O'Neal (5) reinterpreted the data of Barker and Maccoll (3) and proposed the following mechanism for the low pressure region.

$$h\nu + C_2H_5Br \longrightarrow C_2H_5^{\cdot} + Br^{\cdot} \qquad 5$$

$$Br^{\cdot} + C_2H_5Br \longrightarrow HBr + {}^{\cdot}CH_2CH_2Br \qquad 6a$$

$${}^{\cdot}CH_2CH_2Br + HBr \longrightarrow C_2H_5Br + Br' \qquad 6a'$$

$$Br^{\cdot} + C_2H_5Br \longrightarrow HBr + CH_3\dot{C}HBr \qquad 6b$$

$$CH_3\dot{C}HBr + HBr \longrightarrow C_2H_5Br + Br^{\cdot} \qquad 6b'$$

$${}^{\cdot}CH_2CH_2Br + M \longrightarrow C_2H_4 + Br^{\cdot} + M \qquad 13$$

$$Br^{\cdot} + CH_3\dot{C}HBr \longrightarrow CH_3CHBr_2 \qquad 14$$

In contrast to the Barker and Maccoll (3) investigation as well as the present work, Gurman, Dubinskii and Kovalev (6) made no mention of the presence of hydrogen bromide in the 253.7 nm photolysis of liquid phase ethyl bromide at room temperature. As determined by gas chromatography and spectrophotometry the major products reported were ethane, dibromoethane and bromine as well as a small amount of ethylene, less than 3% of the total product yield. The production of the organic products increased linearly with dose up to about 10^{20} quanta/ml. while the bromine plateaued at about 10^{18} quanta/ml. Addition of hydrogen bromide prior to photolysis caused the bromine production to increase and to become more nearly linear while at the same time decreasing the dibromoethane formation. The mechanism suggested to account for these observations was

$$h\nu + C_2H_5Br \longrightarrow C_2H_5^{*\cdot} + Br^{\cdot} \qquad 15$$

$$C_2H_5^{\cdot} + C_2H_5Br \longrightarrow C_2H_6 + C_2H_4Br^{\cdot} \qquad 16$$

$$Br^{\cdot} + Br^{\cdot} \longrightarrow Br_2 \qquad 17$$

$$(C_2H_4Br^{\cdot} + Br^{\cdot}) \longrightarrow (C_2H_4Br_2) \qquad 18$$

$$C_2H_4Br^{\cdot} + Br_2 \longrightarrow C_2H_4Br_2 + Br^{\cdot} \qquad 19$$

The asterisk denotes translationally "hot" species and the brackets indicate a solvent cage. Since butyl bromide was not observed the authors suggested that thermalized ethyl radicals played only a minor role. Furthermore, the decrease in the dibromoethane yield with decreasing temperature was interpreted as support for the "cage" effect.

Donovan and Husain (7) obtained negative results in a search for electronically excited $Br(4^2P_{1/2})$ atoms in the vacuum ultraviolet flash photolysis of ethyl bromide using kinetic spectroscopy. The failure to detect $Br(4^2P_{1/2})$ atoms was attributed to the rapid collisional deactivation of the excited state by ethyl bromide molecules.

Prior to the advent of gas chromatography, Schuler and Hamill (8) studied the fast electron and X-ray decomposition of liquid phase ethyl bromide. Hydrogen bromide and bromine were the only products reported. Addition of triphenylmethane enhanced the G value for hydrogen bromide. Bromine atoms were presumed to abstract hydrogen from triphenylmethane rather than to back react.

$$Br^{\cdot} + (C_6H_5)_3CH \longrightarrow HBr + (C_6H_5)_3C^{\cdot} \qquad 20$$

There has been no other investigation of the radiolysis of ethyl bromide; however, Neddenriep and Willard (9) studied the gamma radiolysis of degassed liquid n-propyl bromide as a function of dose, temperature and concentration of additives. In the pure system, hydrogen bromide, propane, 1,2-dibromopropane and 2-bromopropane were the major products reported. Hydrogen bromide was determined by spectrophotometry and the organic compounds were measured by gas chromatography. Lesser amounts of hydrogen, C_1- and C_2-brominated and unbrominated hydrocarbons as well as a telomeric compound were also reported. As evidenced by the nature of the products, the major primary event is rupture of the C-Br bond. In the additive-free system at room temperature, no bromine was detected by spectrophotometry and the net rate of HBr production decreased to zero with increasing dose. One or more of the elementary steps producing HBr was speculated to have an appreciable activation energy since the G value for HBr formation increased from 0.06 at -78°C to 10.5 at 50°C. Other products also exhibited a temperature sensitivity. These observations suggested that an important step in the radical chain process leading to the decomposition of n-propyl bromide was hydrogen abstraction to form HBr.

$$Br^{\cdot} + CH_3CH_2CH_2Br \longrightarrow HBr + CH_3\dot{C}HCH_2Br \qquad 21$$

In the presence of additives (HBr and O_2) bromine was produced in a substantial amount, a fact attributed to either the reactions between peroxy radicals formed and HBr, or to the prevention of reactions

between organic radicals and bromine. At high dose with added HBr and O_2, the G value for bromine decreased with increasing dose and in some cases even became negative. This indicated that Br_2 was competing with HBr or O_2 for some reaction intermediate. Furthermore, it was found that when bromine was added to the system prior to irradiation, the bromine concentration decreased with dose in agreement with the above observation.

Schindler (10) investigated the gas phase decomposition of ethyl chloride induced by 2.8 Mev electrons. The effects of various additives indicated that roughly half of all primary events were molecular. Ethylene, acetylene, vinyl chloride and hydrogen were assumed to arise in part from molecular processes. In contrast to the alkyl bromides, C-H rather than C-Cl bond rupture was the major primary event. The probability of single bond rupture in the primary event was approximately represented by the ratio $C_2H_4Cl\text{-}H$: $C_2H_5\text{-}Cl$: $CH_3\text{-}CH_2Cl$ = 1 : 0.75 : 0.15. The monochloroethyl and ethyl radicals were the main radicals produced in the primary event. Steps 22 to 26 were characterized as their major reactions.

$$Cl\cdot + C_2H_5Cl \longrightarrow HCl + C_2H_4Cl\cdot \qquad 22$$

$$C_2H_5\cdot + HCl \longrightarrow C_2H_6 + Cl\cdot \qquad 23$$

$$2C_2H_5\cdot \longrightarrow C_4H_{10} \qquad 24$$

$$C_2H_5\cdot + C_2H_4Cl\cdot \longrightarrow C_4H_9Cl \qquad 25$$

$$2C_2H_4Cl\cdot \longrightarrow C_4H_8Cl_2 \qquad 26$$

Five years after Schindler's work, Tiernan and Hughes (11) reported on the role of positive ions in the X-radiolysis of gaseous ethyl chloride. The participation of ionic intermediates in the radiolytic mechanism was related, with the aid of various additives, to the ionic fragmentation scheme from their high pressure mass spectrometer study. Their results on the far ultraviolet photolytic decomposition of excited ethyl chloride molecules were correlated with the data from the other studies to derive a radiolytic mechanism. The data suggested that the major radiolytic reaction mode in the system was neutral unimolecular decomposition rather than ionic reactions.

The gas phase decomposition of ethyl iodide with 2.8 Mev electrons was investigated by Schindler and Wijnen (12). The products formed were hydrogen, methane, ethane, ethylene, acetylene, methyl iodide, vinyl iodide, diiodomethane, 1,1-diiodoethane and a negligible amount of 1,2-diiodoethane. Nonradical processes accounted for all of the ethylene as in the case of ethyl chloride, and 70% of the hydrogen. The probability for single bond rupture in the primary event was roughly represented by the ratio C_2H_5-I : C_2H_4I-H ; CH_3-CH_2I = 1 : >0.06 : 0.01. The primary processes postulated to account for the observed products were similar to those in ethyl chloride (10) except for step 32.

$$C_2H_5I \rightsquigarrow C_2H_5' + I' \qquad 27$$

$$\rightsquigarrow C_2H_4 + HI \qquad 28$$

$$\rightsquigarrow C_2H_2 + H_2 + HI \qquad 29$$

$$\rightsquigarrow C_2H_3I + H_2 \qquad 30$$

$$\rightsquigarrow C_2H_4I' + H' \qquad 31$$

$$\rightsquigarrow CH_4 + 'CHI' \qquad 32$$

$$\rightsquigarrow CH_3' + CH_2I' \qquad 33$$

The wavy arrows in reactions 27 through 33 read "yields under the influence of ionizing radiation" and do not necessarily imply a one-step process. About one third of all the primary events were attributed to molecular processes. Reactions of thermalized ethyl radicals with HI accounted for most of the ethane produced; the contribution of "hot" ethyl radicals was found to be unimportant.

Irsa (13) studied the unimolecular ionic dissociation of ethyl bromide induced by electron impact. On the basis of appearance potential measurements derived from the vanishing current or initial break method and other energetic arguments (bond energies, ionization potentials and electron affinity data) the following fragmentation processes were proposed:

$$C_2H_5Br \longrightarrow C_2H_5Br^+ + e^- \qquad 34$$

$$\longrightarrow C_2H_5^+ + Br + e^- \qquad 35$$

$$\longrightarrow CH_2Br^+ + CH_3 + e^- \qquad 36$$

$$(\text{or } CH_2Br^+ + CH + H_2 + e^-$$

Evidence for the formation of Br^-, C_2H^- and $C_2H_2^-$ was also presented in this study.

Tsuda and Hamill (14) reexamined in more detail the appearance potentials of $C_2H_5^+$ and $C_2H_5Br^+$ by the retarding potential difference method on a Bendix Time-of-Flight mass spectrometer. From the structure in the ionization efficiency curves for $C_2H_5^+$ and $C_2H_5Br^+$ they were able to assign excited states to these ions. Direct measurements of negative ions were also made using a magnetic instrument. Their results indicated that ion-pairing processes always occurred at onset

$$C_2H_5Br \longrightarrow C_2H_5^+ + Br^- \qquad 37$$

where several excited electronic states were associated with the $C_2H_5^+$ ion. At higher energies, the ion-neutral process took place.

$$C_2H_5Br \longrightarrow C_2H_5^+ + Br + e^- \qquad 35$$

Their data suggested that the ion-pair and ion-neutral processes preceded from a common pre-ionized state.

In 1959 Pottie and Hamill (15) reported the first examples of persistent collision complexes between ions and molecules. In a mass spectrometry study of the alkyl halides the bimolecular process was observed.

$$C_2H_5Br^+ + C_2H_5Br \longrightarrow C_4H_{10}Br_2^+ \qquad 38$$

A more detailed exploration of the ion-molecule reactions occurring in ethyl bromide was carried out by Theard and Hamill (16) using high pressure mass spectrometry.

$$C_2H_5Br^+ + C_2H_5Br \longrightarrow C_4H_{10}Br_2^+ \quad 38$$

$$\longrightarrow C_4H_{10}Br^+ + Br \quad 39$$

$$\longrightarrow C_2H_6Br_2^+ + C_2H_4 \quad 40$$

$$\longrightarrow C_4H_9Br^+ + HBr \quad 41$$

$$CH_2Br^+ + C_2H_5Br \longrightarrow CHBr_2^+ + C_2H_6 \quad 42$$

Beauchamp and coworkers (17) reinvestigated the ion-molecule reactions in ethyl bromide using an ion cyclotron resonance spectrometer. In contrast to the results of Hamill and coworkers (15, 16) the ionic dimer was not observed. The primary ions $C_2H_5Br^+$, $C_2H_3^+$, $C_2H_5^+$, Br^+ and CH_2Br^+ were found to undergo reactions 39 and 43 through 47.

$$C_2H_5Br^+ + C_2H_5Br \longrightarrow C_2H_5Br^+C_2H_5 + Br \quad 39$$

$$CH_2Br^+ + C_2H_5Br \longrightarrow C_2H_5^+ + CH_2Br_2 \quad 43$$

$$Br^+ + C_2H_5Br \longrightarrow C_2H_5Br^+ + Br \quad 44$$

$$C_2H_3^+ + C_2H_5Br \longrightarrow C_2H_5Br^+H + C_2H_2 \quad 45$$

$$C_2H_5^+ + C_2H_5Br \longrightarrow C_2H_5Br^+H + C_2H_4 \quad 46$$

$$C_2H_5Br^+H + C_2H_5Br \longrightarrow C_2H_5Br^+C_2H_5 + HBr \quad 47$$

Their double resonance experiments indicated that the bromine atom in the diethylbromonium ion originated with equal probability from the ionic and neutral fragment.

Recently Sieck and Gordon (18) used photoionization mass spectrometry to confirm the observations of Hamill and coworkers (15, 16) regarding the formation of the dimer ion in ethyl bromide. The lower limit for the dissociative lifetime of the ion-molecule collision complex $(C_2H_5Br)_2^+$ was estimated to be 5.4 microseconds.

Negative ions are also important at low electron energies in the alkyl bromides. Christodoulides and Christophorou (19) and Christophorou and coworkers (20) employed the electron swarm beam method to study the mechanism of dissociative electron attachment to several alkyl bromides including ethyl bromide. The dissociative electron attachment rate yielding Br^- for ethyl bromide was a maximum at a mean electron energy of 0.76 e.v. in the energy range of about 0.05 to 2.2 e.v. The process leading to Br^- proceeded through a shortlived ($<10^{-13}$ sec.) compound negative ion state. Although Br^- was the most abundant ion in this study, their data suggested that a second longer lived ($\sim 10^{-10}$ to 10^{-6} sec.) electron attachment process was occurring. Also in this study the mean autoionization lifetime of 55×10^{-14} sec. was determined.

Bansal and Fessenden (21) redetermined the thermal electron attachment rate for ethyl bromide using the microwave conductivity-pulse radiolysis technique. The maximum rate of electron attachment occurred at an electron energy of 0.76 e.v. in agreement with the results of Christodoulides and Christophorou (19).

II. EXPERIMENTAL PROCEDURES AND EQUIPMENT

A. Reagents and Their Purification

1. Ethyl bromide

Baker analyzed reagent grade ethyl bromide was dried overnight with Drierite and then fractionally distilled through a 4 foot glass-helix packed Todd still. The still was operated under total reflux for two hours and then at a reflux ratio of 50 to 1. The middle cut which boils at 38.3 $\pm$ 0.1°C was retained. It was then degassed on the vacuum line and vacuum distilled through a 25 cm. column of barium oxide to storage vessel S_3 (Fig. 1). The barium oxide served not only as a drying reagent but also to remove possible traces of sulfuric acids utilized in the commercial preparation of ethyl bromide. It was then deoxygenated on the vacuum line by a series of freeze-pump thaw cycles.

During the course of this research, several bottles of Baker reagent grade ethyl bromide (Lot No. 39119) were tested for purity with the gas chromatograph-mass spectrometer system. Although alcohol-free as assayed on the bottle's label, several impurities such as methyl bromide, 1,2-dibromoethane and bromoform as well as some other mono-, di-, and tribrominated compounds were present in total amounts on the order of 0.1% (cf 0.0001% analysis on the

bottle's label). In any event, following the distillation procedure no impurities were detected with the flame ionization gas chromatograph. Periodically the purity of the sample in the storage vessel was rechecked on the gas chromatograph.

2. Ethylene

Matheson Company C.P. grade ethylene (99% minimum purity) was passed through a Pyrex drying tube of barium oxide into storage vessel S_1 (Fig. 1) on the vacuum line. Oxygen was then removed by the freeze-thaw method.

3. Oxygen

Matheson Company research grade oxygen was bled into the vacuum system through a 1 in. drying column of 60-200 mesh reagent grade silica gel.

4. Hydrogen bromide

Matheson Company hydrogen bromide (99.8% minimum purity) was admitted through 1/4 in. copper tubing into a Pyrex drying tube filled with P_2O_5 between copper filings. The gas was then stored in a standard volume vessel on the vacuum line (Fig. 3). The sample was deaerated by several cycles of freezing, pumping and melting.

5. Chromatographic calibration standards and other reagents

The gas calibration standards and other miscellaneous reagents were used as received from their vendors.

B. Preliminary Remarks on Sample Preparation and Analysis

1. Principle assumption underlying sample preparation and analysis

In sample preparations and analyses the amount of sample irradiated or photolyzed as well as the corresponding product yields was determined by assuming the applicability of the ideal gas law.

2. Storage of sample

Ethyl bromide was stored in the dark at -196°C because of the possibility of photodecomposition. Also the vacuum line was never flamed to remove adsorbed gas molecules, even under a high vacuum, because it was found that this would lead to the formation of thermolysis products which would contaminate the unirradiated sample. In addition to this precaution, at no time was a Tesla coil applied to the vacuum system while a sample was on the line because of the possibility that it would initiate sample decomposition.

3. Treatment for cleaning radiolysis and photolysis vessels

The vessels used for radiolysis were rinsed at least six times with distilled water and then annealed at 565°C to pyrolyze any

remaining organic residues. The photolysis vessels were cleaned in a similar manner, except that a rinse with nitric acid preceded the distilled water step. The nitric acid rinse was done to remove possible mercury contamination arising from the vessel coming into contact with mercury during the post-photolysis procedures.

The apparent effectiveness of this treatment in eliminating traces of organic and inorganic bromide residues was supported by the observation that water wetted the vessel walls uniformly and that no bromide ions were detected by potentiometric titration. In the case of ethyl bromide-oxygen mixtures, because of the substantial amount of bromine formed, a rinse with sodium thiosulfate was used as an initial step in the cleaning procedure in some of the later experiments.

C. Preparation of Samples for Radiolysis

1. Vacuum system

The vacuum system used for sample preparation for radiolysis experiments is shown in Figs. 1 and 2. It consisted of four sections: a pumping section capable of reaching pressures of 0.1 to 0.5 microns, a section for pre-radiolysis sample preparation, another for post-radiolysis sample preparation and analysis and a main manifold interconnecting the three sections.

The pumping station was the conventional high vacuum type. It consisted of a two-stage mercury diffusion pump, P, backed by a

Welch Duo-Seal Model 1400B forepump, and two liquid nitrogen traps, T_1 and T_2. Two 8 mm. bore two-way ground glass stopcocks, V_1 and V_2, could be rotated 180 degrees to allow pumping by the diffusion and mechanical pump in union, or the mechanical pump alone. These glass valves as well as the two glass valves, V_8 and V_9, in the sample analysis section were lubricated with Dow Corning high vacuum grease; the halocarbon greases proved unsatisfactory as ethyl bromide tended to dissolve in them. All other stopcocks, with the exception of a single 6 mm. West valve, V_3, were Fischer-Porter 4 mm. O-ring sealed Teflon-glass valves.

The pumping station communicated with the main manifold through the West stopcock, V_3. Attached to the main manifold were a mercury manometer, M_1, two one liter reservoirs, S_1 and S_2, for reagent storage, three inlets, I_1, I_2 and I_3, for introducing samples and a vacuum thermocouple gauge, G_1. Strategically located, this vacuum gauge as well as gauges G_2 and G_3 on the submanifolds, allowed the pressure to be monitored independently through a multiposition thermocouple meter.

A valve, V_4, connected the center of the main manifold with the submanifold which was used mainly for pre-radiolysis sample preparation. Ethyl bromide was stored in a detachable 500 cc. vessel, S_3, connected to this submanifold through an O-ring joint. Depending on whether irradiation was to be carried out in a large or a small radiolysis vessel (Figs. 5 and 6), the sample was metered to the 30.39 cc. standard volume vessel, W_1, or to the 324.7 cc. standard

volume vessel, W_2. The amount of sample was measured with the mercury manometer, M_2. Attached to this submanifold through valve V_7 was a tubulation connected to the radiolysis vessel, R, shown in Figs. 1, 5 and 6. The O-ring joint between the stopcock and the radiolysis vessel served both as an entry port for glass blowing and as a means for attaching a 29.76 cc. standard volume vessel used in the oxygen scavenger experiments.

The second submanifold in Figs. 1 and 2, which was used for sample analysis following irradiation, communicated with the main manifold through two valves, V_5 and V_6. The tubulation on this submanifold isolated by valve V_{12} was for attaching the irradiated sample. Valve V_{13} opened to the gas loop, L_1 (Figs. 1 and 12), employed in the gas chromatographic end product analysis. Also connected to this manifold through values V_{10} and V_{11} was a Toepler pump-McLeod gauge combination, C, with an intermediary glass-helix packed U-trap, T_3. The U-trap was used to prevent passage of condensibles into the combined Toepler pump-McLeod gauge during analysis of non-condensibles. The three-way ground glass stopcock, V_8, was generally kept at a high vacuum by pumping through valve V_6. Valve V_8 channelled the non-condensible gases from the radiolysis vessel to the McLeod gauge, D, or to the gas loop, L_3 (Figs. 1 and 12), or from the McLeod gauge to the gas loop, L_3.

2. Ethyl bromide

Ethyl bromide in storage reservoir S_3 was deaerated by repeated cycles of freezing, pumping and melting until the thermocouple

Fig. 1 Radiolysis vacuum system

1. Pumping station
   - V_1, V_2 Ground glass stopcocks
   - T_1, T_2 Liquid nitrogen traps
   - P_1 Mercury diffusion pump

2. Main manifold
   - V_3 - V_6 O-ring sealed Teflon-glass valves
   - I_1 - I_3 Inlet ports
   - M_1 Mercury manometer
   - S_1, S_2 Storage reservoirs (1000 cc.)
   - G_1 Thermocouple vacuum gauge

3. Submanifold for pre-radiolysis preparation
   - V_7 O-ring sealed Teflon-glass valve
   - R Radiolysis vessel
   - M_2 Mercury manometer
   - W_1 Standard volume vessel (30.93 cc.)
   - W_2 Standard volume vessel (324.7 cc.)
   - S_3 Storage reservoir for ethyl bromide
   - G_2 Thermocouple vacuum gauge

4. Submanifold for sample analysis (see Fig. 2)
   - V_8, V_9 Ground glass stopcocks
   - V_{10} - V_{13} O-ring sealed Teflon-glass valves
   - L_1, L_2 Gas sampling loop (see Fig. 12)
   - C Toepler pump-McLeod gauge combination
   - T_3 U-trap
   - D McLeod gauge
   - G_3 Thermocouple vacuum gauge

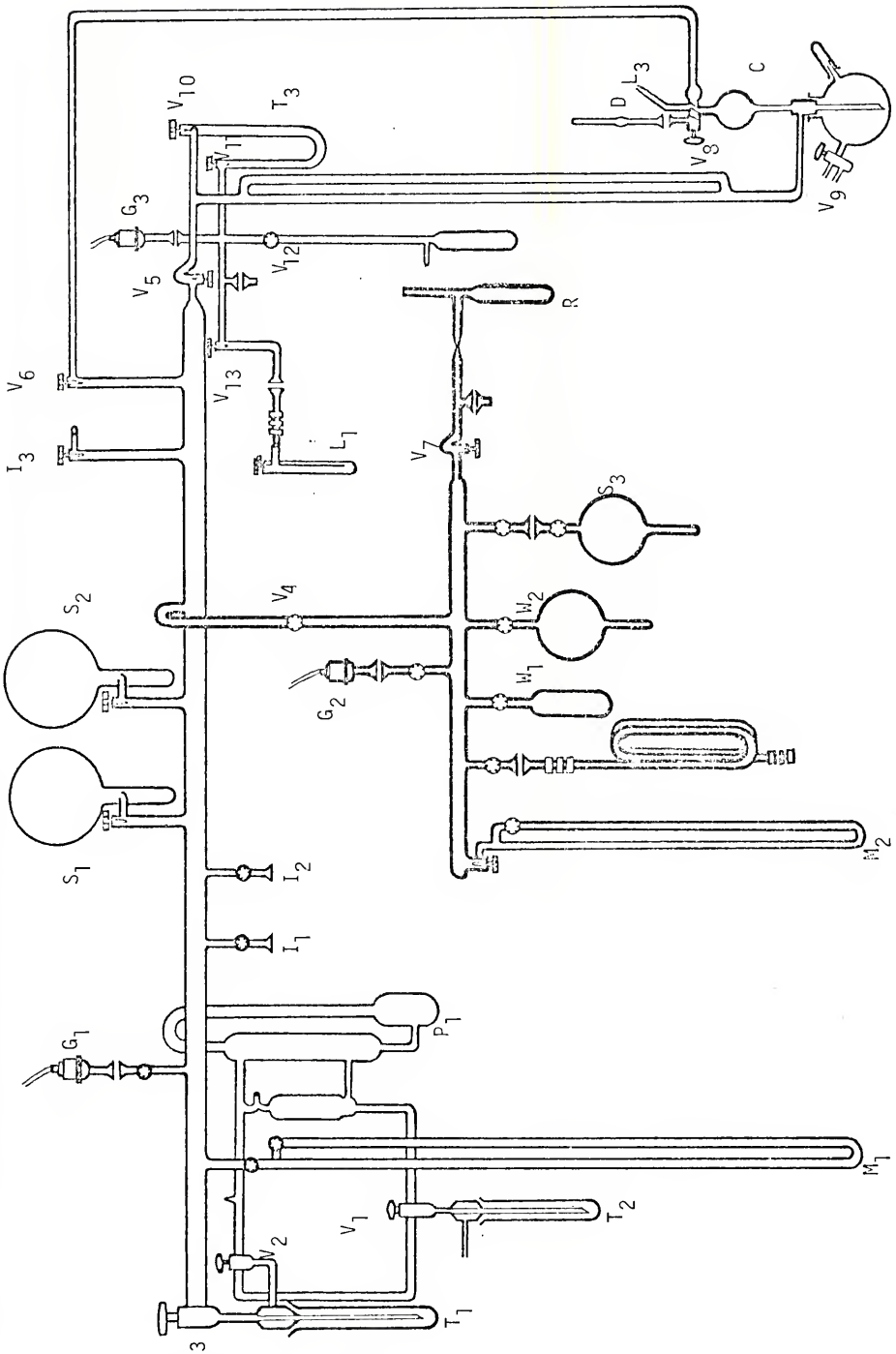
V10
T3
V11
G3
V5
V12
V6
V13
I3
L1
R
V7
S3
S2
V4
W2
W1
G2
S1
I2
I1
G1
P1
M2
M1
T2
V1
V2
T1
V3
D
L3
C
V8
V9

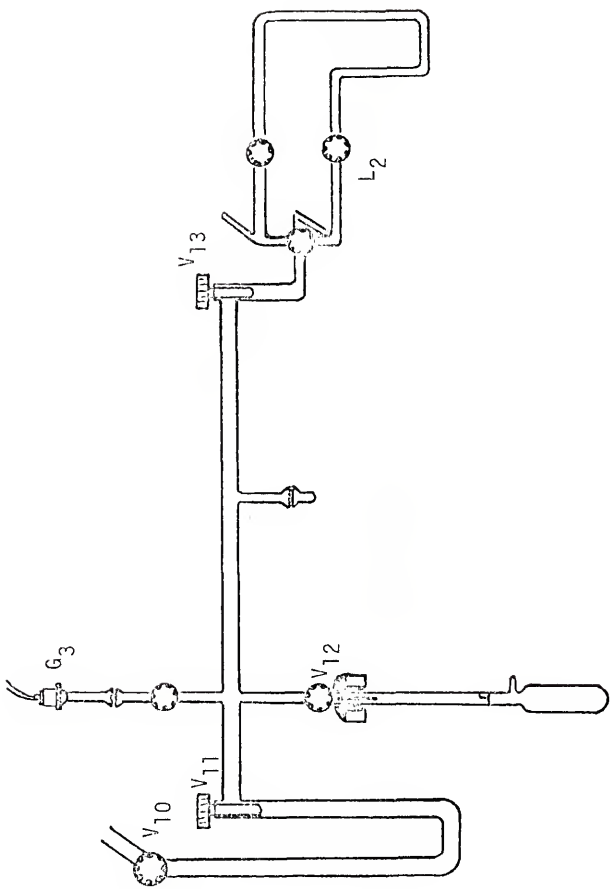

Fig 2. Sample analysis submanifold (see legend for Fig. 1)

vacuum meter indicated the absence of air. Valve V_4 was then closed and the sample was allowed to expand into standard volume vessel W_1 or W_2 while the pressure was monitored with mercury manometer M_2. The final pressure was read with an Ealing cathetometer. At the desired pressure required in the radiolysis vessel, the valve to the standard volume vessel was closed and the excess material was condensed back into the cold finger on the storage vessel with liquid nitrogen. Following reevacuation of the submanifold, value V_4 was again closed and the material in the standard volume vessel was vacuum transferred to the radiolysis vessel by means of liquid nitrogen. Although the transfer was essentially complete within 3 to 4 minutes as indicated on the thermocouple meter, 20 minutes was allotted for this process. The radiolysis vessel was then sealed off from the vacuum line with an oxygen-methane torch at a reproducible mark. Recalibration of the vessel volume at a later time confirmed that its volume never deviated more than 1% from its original calibrated volume. After the glass cooled, the liquid nitrogen was removed from under the vessel and it was allowed to warm to room temperature before irradiation.

All irradiations were carried out at a pressure of 100 torr except those intended for the analysis of hydrogen bromide, in which case, the irradiation was at 300 torr.

3. Ethyl bromide with added oxygen

Under the condition that the radiolysis vessel was almost entirely at -196°C, it was estimated that the amount of oxygen

transferred could be calculated by the ideal gas law with a correction factor of 4 corresponding to the difference in temperature between ambient and -196°C. However, such a temperature correction is inadequate because of the uncertain extent of localized heating as the vessel is sealed off using a hand torch. The actual quantity of oxygen transferred to the vessel was measured with the Toepler-McLeod gauge assembly. Knowing the actual quantity of oxygen transferred in a given case, an empirical correction was determined. Thus, the quantity of oxygen introduced into the radiolysis vessel is stated mathematically as

$$P_V = \beta \cdot \left(\frac{T_R}{T_{N_2}}\right) \cdot P_L$$

or, in words, that the pressure desired in the radiolysis vessel, P_V, equals an empirical constant, $\beta(=0.8)$, times the ratio of room temperature to liquid nitrogen temperature, T_R/T_{N_2}, times the oxygen pressure in the vacuum line, P_L. Although it is perhaps evident, it should, nevertheless, be pointed out that for complete vacuum transfer of the ethyl bromide, its transfer should precede that of oxygen.

In all irradiations with oxygen, the oxygen constituted 5% of the total pressure except in the case of samples intended for HBr determination, where it was 12% of the total pressure. The corresponding ethyl bromide pressures were 100 and 300 torr respectively.

4. Ethylene

The preparation of ethylene differed from that of ethyl bromide (Sec. II-C-2) only in that the former originated from storage vessel S_1 or S_2 rather than from S_3.

D. Preparation of Sample for Photolysis

1. Vacuum system

To avoid mercury sensitized reactions in photolysis experiments, a mercury-free vacuum system was utilized for sample preparation. This system is illustrated in abbreviated form in Fig. 3. The pumping station consisted of the Labglass LG-10980 two stage oil diffusion pump, P_2, heated by a 50 ml, Glas-Col heating mantle, backed by a Welch Duo-Seal Model 1400B forepump, and two liquid nitrogen traps, T_4 and T_5. The oil diffusion pump and the traps were attached to the vacuum line by means of O-ring joints. Three 10 mm, West O-ring sealed Teflon-glass valves, V_{14}, V_{15} and V_{16}, allowed pumping by the diffusion and mechanical pump together or the mechanical pump alone. The pumping station and the submanifold each communicated with the main manifold through the 10 mm. West valves, V_{17} and V_{18}. All other valves on the vacuum line were Fischer-Porter 4 mm. O-ring sealed Teflon-glass valves.

Preparation of samples for photolysis was conducted on the submanifold. All pressure measurements were determined with a Wallace and Tiernan, Model 62-075 series 1000 differential pressure gauge

Fig. 3 Photolysis vacuum system

1. Pumping station

   V_{14} - V_{17} O-ring sealed Teflon-glass valves

   T_4, T_5 Liquid nitrogen traps

   P_2 Oil diffusion pump

2. Submanifold

   V_{18} - V_{26} O-ring sealed Teflon-glass valves

   S_4 Storage reservoir for ethyl bromide

   F Photolysis vessel

   G_4 Wallace and Tiernan differential pressure gauge

   G_5 Kollsman pressure gauge

   G_6 Thermocouple vacuum gauge

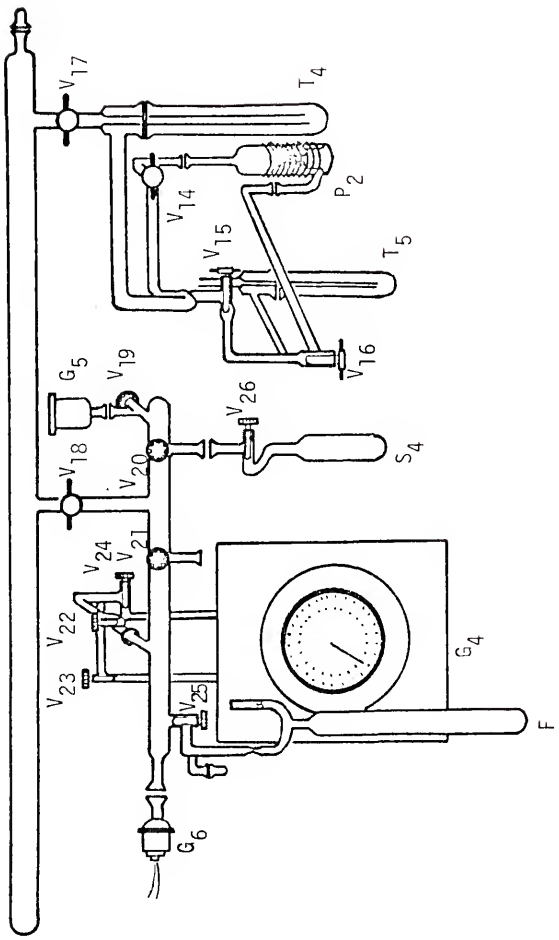
V17
T4
V14
P2
V15
T5
V16
G5
V19
V26
V18
V20
S4
V24
V21
V22
V23
V25
G4
F
G6

G_4, except those for actinometry (Sec. II-F-2) which were made on a Kollsman 10 in. absolute mercury pressure gauge, G_5. The extent of vacuum was monitored through a thermocouple vacuum gauge G_6. Ethyl bromide was stored in a detachable 120 cc. vessel, S_4, connected to the submanifold by an O-ring joint. The amount of sample delivered to the photolysis vessel was determined by PV measurements using the standardized 223 cc. volume submanifold in conjunction with the Wallace and Tiernan gauge. The standardized volume refers to that portion of the submanifold resulting when valves V_{22} and V_{24} are opened and all other valves are closed.

2. Ethyl bromide

The experimental procedure for preparing ethyl bromide for photolysis is analogous to that for radiolysis. Ethyl bromide in storage reservoir S_4 was deaerated by repeated freezing, pumping and melting cycles until the thermouple vacuum meter registered no change. Next, with valves V_{20}, V_{22}, and V_{24} opened and the rest of the valves on the submanifold closed, valve V_{26} to the storage vessel, S_4, was cracked open to admit ambient ethyl bromide to the submanifold while the pressure was monitored on the Wallace and Tiernan gauge. When the desired pressure was reached, valves V_{20} and V_{26} were closed and then valve V_{25} was opened to the photolysis vessel, F. The material in the standard volume submanifold was then condensed into the photolysis vessel and frozen at -196°C using a Dewar of liquid nitrogen over a period of 20 minutes. After pumping on the frozen

residue for 3 minutes, the vessel was sealed with an oxygen-methane torch and then allowed to warm to room temperature after the heated glass had cooled. As with the radiolysis vessel, the photolysis vessel was sealed at a reproducible position to minimize the deviation from its original calibrated volume.

A pressure of 100 torr was used in all photolyses of the pure sample.

3. Ethyl bromide with added oxygen

The general experimental procedure described in Sec, II-C-3 was followed. In all photolyses, the pressure of the ethyl bromide was kept at 100 torr and the oxygen was 5% of the total pressure,

4. Hydrogen bromide

Because of the corrosiveness of the hydrogen halide, the pressure gauge G_5 was employed in place of the Wallace and Tiernan gauge, G_4, used in the earlier sample preparations.

The hydrogen bromide was bled into the submanifold which was open to a standard volume vessel, as detailed in Sec, II-A-4, until a pressure of about one atmosphere was read on gauge G_5. The hydrogen bromide was then condensed into the standard volume vessel with liquid nitrogen and the residue gas pumped off. Utilizing the volume of the submanifold, except for the section beyond valve V_{22}, the sample was degassed by the freeze-thaw method, Next the degassed sample was expanded into the submanifold and valve V_{18} was cracked

open. When the desired pressure was registered on the gauge G_5, the valve to the standard volume vessel was closed and the remaining material pumped off. After evacuation, the hydrogen bromide was vacuum transferred to the photolysis vessel by means of liquid nitrogen and the vessel was then sealed off with the torch.

Depending on whether the small or the large photolysis vessel (Fig. 9) was being used, the standard volume vessel described above was either 29.76 cc. or 120.5 cc. All actinometry experiments with hydrogen bromide were carried out at a pressure of 129.7 torr.

E. Sample Irradiation

1. Radiation source, vessel and ancillary equipment

The cobalt-60 source employed in this investigation has been detailed elsewhere (22). Fig. 4 shows a cross-sectional view of the irradiator.

Two types of radiation vessels (Figs. 5 and 6) were used in this investigation. Each was made of Pyrex and equipped with a single breakseal. The large annular vessel (Fig. 5) with the 10 cm. quartz optical cell was used principally for the spectrophotometric analysis of bromine (Sec. II-H-5) and for the unscavenged hydrogen determination. The annular portion of the vessel efficiently utilized the radiation flux from the source, which could be positioned in its

center, and the vessel's optical cell made spectrophotometric analysis simple. However, because of its large volume and shape, this type of vessel was less convenient than the smaller cylindrical ones (Fig. 6) for gas chromatographic (Sec. II-H-1) and hydrogen bromide (Sec. II-H-4) analyses.

The volumes of the two annular vessels and the three cylindrical vessels are listed below.

Annular Vessels

Vessel No.	Volume
2	341.2 cc.
3	368.1 cc.

Cylindrical Vessels

Vessel No.	Volume
8	29.92 cc.
9	29.96 cc.
10	30.24 cc.

The sample holders (Figs. 5 and 6) allowed reproducible positioning of the radiolysis vessels during irradiation. The annular vessels fit snugly on a Teflon cap on a metal post; the height of this combination insured that the cobalt-60 source was situated in the center of the vessel. After frequent exposure to the radiation flux for about a year, however, the Teflon cap disintegrated and had to be replaced.

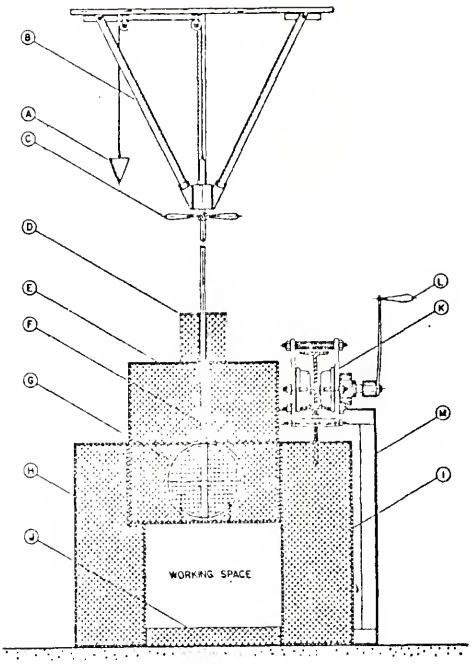

Legend=(A) counterweight; (B) upper support; (C) control rod handle; (D) extra top shielding; (E) storage turret; (F) 400 curie Co^{60}; (G) shutter shown open; (H) rear wall; (I) door; (J) downward shielding; (K) door carriage; (L) door crank; (M) door frame.

Emergency 6 foot tube in ground, under source, is not shown.

Fig. 4 Cross section of cobalt-60 gamma ray source

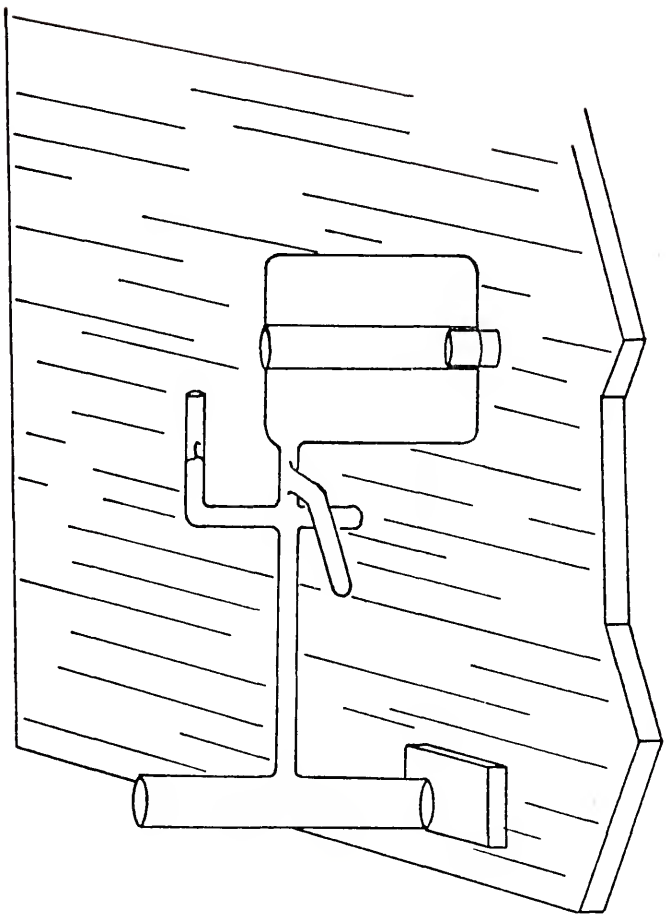

Fig. 5 Annular radiolysis vessel and holder

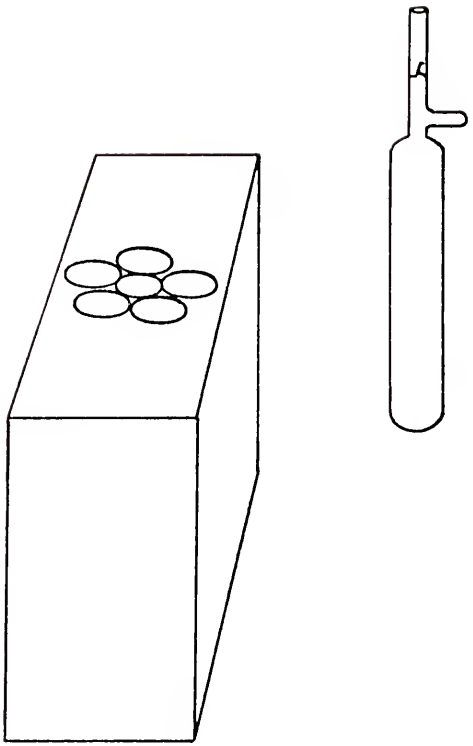

Fig. 6 Cylindrical radiolysis vessel and holder

The vessel holder (Fig. 6) for the smaller vessels was an aluminum block with a 0.630 in. diameter center hole for the source and five peripheral holes of 0.787 in. diameters for the 0.786 in. diameter vessels. Each peripheral hole was equally spaced on a circle of 0.727 in. radius. A metal wall of 0.018 in. thickness was left between the center hole and each of the peripheral holes. The depth of the center hole was 3.125 in. and 4.25 in. for each of the peripheral holes. The small cylindrical radiolysis vessel was, therefore, positioned securely within the vessel holder and cobalt-60 wafers midway along its length.

2. Dosimetry

In the pressure range of 150 to 1000 torr at room temperature, the hydrogen yield in ethylene under gamma radiolysis has been reported (23) to be independent of absorbed dose up to about 5% conversion. Furthermore, the G value for hydrogen production in ethylene has been established (23, 24) as 1.2 molecules/100 e.v.

The absorbed dose rate of the ethyl bromide system was determined using ethylene dosimetry. The irradiation of ethylene was carried out at 23 $\pm$ 2°C from 4 to 24 hours between the pressures of 200 and 600 torr in the vessels shown in Figs. 5 and 6. Following irradiation the total pressure of hydrogen along with a small quantity of methane and ethylene was determined using the Toepler-McLeod apparatus, C (Fig. 1). Knowledge of the total pressure of the mixture and the quantitative contribution of methane and ethylene allowed the hydrogen yield to be calculated. From the slope of the plot in

Fig. 7 and the accepted G value for hydrogen formation, the energy absorbed by the system was calculated. For the two types of vessels used and the geometries in which the irradiations were carried out, the absorbed dose rate of ethylene was 2.06×10^{19} e.v./gram-hr. on March 7, 1972, for the annular vessels and 2.72×10^{19} e.v./gram-hr. on January 10, 1973, for the small cylindrical vessels.

To the extent that the radiolysis vessels approximate the Bragg-Gray cavity (25, 26), the rate of energy deposition in ethylene can be correlated to that in ethyl bromide. Since the application of the Bragg-Gray principle is justified (27), the ratio of the energy deposited per unit mass in the sample and in the dosimeter can be determined by the ratio of their mass stopping power as detailed elsewhere (28).

The final form of the equation used to calculate the absorbed dose rate in ethyl bromide is

$$\text{Dose}(C_2H_5Br) = 0.729\ \text{Dose}(C_2H_4)$$

in units of e.v./gram-hr. The absorbed dose rate, therefore, of ethyl bromide on March 7, 1972, for the large annular vessel was 1.50×10^{19} e.v./gram-hr. and on January 10, 1973, for the smaller radiolysis vessel was 1.98×10^{19} e.v./gram-hr. During subsequent irradiations, the absorbed dose rates were corrected for cobalt-60 decay.

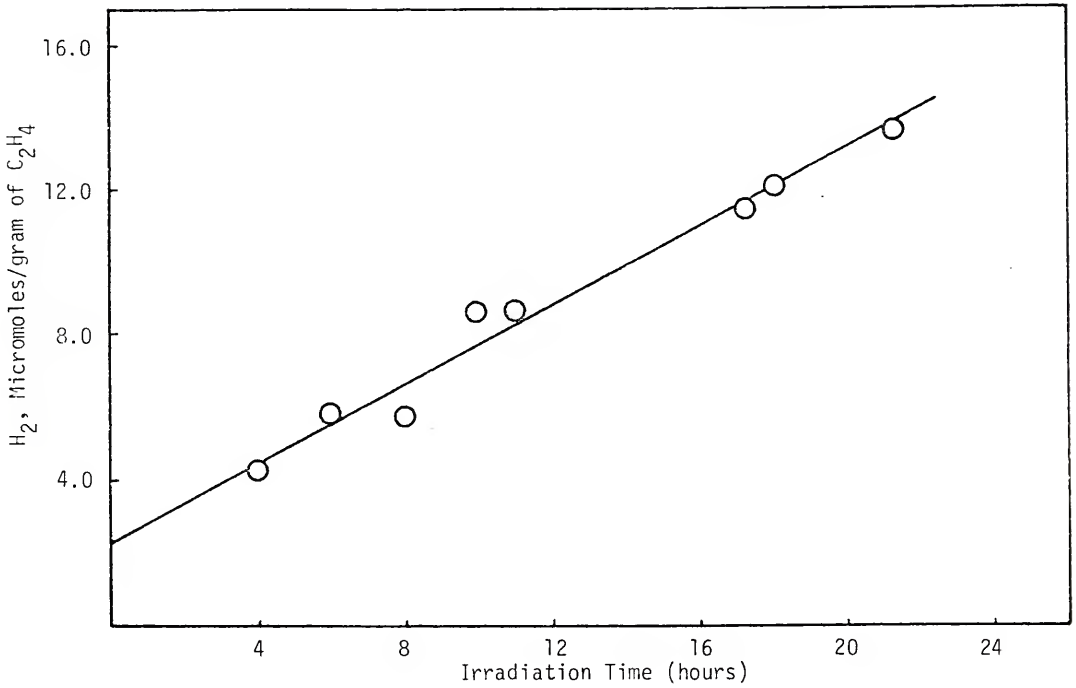

Fig. 7 Dosimetry: hydrogen yield from ethylene as a function of irradiation time

F. Sample Photolysis

1. Photolysis lamp and vessels

The photolysis lamp employed in this study was a General Electric 15 watt Germicidal lamp which is illustrated in Fig. 8. The Germicidal lamp is essentially a low pressure mercury lamp in a quartz envelope.

The emission spectrum of this lamp was examined with a McPherson Model 218 Vacuum Ultraviolet monochromator with double-beam attachment and ratio-recording electronics. The McPherson monochromator was operated with an entrance and an exit slit of 10 microns and at a scan rate of 5 nm/min. The window on the monochromator was 3 mm, thick Far-UV Silica.

In the spectral range of 170.0 to 450.0 nm, the principal lines are 253.7 nm, 296.7 nm, 313.0 nm, 365.0 nm, 404.6 nm and 435.8 nm. It should be noted (Table 1) that the output of the lamp is rich in the 253.7 nm resonance line and that the 184.9 nm line is unobserved.

Fig. 9 shows the two types of photolysis vessels used in these experiments. The smaller vessel was essentially a 10 cm. quartz cell attached to a Pyrex cold finger and break seal. The long cylindrical vessels were constructed of 20 mm. O.D. x 18 mm. I.D. General Electric Type 204 clear fused quartz with a Pyrex breakseal. The General Electric quartz was later found to be inferior to several other brands, for instance, that of the American Quartz Company. A number of pieces of quartz received from G.E. had striations that

marred their optical quality and so care had to be exercised in the selection of the pieces used. Also glass blowing on this material proved difficult because slight overheating of the glass caused bubbles to form in it.

The smaller vessel was used only for the spectrophotometric analyses of bromine. All other product yields were determined using the large vessels.

The volumes of the photolysis vessels are listed below.

Small Vessel No.	Volume
5	34.2 cc.

Large Vessel No.	Volume
2	88.22 cc.
3	91.81 cc.
4	93.68 cc.

The lamp fixture was a standard desk lamp designed to hold two fluorescent lamps. In the original experimental arrangement, two Germicidal lamps were used together with the large photolysis vessel positioned between them. Their total output, however, led to too rapid photodecomposition of the HBr actinometer. One of the lamps was then removed and replaced by three Pyrex tubes that aided in the positioning of the long photolysis vessel. The vessel was positioned longitudinally and parallel to the single lamp and at a perpendicular distance of about 2 cm. Marks on the glass tubing allowed the vessels to be positioned reproducibly. The vessel's length allowed it

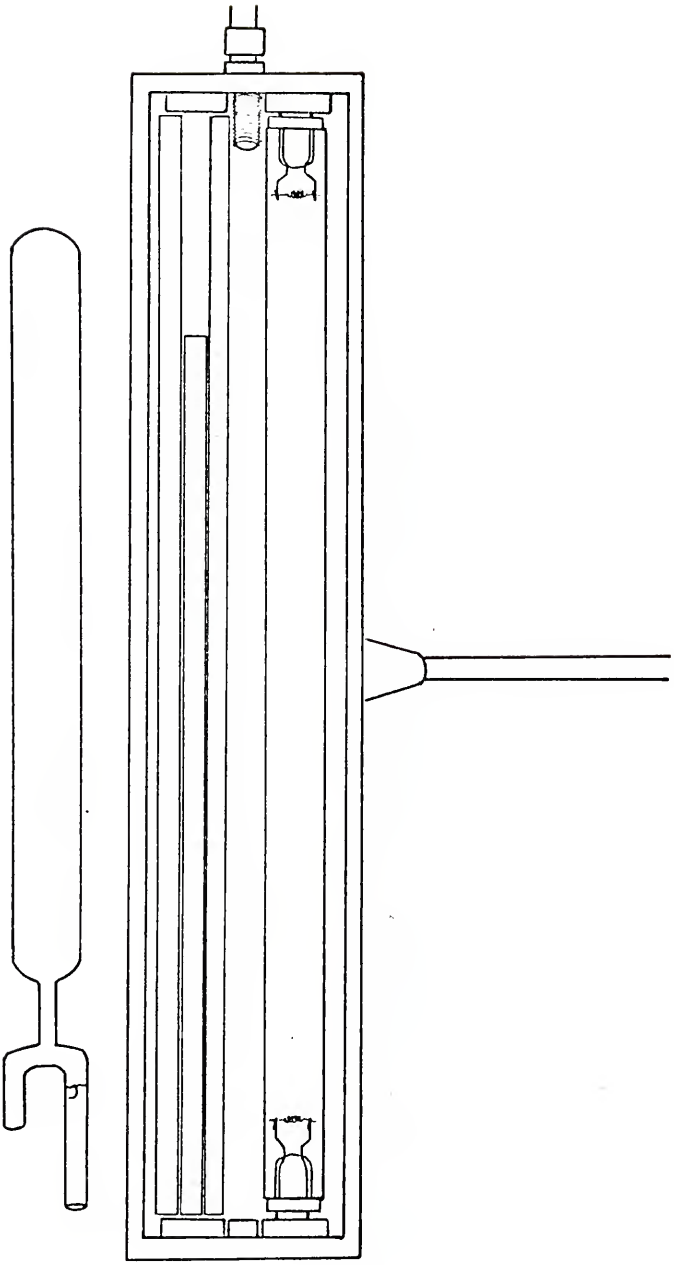

Fig. 8 Photolysis lamp

Table 1

The Relative Intensity Distribution on a Logarithmic Scale of the Emission Lines in the Spectral Range from 170.0 to 450.0 nm for the General Electric 15 Watt Germicidal Lamp

Wavelength (nm)	Log Relative Intensity
253.7	1.00
296.7	0.05
313.0	0.14
365.0	0.06
404.6	0.48
435.8	0.56

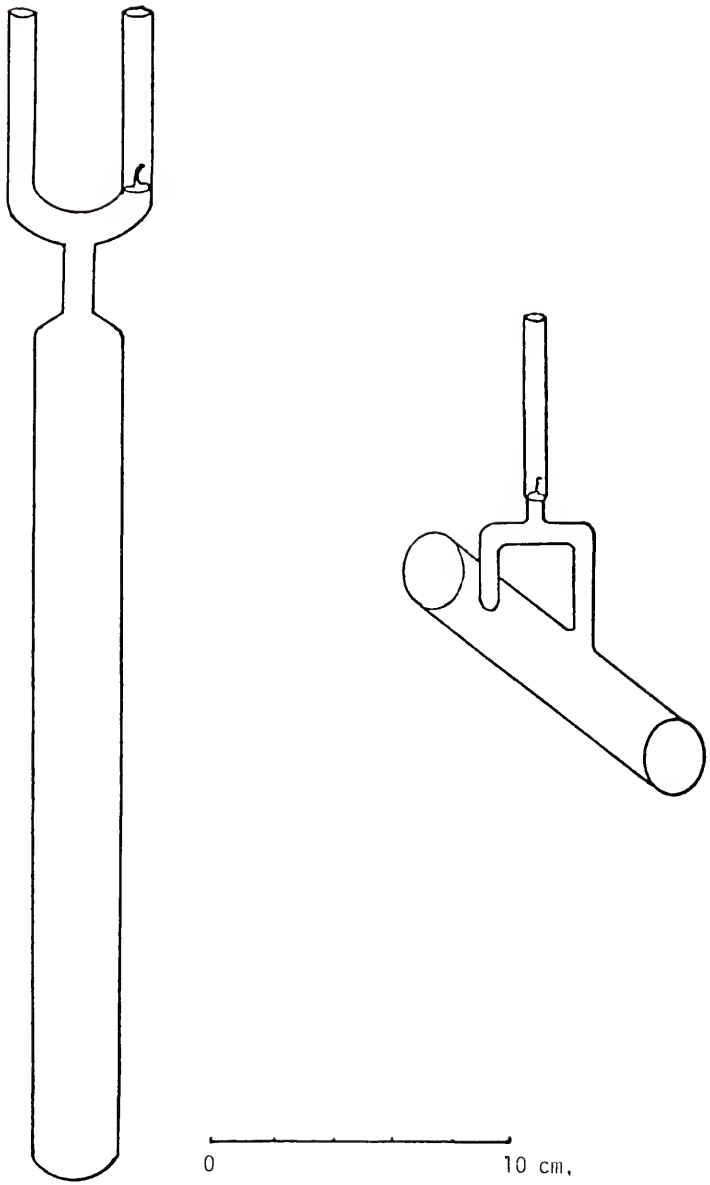

Fig. 9 Photolysis vessels

to be situated between the lamp's filaments, and air was passed between the vessel and the lamp to avoid thermal effects and to remove possible ozone formed. The latter has a strong absorption band at 253.7 nm (29). Prior to each photolysis, the lamp was turned on for a period of five minutes to allow it to stabilize. In addition, to minimize voltage fluctuations from the power line, a Sola transformer was employed. The geometry of the arrangement and the lamp's output allowed the photolysis to be carried out in periods of less than 10 minutes.

2. Actinometry

Gaseous hydrogen bromide was employed for actinometry with the Germicidal lamp. The near ultraviolet absorption spectrum of hydrogen bromide resembles closely that of ethyl bromide as would be expected if the electronic transition originates from an orbital on the bromine atom. The replacement of a hydrogen atom by an ethyl group shifts the absorption maximum to the red. The hydrogen bromide absorption band is rather broad with a maximum at about 185 nm and a long wavelength tail extending to 299 nm (30), while the absorption band of ethyl bromide reaches a broad maximum at 203 nm and tails to approximately 300 nm (31). At longer wavelengths extending out to at least 400 nm both molecules are optically transparent. The lower energy lines of the Germicidal lamp above 253,7 nm should, therefore, contribute insignificantly to the photolytic decomposition of these gases; and hydrogen bromide, it may be concluded, was an excellent choice as an actinometer for this investigation.

Hydrogen bromide was photolyzed at a pressure of 129.7 torr and a temperature of 22.5 $\pm$ 0.5°C in a mercury-free system. The quantum yield for hydrogen production with less than 1% conversion has been taken as unity (32, 33). The hydrogen yield corresponded to an absorbed intensity of 8.5 $\pm$ 0.1 x 10^{13} quanta/cc.-sec. (7.7 $\pm$ 0.2 x 10^{15} quanta/sec.) for the large vessels and 8.0 $\pm$ 0.1 x 10^{13} quanta/cc.-sec. (2.7 $\pm$ 0.1 x 10^{15} quanta/sec.) for the small photolysis vessel. The experimental conditions of the actinometry were designed so that the absorbance of the hydrogen bromide actinometer was the same as that of the ethyl bromide. Combination of the deal gas law with the Beer-Lambert law for equal absorbance of the hydrogen bromide and ethyl bromide yielded the expression

$$P(HBr) = \left[\frac{a(C_2H_5Br)}{a(HBr)}\right] P(C_2H_5Br)$$

$$= \left[\frac{7.82 \times 10^{-5} \text{ torr}^{-1}\text{cm.}^{-1}}{6.03 \times 10^{-5} \text{ torr}^{-1}\text{cm.}^{-1}}\right] 100 \text{ torr}$$

where the extinction coefficients at 253.7 nm, a, for hydrogen bromide and ethyl bromide respectively were interpolated from the graphical data of Porret and Goodeve (30) and Goodeve and Taylor (31) and the pressure of ethyl bromide, $P(C_2H_5Br)$, was that employed in this study.

The configuration of the photolysis apparatus (Fig. 8) precluded straightforward determination of the incident light intensity, I_o, because the path length of light through the photolysis

vessel was not easily ascertained. However, since actinometry experiments were carried out at several pressures it was possible, as a matter of interest, to determine this path length. Using the absorbed light intensities I_a^P at 129.7 torr (7.7×10^{15} quanta/sec.) and $I_a^{P'}$ at 389.5 torr (20.5×10^{15} quanta/sec.) of the large vessels, the path length was calculated through successive iterations on a computer with the equation

$$\frac{I_a^P/I_o}{I_a^{P'}/I_o} = \frac{1-e^{-abP}}{1-e^{-abP'}}$$

The path length, b, was found to be 16.0 cm., in contrast to the 2 cm. diameter of the photolysis vessel. Apparently, a major portion of the light traversed the tube obliquely. Considerable internal scatter from the cylindrical glass walls may also have occurred. Insertion of the value of b into the Beer-Lambert law gives an incident light intensity of 6.5×10^{16} quanta/sec.

G. Preparation and Spark Discharge of Sample

The technique of using a Tesla discharge to produce good yields of the same kind of products formed by radiolysis has been employed before in this laboratory (34).

The spark discharge vessel (Fig. 10) was a 500 ml, round-bottom flask provided with two stainless steel electrodes opposite each other, about 1 in. apart, and with a Fischer-Porter Teflon plug

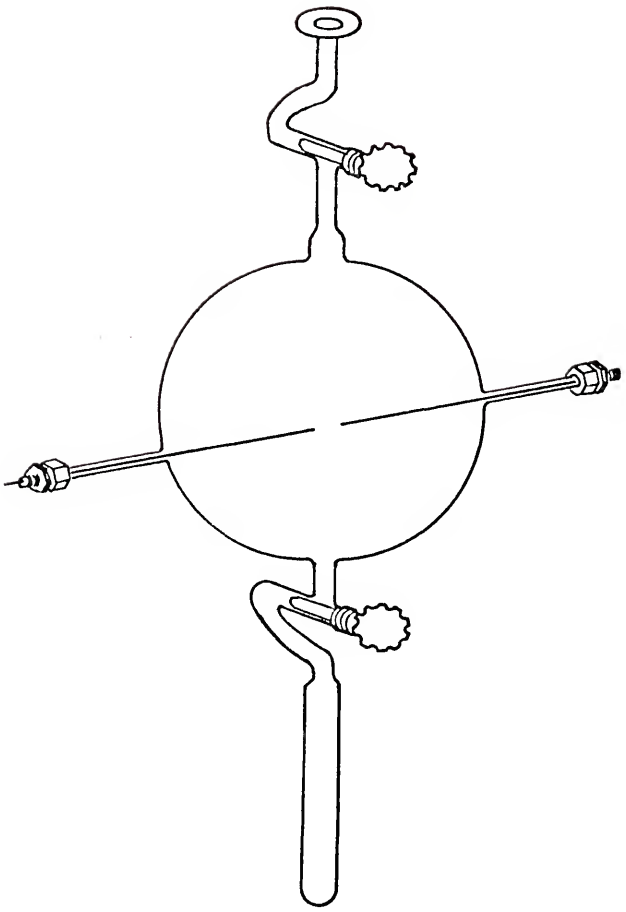

Fig. 10 Spark discharge vessel

needle valve. The incorporation of the second Fischer-Porter Teflon needle valve to the cold finger at the bottom of the vessel for the sparking of gaseous mixtures followed the design by D. R. Johnson in this laboratory.

In the vacuum preparation of ethyl bromide with oxygen, the ethyl bromide was first admitted to the vessel from storage reservoir, S_3 (Fig. 1). After the desired pressure was read on the cathetometer, the valve to the discharge vessel was closed, the sample was condensed into the cold finger and the valve to the cold finger closed. Following reevacuation of the submanifold, valve V_4 was closed and the valve to the discharge vessel reopened. A determined amount of oxygen was then admitted and the valve to the vessel again closed. After removing the vessel from the submanifold, the condensed sample was warmed to room temperature and the valve to the cold finger opened to allow the two gases to mix by diffusion.

In the spark discharge, one electrode was grounded to a cold water pipe and the other was in contact with a Tesla coil. Power to the Tesla coil was supplied through a Variac set at about 30 volts. During the discharge, a pale violet-blue color surrounded the electrode ends; however, the low voltage setting caused no distinguishable arcing.

For the purpose of column evaluation (Sec. II-H-1-b), the spark discharge was carried out at an ethyl bromide pressure between 4 and 6 torr for a period of about 5 minutes. Approximately 12 torr

sparked for 12 minutes provided sufficient products for product identification on the gas chromatograph mass-spectrometer system (Sec. II-H-2). When oxygen was added, it comprised about 5% of the total pressure.

H. Analytical Equipment and End Product Analysis

1. Gas chromatography

a. Principle instruments

A modified MicroTek 1600 gas chromatograph with a hydrogen flame ionization detector was the principal instrument used in the quantitative analysis of the organic products. The output of its detection system was fed to the 1 mv. pen of a Minneapolis-Honeywell double pen, 1 mv. and 10 mv. full scale, recorder. The instrument had an output attenuator with a range of 1, 2, 4, 8, . . . , 128 and an input attenuator marked X1 (most sensitive), X100 and X10000. It was found experimentally, however, that the input attenuator ranges were X1, X573 and X57300.

The flow system for this instrument is illustrated in Fig. 11. An L-206-6 Loenco multiport valve with Viton-A O-rings (valve A) was arranged so that in a two-column series, the down-stream column could be switched out of the flow system, while a Hoke "Milli-Mite" needle valve introduced into the bypass compensated for the flow restriction of the switched-out column. This arrangement was designed to prevent the proportionately large quantity of

unreacted ethyl bromide from the irradiated or photolyzed sample from flooding the detector. In practice, however, it was found that the flooding of the column with the excess parent compound was more important than the saturation of the detector. Also incorporated into the flow system was an Air Products tri-tube flow meter unit to adjust and monitor the flow rates of the carrier gas, hydrogen and air. Accurate control of the carrier gas flow rate is necessary to reproduce elution times, and of substantial importance in reproducing flame sensitivity. The critical factor in control of the flame sensitivity, however, is the hydrogen flow rate. Control of the air flow rate is not crucial and could be done at the air tank pressure regulator.

As a result of the replumbing of the flow system, a heating cartridge and blower were installed into the MicroTek sampling compartment to prevent the high boiling components of a sample from distilling out of the carrier gas onto the relatively cool metal surfaces of the sliding valve and stainless steel tubing enroute to the detector.

The instrument provided for the vacuum transfer of a sample from an externally attached vessel to a sample loop attached to the front of the chromatograph by Swagelok fittings. This sample module, which was installed by J. M. Donovan (35), is similar to a design by Marcotte (36).

In the present work, however, all samples were transferred on the vacuum line submanifold (Figs. 1 and 2) to one of the gas

loops shown in Fig. 12 and these introduced the sample through the sample loop ports on the front of the chromatograph instrument.

Three types of gas sampling loops (Fig. 12) were employed in this work. Differences in the design of loops L_1 and L_2 were to accommodate the instruments on which they were used. The former was used on both a 550 Tracor instrument and a Loenco gas chromatograph, the latter solely on the 1600 MicroTek, In the analysis of gases non-condensible at liquid nitrogen temperature, a gas sampling loop similar to one designed by J. W. Buchanan (37) was employed. This loop, L_3, was attached directly above the Toepler pump as indicated in Fig. 1 by means of a 10/30 tapered ground glass joint. Loops L_1 and L_2 were attached through a single inlet arm to the vacuum submanifold shown in Figs. 1 and 2 via a 1/4 in. stainless steel Swagelok union or elbow joint assembled with two Viton-A O-rings as a front ferrule and with the back ferrule reversed from normal.

b. Evaluation of column packing

The radiolytic and photolytic decomposition of a compound is generally limited to much less than 1% to prevent secondary and higher order product formation. Experimentally this means that the products are formed in submicromolar quantities and that the parent compound is essentially unconsumed. Accordingly, since the preponderance of sample is the parent compound, a very desirable and perhaps essential characteristic is a rapid unloading of the column to determine the compounds eluting after the parent. Furthermore, as is the case

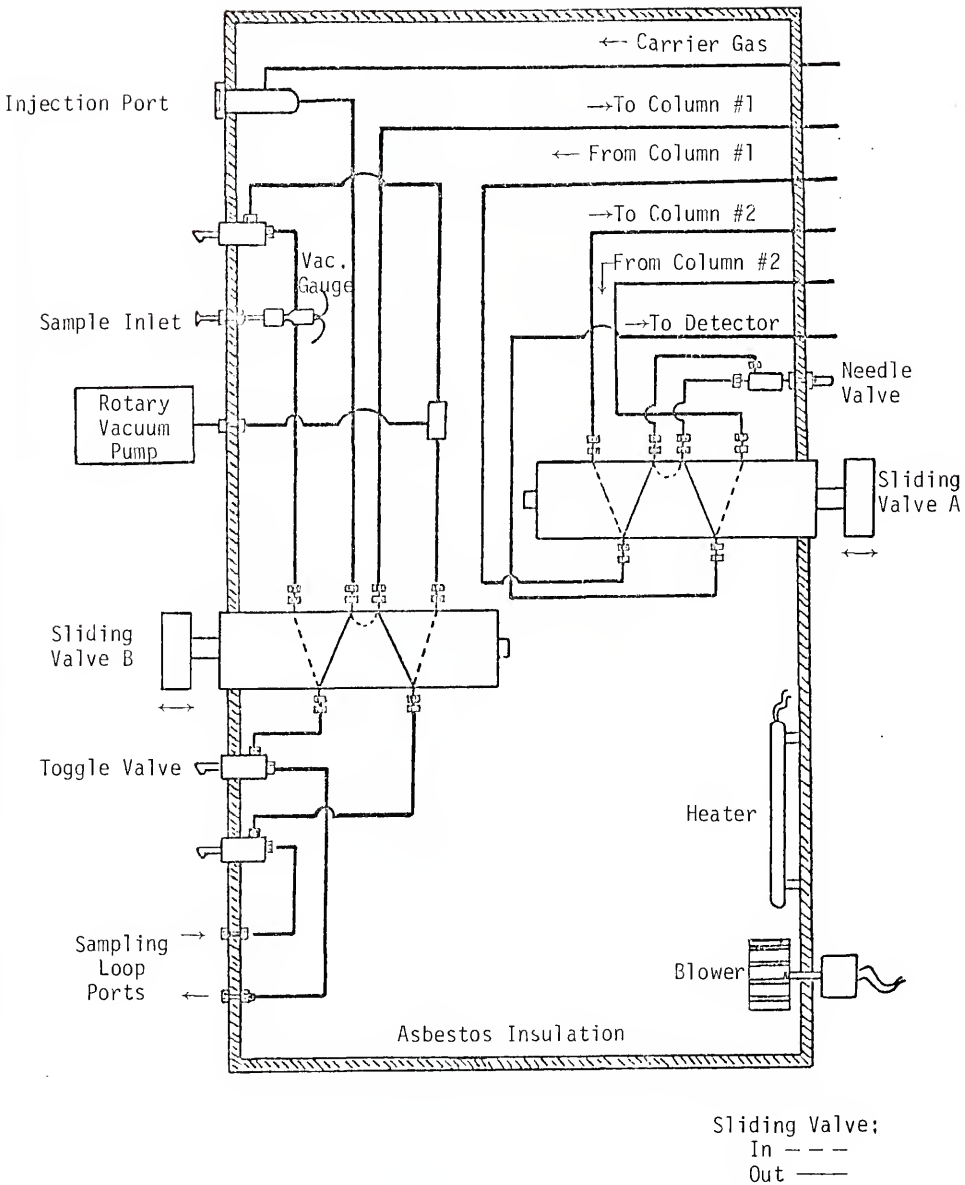

Fig. 11 1600 MicroTek gas chromatograph sampling module

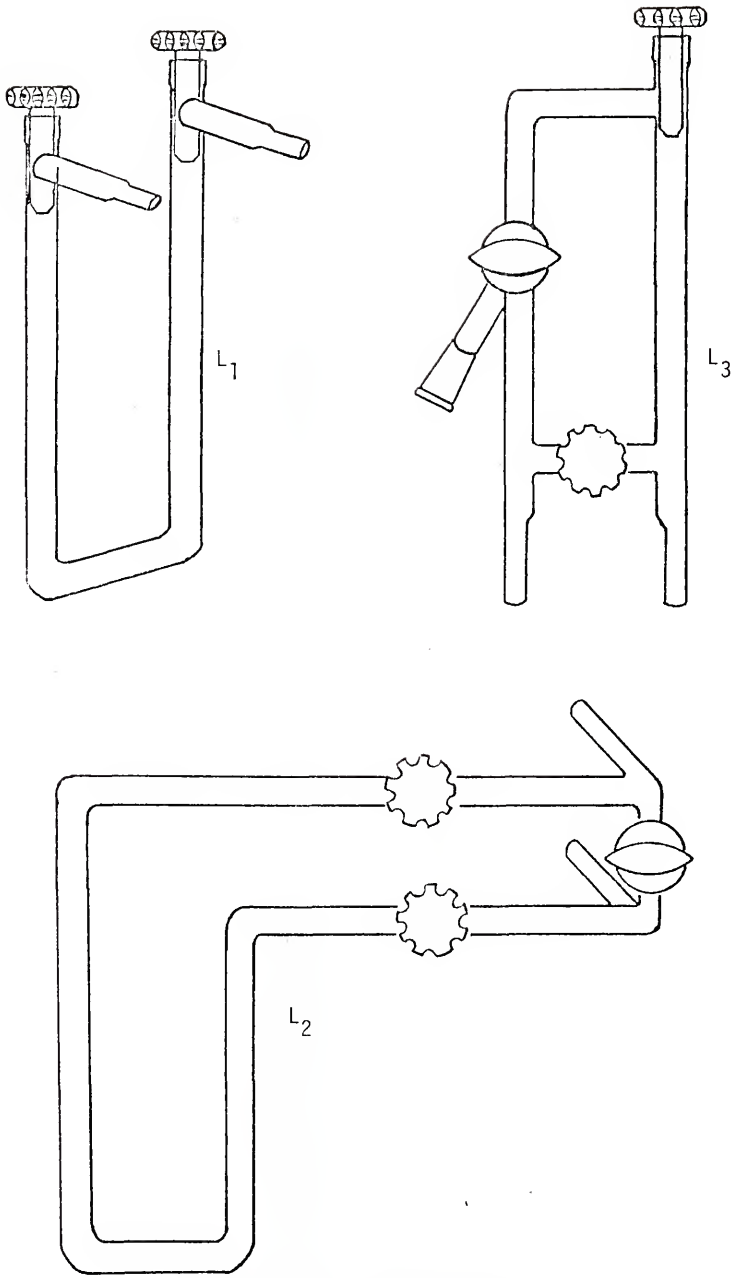

Fig. 12 Gas sampling loops.

in the ethyl bromide system, the number of products formed may exceed 25 and cover a boiling point range of 400°C. Such a wide boiling range generally requires temperature programming and this may limit the nature of the column material employed, especially if it is to be used with a flame ionization detector. The upper temperature limit of a column given in the literature is usually determined for a thermal conductivity detector. For a flame ionization detector, the operating temperature must be kept substantially lower than the maximum temperature if noise and rising baseline resulting from column bleed are to be avoided. There is also a lower temperature limit determined by the viscosity of the phase. The less viscous phases at the analysis temperature give the most efficient separation.

The properties of a number of solid adsorbents and stationary phases were evaluated under conditions that simulated those in this study (Secs. II-H-1-c and -d). The gaseous mixture was obtained by spark discharge (Sec. II-G). Most of the stationary phases examined were methyl silicones which had low selectivity according to the McReynolds constants (38). All of the liquid phases, including Porapak Q, separate a homologous series of compounds according to their boiling points. Only the solid adsorbent, silica gel, was capable of separating all of the C_2 hydrocarbons. Ethylene and acetylene were unresolved in all other cases.

A brief comparison of some of the column materials examined follows below:

(1) 10% Diethylene glycol adipate and 90% GE SF-96 (28.6% liquid phase) provided the most symmetrical peaks and unloaded the most rapidly of the liquid phases; however, its thermal stability was much poorer as bleeding occurred at a lower temperature.

(2) 30% SE-30 GC Grade behaved similar to 30% OV-101. It unloaded fairly well; however, its thermal properties were not as good.

(3) 30% OV-101 showed some tailing of peaks. A slight base-line rise began at 160°C but did not become excessive until 190 to 200°C. 10% OV-101 did not separate as well as the 30% loaded column although it unloaded more rapidly as expected.

(4) Porapak Q (polystyrene-type porous polymer) recovered relatively slowly from overloading and the alkyl bromides tailed considerably unless rapid temperature programming was used.

(5) Baker reagent grade 60-200 mesh and Analabs' Anasorb 40-50 mesh silica gel were comparable in their separation of the C_2 hydrocarbons when the former was used at room temperature and the latter at 85°C. The bromides did not easily elute off of either material.

All of the liquid phases described were coated on acid washed Chromosorb P. Column dimensions in each case were about 3.1 m. x 0.25 in. O.D. except for Porapak Q in which they were 1 m. x 0.25 in. O.D. Several different temperature programming rates and flow rates were also explored to determine the conditions which gave the optimum separation of the compounds. Of the columns evaluated,

the 40-50 mesh silica gel was chosen for the determination of the low molecular weight C_2 hydrocarbons and the 30% OV-101 on acid washed Chromosorb P was selected for the analysis of the intermediate and high molecular weight organic compounds. Typical gas chromatograms from the analysis of irradiated ethyl bromide are given in Fig. 15.

c. Products non-condensible at -196°C

Immediately after radiolysis or photolysis, the vessel was immersed in a Dewar of liquid nitrogen to reduce the possibility of post-irradiation and post-photochemical effects (Sec. III-B).

In the determination of the non-condensibles and the condensible organic products, the vessel was attached to the submanifold of the mercury vacuum line (Fig. 2) by means of the breakseal fitting. After a good vacuum had been reached, the U-trap, T_3, was cooled in liquid nitrogen for 20 minutes and then valve V_5 was closed. The hammer above the breakseal was then released and the gases non-condensible at -196°C were collected in two stages of Toeplering. In the first stage, they were collected in 12 Toepler pump cycles at one minute intervals. Next, valve V_{10} was closed and the condensible material was vacuum transferred to loop L_2 with liquid nitrogen over a 20 minute period. The valve to the loop was then closed and valve V_{10} on the U-trap reopened. Another series of 12 Toepler cycles were carried out to complete the transfer of the non-condensibles. By the sixth or seventh cycle the transfer was, in general, complete as monitored through the thermocouple vacuum gauge, G_3, directly above the sample vessel. The main procedural differences

for the dosimetry and the actinometry were that the condensible material was not transferred to the gas loop L_2 and the Dewar of liquid nitrogen was kept under the U-trap during the second stage of Toeplering.

Hydrogen was determined by two methods. In ethylene dosimetry and in the radiolysis and photolysis of pure ethyl bromide, the non-condensibles were Toeplered to the McLeod gauge, D, for a PV measurement and then to the non-condensible gas loop, L_3, for gas chromatographic analysis by flame ionization of the small quantity of organic products that contributed to the pressure measurement as described below in the discussion of methane. The hydrogen was then determined by difference. In actinometry and in the oxygen scavenged radiolysis, the non-condensible gases were Toeplered to the gas loop L_3 for analysis on the Tracor Model 550 gas chromatograph equipped in this laboratory by A. R. Ravishankara with a Gow-Mac Model 10-285 thermal conductivity detector using WX filaments. The hydrogen was separated on a 20 ft. x 0.25 in. O.D. copper column of molecular sieve with nitrogen carrier gas at room temperature.

Direct analysis of hydrogen with thermal conductivity gas chromatography could be employed only if one lambda or more of hydrogen was being measured. When applicable, however, this method left less doubt about the presence of air and was more expedient than the PV measurement. When the McLeod gauge is used, it is necessary to make an empirical correction for the small amount of air present in the apparatus; otherwise, there will be an apparent finite yield of hydrogen at zero radiation dose.

In the radiolysis and photolysis, methane was in sufficiently small yield that essentially all of it could be Toeplered to the non-condensible gas loop for analysis on the MicroTek Model 1600 gas chromatograph (Sec. II-H-1-a). Methane was separated from the C_2 hydrocarbons isothermally at 85°C on a 3.1 m. x 0.25 in. O.D. stainless steel column packed with Anasorb 40-50 mesh silica gel with a nitrogen carrier gas at a flow rate of 95 cc./min. In dosimetry only ethylene was present while in ethyl bromide radiolysis and photolysis, both ethane and ethylene contributed to the non-condensibles. In each instance, the components were quantitatively determined relative to three methane standards injected with a Unimetric 50 µl gas-tight syringe immediately prior to the actual analysis. In 16 consecutive radiolysis experiments over a three-week period, the maximum variation of the detector's response to methane was 11% with a relative standard deviation of 3,3%. The peak areas were determined by approximation of the peaks with several triangles which gave more consistent values than the method of single triangulation commonly referred to in the literature.

d. Organic products condensible at -196°C

The organic condensibles were transferred to the gas loop L_2 on the submanifold of the mercury vacuum line as described in Sec. II-H-1-c. The low molecular weight C_2 products ethane, ethylene and acetylene were determined in separate experiments from the intermediate and high molecular weight products on the 1600 MicroTek gas chromatograph.

The low molecular weight hydrocarbon analysis was carried out under the same conditions described in Section II-H-1-c in the discussion of methane. The C_2 saturates and unsaturates were identified by retention times and confirmed on the gas chromatograph-mass spectrometer-computer system (Sec. II-H-2). After each analysis the column was conditioned at 250°C for several hours to elute ethyl bromide and other adsorbed alkyl bromides.

The intermediate and high molecular weight products were separated on a 4.2 m. x 1/4 in. O.D. stainless steel column packed with 30% OV-101 on 60-80 mesh acid washed Chromosorb P with a nitrogen carrier gas flow rate of 32 cc./min. The gas chromatograph was ballistically programmed from room temperature to 200°C according to the following Variac schedule:

Variac (volts)	Time (min.)	Temperature (dg C)
0	0-45	ambient
45	45-67	ambient-80
50	67-127	80-133
increment 1v. every 5 min.	127-210	133-200

At the end of each analysis, the column was conditioned at 250°C for several hours. The products were identified on the gas chromatograph-mass spectrometer-computer system (Sec. II-H-2) and confirmed when possible (Table 2) on the 1600 MicroTek gas chromatograph.

The response of the flame ionization detector to the products was calibrated relative to the mean of three standard propane

injections made immediately prior to each analysis. All gas standards were injected with a Unimetric 50λ gas-tight syringe and liquid standards with a Unimetric 10λ liquid syringe. Reproducibility of the standards based on 4 or 5 injections typically had a relative standard deviation of much better than 1%.

2. Gas chromatography-mass spectrometry-computer system in the identification of organic products

A detailed description of the gas chromatograph-Bendix Model 14-107 system has been given elsewhere (39). Recently, however, the instrument has been interfaced with a single stage jet molecular separator designed by R. J. Hanrahan and J. E. Prusaczyk in this laboratory. The critical dimensions, which were suggested by an earlier design of Ryhage (40), are jet and skimmer orfices of 0,010 in, separated by a gap of 0.020 in. The separator was installed in an existing U-trap of the gas chromatograph-output trapping manifold (39) without interfering with the original design of the unit (Fig. 13). Since the molecular separator allows the effluent from the gas chromatograph column to be continuously diverted into the ion source of the Bendix mass spectrometer, use of this modification is more convenient and efficient than the old trapping system.

In principle, the molecular separator compresses and accelerates the gas chromatograph effluent into a narrow jet from which the light helium atoms (carrier gas) are scattered and the heavy organic molecular weight molecules are retained. In practice, it allows the gas chromatograph to operate at atmospheric pressure and the mass

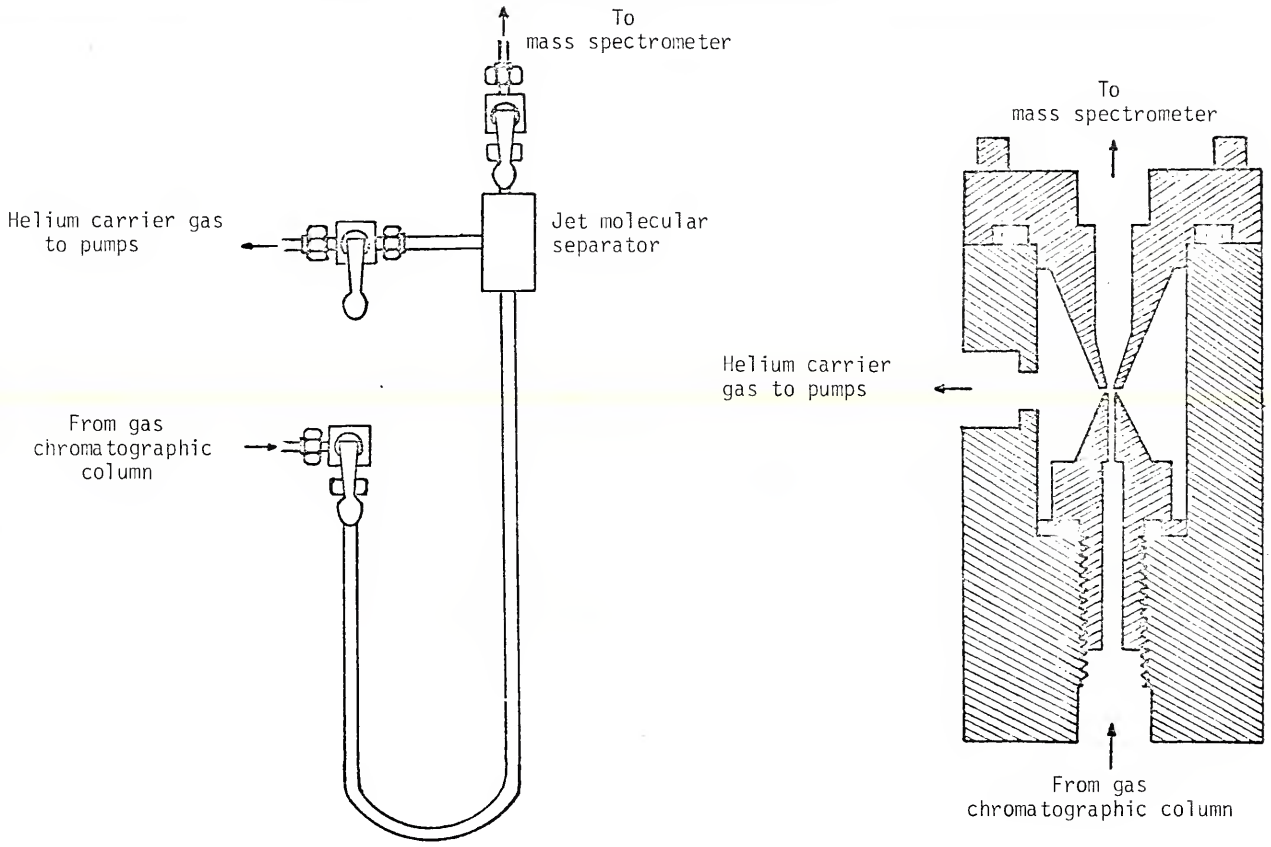

Fig. 13 Portion of product trapping assembly and jet molecular separator

spectrometer at 10^{-5} torr. Helium is used as the carrier gas because it is easily skimmed off by the separator; fortunately, it also provides minimum interference with the mass spectral cracking pattern of other species.

A Hoke "Milli-Mite" metering valve diverted about 1/4 of the column effluent to the detector of the gas chromatograph and the remaining fraction to the ion source of the Bendix mass spectrometer. The gas chromatograph separated the components while the mass spectrometer provided information on the empirical formula and the structure of the compounds. Data acquisition of the mass spectra was accomplished under semi-automatic control of a General Automation SPC-12 minicomputer. The SPC-12 computer is capable of making about 500 complete digitizations per second and taking 20 digitizations per peak. The mass spectrometer software (41) includes a conversational executive system which permits the operator to communicate with the computer via an ASR-38 Teletype in 2 letter mnemonics. A PEC 9-track IBM magnetic tape unit facilitates the transfer of information to and from the computer. In particular, during a gas chromatograph-mass spectrometer run, data are collected and stored on magnetic tape and at a later time are retrieved and reduced.

At a scan rate of 9 on the Bendix mass spectrometer, 20 sec. is required to cover a mass spectral range of 14 to 400. At a more rapid scan speed, resolution is sometimes sacrificed, while at a slower speed there may not be sufficient time to scan the fragments

in the heavy mass range. Normally, both the gas chromatogram on the chart recorder and the oscilloscope screen on the Bendix are visually monitored, and when a peak is observed the spectral scan is manually initiated from the mass spectrometer. Frequently, it is possible to detect samples in small quantities that appear neither on the chromatogram nor on the oscilloscope screen by repeated scans and comparisons of the number of peaks in the spectra that are printed out on the Teletype,

One problem encountered in optimizing experimental conditions is the adjustment of the stream splitter to properly partition the column effluent between the flame ionization detector and the ion source. If insufficient carrier gas is proportioned to the gas chromatograph detector, not only the column effluent but also air and hydrogen from the ionization detector are pumped into the mass spectrometer. In most operations, a supplemental carrier gas flow is added between the column exit and the stream splitter to circumvent this effect (39).

Another problem related to flow control is the possibility of lag time between the sample reaching the flame ionization detector and the mass spectrometer. This presents a particular problem when the column is heated during temperature programming. As the oven temperature rises the sample tends to reach the mass spectrometer before the gas chromatograph detector. The delay time may be as great as 30 sec. at 150°C if the experiment was begun at room temperature and signals were then being received concurrently. The

difficulty is resolved somewhat by proportioning additional carrier gas to the gas chromatograph detector while the experiment is in progress.

Column bleeding from the 30% OV-101 on Chromosorb P caused only minor interference with the cracking pattern of the unknown compounds until temperatures exceeded 160°C.

3. High pressure mass spectrometry

a. Equipment for ion molecule studies

The Bendix mass spectrometer could be readily modified from the analytical to the ion-molecule mode (42). The high pressure source and accessories were patterned after a design described in detail by Futrell and coworkers (43). The ions were generated in a continuous mode with 100 e.v. electrons. With the exception of reducing the pulse height signal on grid No. 1 from +25 volts to +23 volts, the ion source potentials were the same as those reported by Futrell and coworkers (43). The horizontal and vertical deflection control settings including the ion focus control were varied to optimize resolution which would change as a function of the source pressure. Because the relative ion intensity in the mass spectra would change with slight variation of these controls, it was necessary to visually monitor the mass spectra on an oscilloscope while making these changes to insure that the ion intensities throughout the whole spectrum would change uniformly.

b. Chemical ionization study

Chemi-ionization mass spectrometry is similar to electron impact mass spectrometry except that in the former, the ionization of a substance is effected by the reactions between the molecules of the substance and chemical species other than electrons. The chemical species are reactant ions or electronically excited metastable neutrals formed by electron impact and ion-molecule reactions.

Only a cursory study was undertaken using this method for the identification of products formed in the spark discharge of ethyl bromide (Sec. II-G). Field (44) employed this method and found that identification of a compound in methane was drastically simplified over electron impact mass spectrometry.

The experimental arrangement used in the present study was modeled after the set up in Sec, II-H-2 except that the high pressure source replaced the analytical source. Helium from the gas chromatograph served as the ionizing reactant and the pressure in the source was 0.5 torr.

Helium produced substantially more fragmentation than electron impact making identification more complex, a result which suggests that helium is more effective than 100 e.v. electrons in funneling energy into the molecules. Such an explanation is not unreasonable since the existence of states with excitation energy up to helium's first ionization potential, 24.6 ev. (45), and above have been known for some time. In the rare gases, some of these states participate in Penning ionization, Hornbeck-Molnar reactions or charge exchange.

4. Potentiometric titration of hydrogen bromide

The hydrogen bromide yield was determined electrochemically. Immediately after irradiation and photolysis, the reaction vessel was cooled to liquid nitrogen temperature, slightly acidified distilled water was added to the solid sample through the breakseal fitting. The vessel was removed from liquid nitrogen and the contents were shaken until the solid melted. The hydrobromic acid solution was then poured into a beaker and the vessel walls were rinsed several more times with small quantities of the acidified water to extract the remaining acid. About 30 ml. in total were used in the extraction of the hydrogen bromide.

The Br^- ion was titrated using either 0.02 or 0.05 M $AgNO_3$ in a 50 λ gas-tight Hamilton syringe with a platinum needle. Differences in the EMF between an Orion Model 94-35A bromide ion specific electrode and a double junction calomel electrode were monitored using a high input impedance (10 megohms) Hickok digital volt-ohm meter having a minimum voltage range from 0 to 199 mv. The reference electrode was in fact a Beckman Model 39270 fiber junction calomel electrode in a slightly cracked test tube containing a 1 molar solution of KNO_3. To insure adequate mixing, the solution was continuously stirred with a Teflon coated magnetic stirrer.

A representative titration curve is reproduced in Fig. 14. The equivalence points were always easily identifiable. For example, when a 0.0200 molar KBr solution was titrated with a 0.0200 M $AgNO_3$ solution, the equivalence point agreed to within

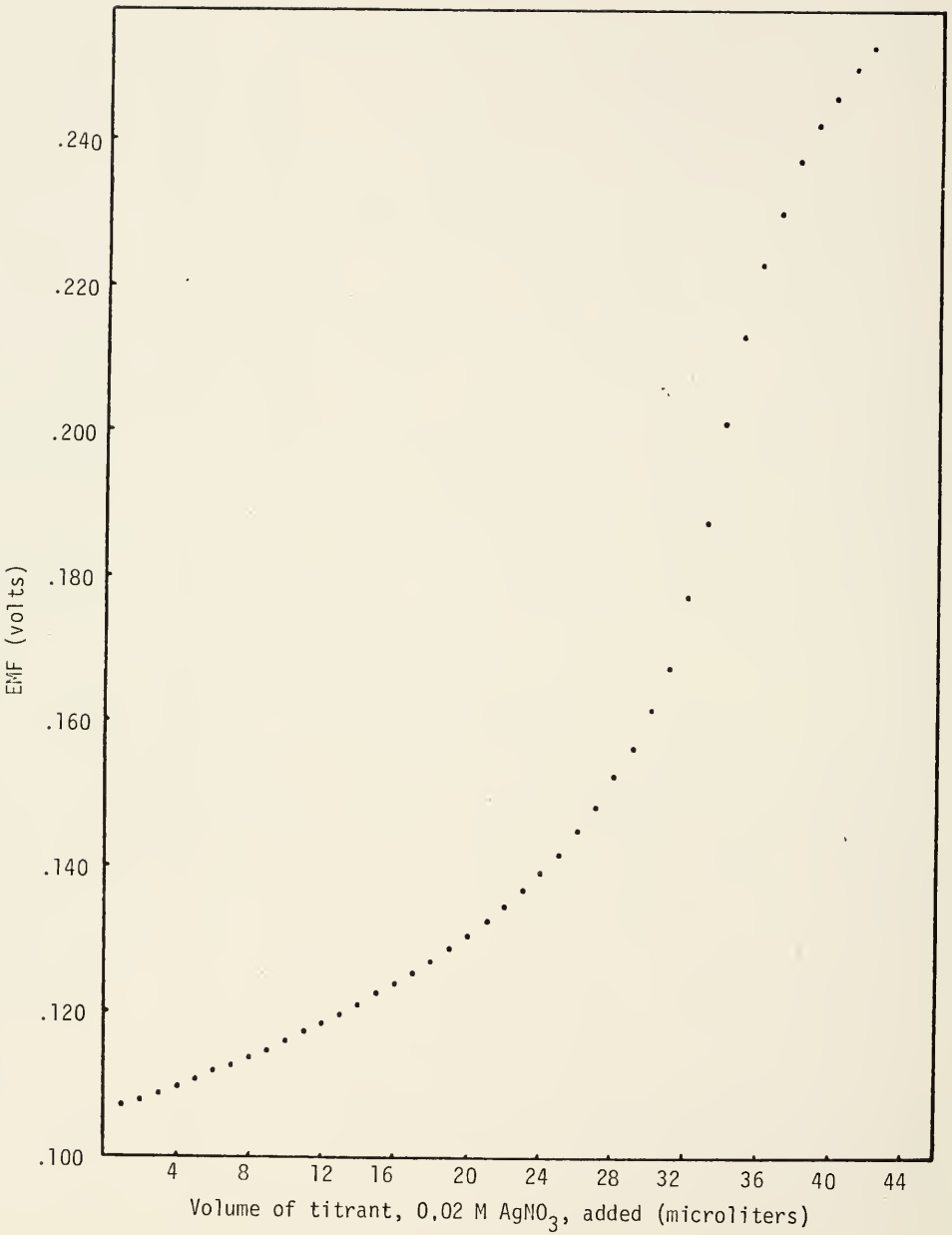

Fig. 14 Potentiometric titration curve of hydrogen bromide

$\pm$ 0.0002 M. In the actual determination, the uncertainty should be within $\pm$ 1%.

5. Spectrophotometric and chemical analysis of bromine

The determination of bromine in the pure and scavenged radiolysis sample was made spectrophotometrically at room temperature in the vapor state. For the analysis, the annular radiolysis vessel with the attached optical cell (Fig. 5) was used. Absorbance measurements at 416 nm were carried out between successive irradiations on the Beckman DU spectrophotometer with the Gilford Model 222 photometer and power supply. In a typical analysis, the sample was condensed into the cold finger of the reaction vessel and the cell absorbance determined. An optical measurement was then made of the thawed sample and the difference in the optical density was taken to be proportional to the concentration of bromine. The amount of bromine present was determined using the extinction coefficient 170 M^{-1} $cm.^{-1}$ (46). The uncertainty in measurement may be as large as 20%.

The same method was employed in the determination of bromine in the photolysis.

In addition to the direct spectrophotometric measurement for bromine in the pure radiolysis, a color test using dithizone (47) was also tried. An irradiated sample was vacuum transferred to a cold finger on the vacuum submanifold (Fig. 2) and the neck of the tubulation was sealed off with a torch. The sealed sample was then

broken open under anhydrous carbon tetrachloride and dithizone (diphenylthiocarbazone) was added dropwise. A change in color from yellow to red would have indicated the presence of bromine. To facilitate breaking open the sealed sample, the glass had been scored with a file.

Another test carried out for bromine in the pure ethyl bromide radiolysis involved breaking the sealed sample under a strip of filter paper saturated with a solution of fluorescein in a 1:1 methanol-water mixture. The development of a red spot on the filter paper would have pointed to the presence of bromine. This test detects as little as 2 gamma ($1\gamma = 10^{-6}$g.) of bromine (48).

Also, after each radiolysis and photolysis the sample was cooled to -196°C and inspected for yellow spots or colorations testifying to the existence of bromine in the sample.

III. EXPERIMENTAL RESULTS

A. Qualitative Identification of Products

The inorganic products formed from the radiolysis of ethyl bromide were identified as hydrogen, hydrogen bromide and in the oxygen-scavenged system, bromine. In the photolysis the same inorganic products were likewise detected except that no hydrogen was observed. These compounds were identified using thermal conductivity gas chromatography, potentiometry and absorption spectroscopy respectively.

The organic products were identified by their gas chromatographic retention times and when possible confirmed by their mass spectral cracking patterns. The array of peaks present in a gas chromatogram for a 24 hour radiolysis of the pure sample is shown in Fig. 15. The low molecular weight hydrocarbons methane, ethane, ethylene and acetylene were identified by retention times on a silica gel column and later confirmed by mass spectrometry. Identification of a number of the heavier products on the Bendix mass spectrometer was made possible by the larger yields produced in the spark discharge of ethyl bromide. N-butane, methyl bromide, vinyl bromide, methylene bromide, 1,1-dibromoethane, *cis*-1,2-dibromoethylene, 1,2-dibromoethane, bromoform, and 1,1,2-tribromoethane were identified using this means. The remaining products were identified only by their gas chromatographic

Fig. 15 Gas chromatograms of irradiated ethyl bromide

(a) Non-condensible hydrocarbons (3.1 m. x 0.25 in. O.D. stainless steel, Anasorb 40-50 mesh silica gel, 85°C, N_2 95 cc./min.)

(b) Condensible low molecular weight hydrocarbons (same as in (a))

(c) Condensible intermediate and high molecular weight products (4.2 m. x 0.25 in. O.D. stainless steel, 30% OV-101 on Chromosorb P, programmed as given in Sec. II-H-1-d, N_2 32 cc./min.)

Peak Identification

1. CH_4
2. C_2H_6
3. C_2H_4
4. C_2H_2
5. C_4H_{10}
6. CH_3Br
7. C_2H_3Br
8. C_2H_5Br
9. 1-C_3H_7Br
10. 2-C_4H_9Br
11. CH_2Br_2
12. 1-C_4H_9Br
13. 1,1-$C_2H_4Br_2$
14. *cis*-1,2-$C_2H_2Br_2$
15. 1,2-$C_2H_4Br_2$
16. C_3 dibrominated at 120°C
17. 1,2-$C_3H_6Br_2$
18. C_3 or C_4 brominated at 128°C
19. $CHBr_3$
20. *meso*-2,3-$C_4H_8Br_2$
21. 1,3-$C_3H_6Br_2$ and/or *racemic*-2,3-$C_4H_8Br_2$
22. 1,3-$C_4H_8Br_2$
23. C_3 or C_4 brominated at 140°C
24. 1,1,2-$C_2H_3Br_3$
25. 1,4-$C_4H_8Br_2$
26. Unknown at 170°C

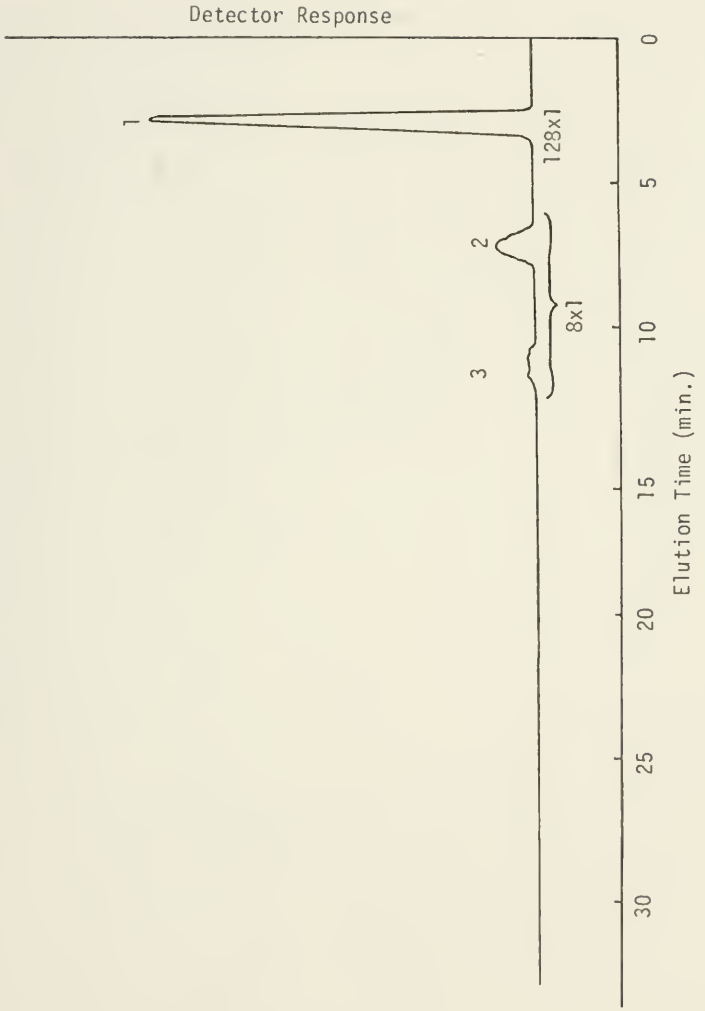
Detector Response
1
2
3
128x1
8x1
0
5
10
15
20
25
30
Elution Time (min.)

Fig. 15a

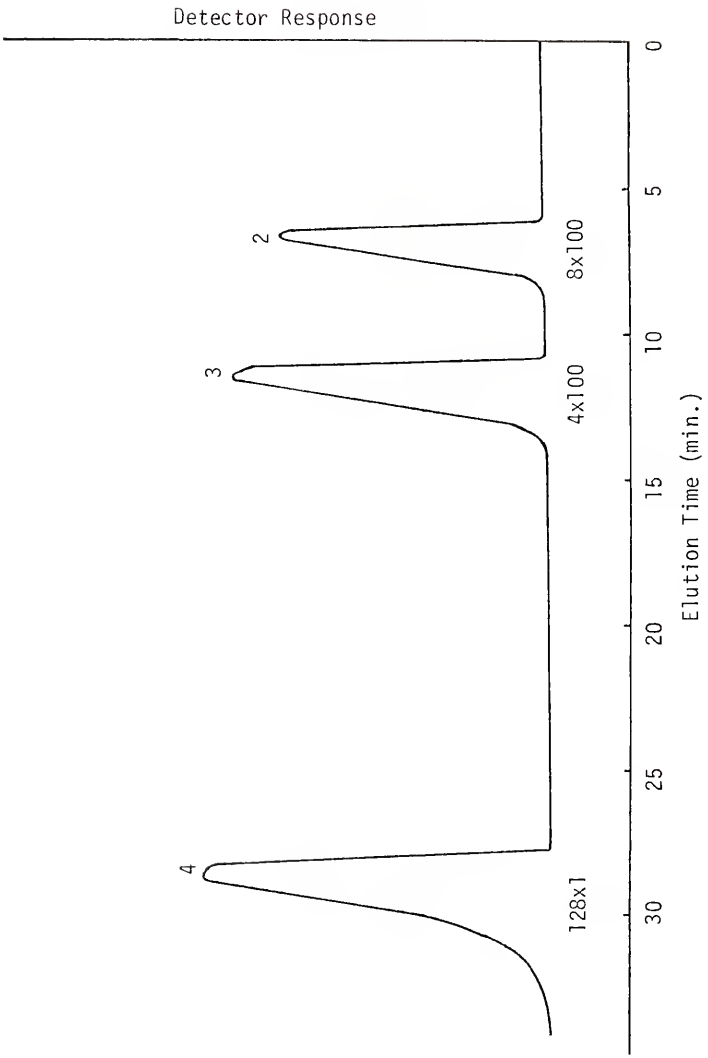
Detector Response
4
3
2
128x1
4x100
8x100
0
5
10
15
20
25
30
Elution Time (min.)

Fig. 15b

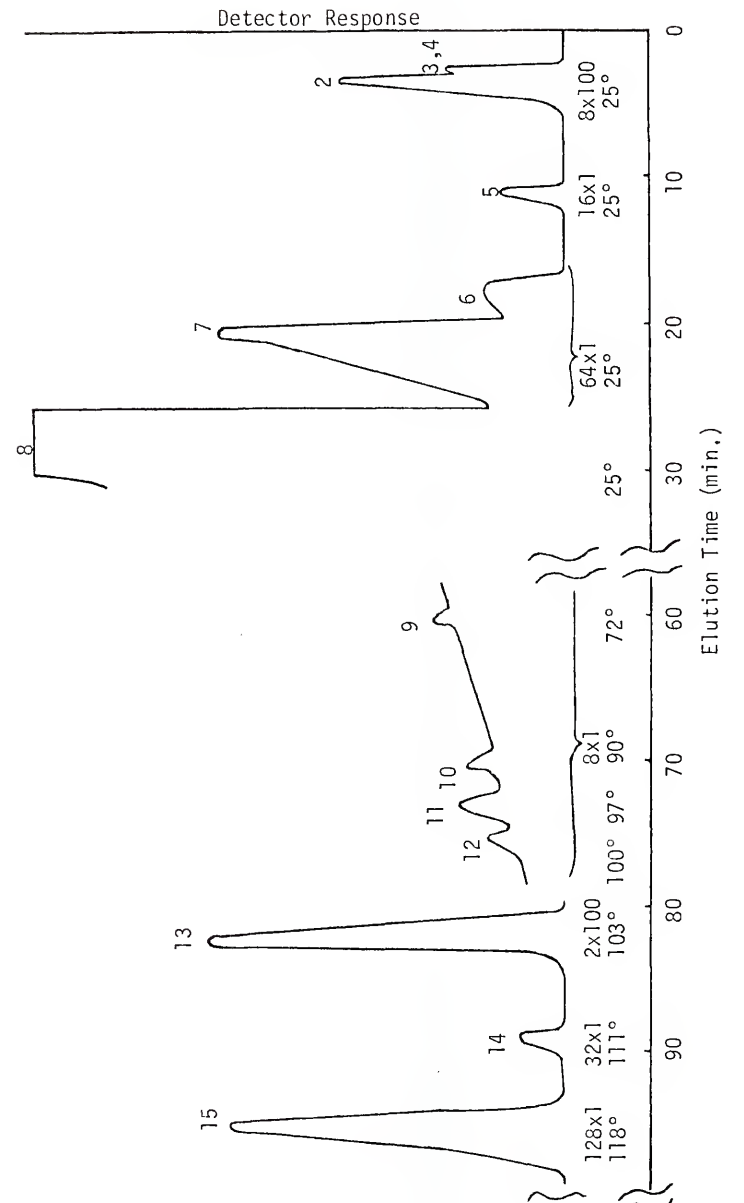
Detector Response
Elution Time (min.)
0
10
20
30
60
70
80
90
2
3,4
5
6
7
8
9
10
11
12
13
14
15
8x100
25°
16x1
25°
64x1
25°
25°
72°
8x1
90°
97°
100°
2x100
103°
32x1
111°
128x1
118°

Fig. 15c

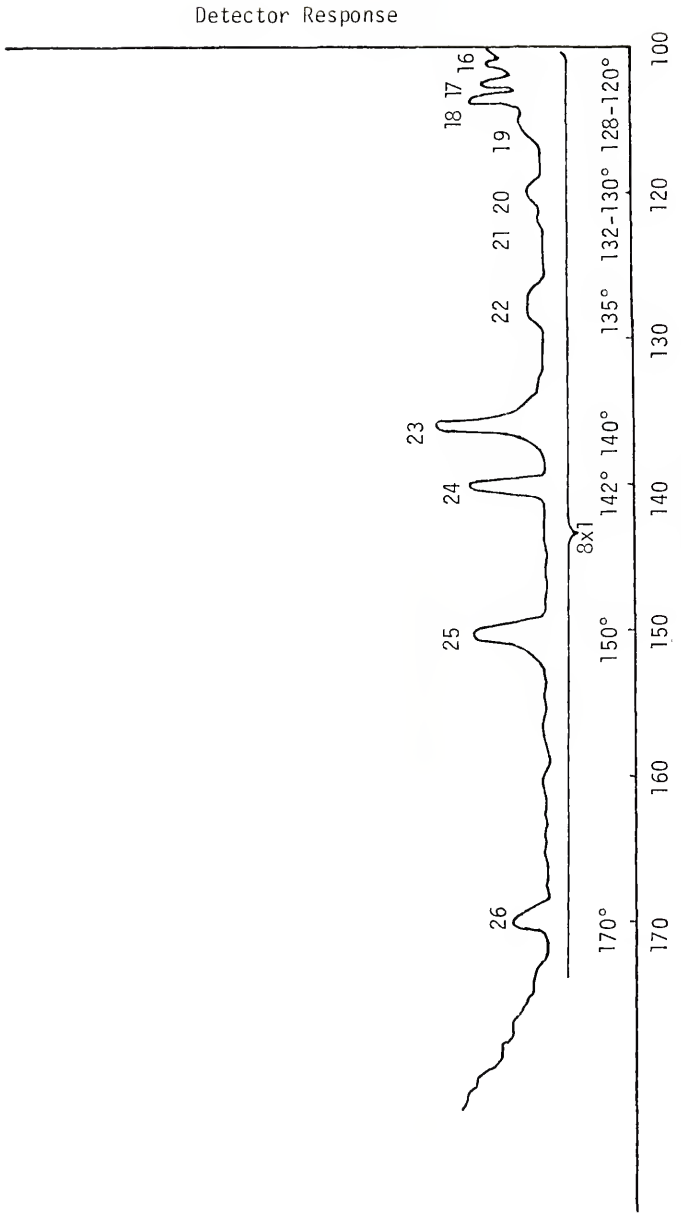

Fig. 15c continued

Table 2

Products in Spark Discharge of Ethyl Bromide

Organic Compounds[a]	Boiling Points (°C)[b]	Method of Identification[c]
CH_4	-161.5	1,2
C_2H_6	- 88.6	1,2
C_2H_4	-103.7	1,2
C_2H_2	- 84	1,2
C_3H_8	- 42.1	1,2
C_4H_{10}	- 0.5	1,2
CH_3Br	3.5	1,2
C_2H_3Br	15.8	1,2
C_2H_5Br	38.4	1,2
$2\text{-}C_3H_7Br$	59.4	1
$1\text{-}C_3H_7Br$	71.0	1
$2\text{-}C_4H_9Br$	91.3	1
$1,1\text{-}C_2H_2Br_2$	92[d]	2
CH_2Br_2	97	1,2
$1\text{-}C_4H_9Br$	101.6	1
$1,1\text{-}C_2H_4Br_2$	108-10	1,2
trans-$1,2\text{-}C_2H_2Br_2$	108	1,2

Table 2 (continued)

Organic Compounds[a]	Boiling Points (°C)[b]	Method of Identification[c]
cis-1,2-$C_2H_2Br_2$	112.5[e]	1,2
1,2-$C_2H_4Br_2$	131.7	1,2
C_3-dibrominated at 120°C		3
1,2-$C_3H_6Br_2$	141.6	1
$CHBr_3$	149.6	1,2
C_3 or C_4 brominated at 128°C		3
meso-2,3-$C_4H_8Br_2$	157.4[f]	1
1,3-$C_3H_6Br_2$ and/or *racemic*-2,3-$C_4H_8Br_2$	167.3/160.6[f]	1
1,3-$C_4H_8Br_2$	174-5	1
C_2HBr_3	163-4	1,2
C_3 or C_4 brominated at 140°C		3
1,1,2-$C_2H_3Br_3$	188.9[g]	1,2
1,4-$C_4H_8Br_2$	197-8	1
Unknown at 170°C		

[a]Methane through acetylene were separated under the conditions described in Fig. 15 a and b, while the remaining products were separated according to the conditions in Fig. 15c

[b]Boiling point data are from reference (49) unless otherwise indicated.

[c]Numbers represent: 1-Mass spectral cracking pattern.
2-Comparison of gas chromatographic retention times with standard samples.
3-Gas chromatographic retention time and boiling point data--see Sec. III-A.

Table 2 (continued)

[d]Reference (50).

[e]Reference (51).

[f]Reference (52).

[g]Reference (53).

retention times since their yields were too small to be amenable to mass spectrometric analysis. The list of products identified in the spark discharge is given in Table 2. Not all of these products appeared in the radiolysis, for instance, *trans*-1,2-dibromoethylene and tribromoethylene were not observed.

Mass spectral tables for the brominated compounds appearing in the radiolysis are collected together for convenience at the end of this section. Air and water background has been subtracted out of the spectra. The bleeding of the methyl silicone column contributed a number of minor peaks that did not correspond to any hydrocarbon fragments in this system such as 45,47, 90 and 208 as well as several that did correspond such as 92, 93, 107 and 121. The former type of peak has also been omitted from the spectra. These contaminants were only minor, less than 1% of the base peak, and could be observed to grow during temperature programming of the column.

The mass spectra of brominated compounds exhibit several distinguishing features. The most prominent one arises from the existence of two bromine isotopes which are two mass units apart and in approximately equal abundance. Application of the binomial expansion to the natural abundance of the two isotopes allows their contribution to a compound to be estimated (54). Furthermore, the molecular C_1 and C_2 brominated

ions are quite stable and their presence in the spectrum immediately identifies the compound.

The following discussion will consider the mass spectrum of each compound (Tables 3, 4, and 5) in the order that it elutes from the gas chromatograph column (Fig. 15) into the mass spectrometer.

Peak No. 6, CH_3Br: Peaks 96 and 94 clearly correspond to the molecular ion. Loss of Br, HBr and H_2Br produces the peaks 15, 14 and 13. A comparison of the relative intensities of the CH_3^+, CH_2^+ and CH^+ fragments with those of the Br^+, HBr^+ and H_2Br^+ fragments indicates that during bond fission the ionization of the hydrocarbon fragment is more important relative to the complementary bromine fragment, presumably due to the greater electron affinity of the Br atom. With the exception of the large 93 peak whose origin is partially in doubt, the remaining fragments agree with the methyl bromide assignment.

Peak No. 7, C_2H_3Br: Peaks 106 and 108 correspond to the molecular ion. Loss of Br, HBr and H_2Br leaves relatively intense 27, 26 and 25 peaks. The CBr^+ fragment corresponds to a C-C fission. The mass spectrum is that of vinyl bromide.

Peak No. 8, C_2H_5Br: The peak is the parent compound, ethyl bromide.

Peak No. 11, CH_2Br_2: The molecular ion identifies the compound as methylene bromide. Supportive evidence is provided by the CH_2Br^+, CH^+ and CH_2^+ ions resulting from the loss of Br, HBr_2 and Br_2. In general, the loss of HBr_2 rather than Br_2 is more probable in the heavier di- and tri-brominated compounds. The relative abundances of the three peaks 176: 174: 172 are in reasonable agreement with the expected 1:2:1 ratio considering that the amount of sample eluting from the column is continuously changing during the mass spectral scans.

Peak No. 13, 1,1-$C_2H_4Br_2$: Mass peaks 190, 188 and 186 correspond to the empirical formula $C_2H_4Br_2$. The presence of the $CHBr_2^+$ ion as mass numbers 175, 173 and 171 and the absence or at least insignificant intensity of the CH_2Br^+ fragments at 92 and 94 establishes the compound as 1,1-dibromoethane rather than 1,2-dibromoethane.

Peak No. 14, *cis*-1,2-$C_2H_2Br_2$: The mass spectrum corresponds to a compound with the empirical formula $C_2H_2Br_2$. The retention time data indicate the compound to be *cis*-1,2-dibromoethylene rather than *trans*-1,2-dibromoethylene or 1,1-dibromoethylene.

Peak No. 15, 1,2-$C_2H_4Br_2$: Absence of peaks at 171, 173 and 175 and comparison with the mass spectrum of Peak No. 13 identifies the compound as 1,2-dibromoethane.

Peak No. 19, $CHBr_3$: The ratio of the relative intensities and mass numbers of the peaks at 256, 254, 252 and 250 corresponds to $CHBr_3$. Loss of Br, HBr_2 and Br_2 yields the $CHBr_2^+$, CBr^+ and $CHBr^+$ fragments.

Peak No. 24, 1,1,2-$C_2H_3Br_3$: The largest mass numbers at 270, 268, 266 and 264 identify $C_2H_3Br_3^+$. Loss of Br and HBr_2 results in the formation of the $C_2H_3Br_2^+$ and $C_2H_2Br^+$ ions and C-C bond rupture yields the $CHBr_2^+$ fragment.

Four minor compounds which were never identified appeared in the radiolysis. These correspond to the peak numbers 16, 18, 23 and 26 in Fig. 15. The position of these peaks in the gas chromatogram reveals some information about them. The OV-101 column separates a homologous series of compounds by their boiling points (Table 2), and for a given number of carbon and bromine atoms the most unsaturated compound elutes first. Peak No. 16 occurs before the simplest tribrominated compound, $CHBr_3$, but after all the dibrominated C_2 compounds. Furthermore, it elutes before 1,2-$C_3H_6Br_2$ whose boiling point is 141.6°C. The compound may be 1,1-$C_3H_6Br_2$ which boils at 130°C or an unsaturated dibrominated C_3 compound. Peak No. 18 is bracketed between the two highest boiling saturated dibrominated C_3 compounds, 1,2-$C_3H_6Br_2$ and 1,3-$C_3H_6Br_2$ so it is probably either 1,3-$C_3H_4Br_2$ or a dibrominated C_4 compound. Peak No. 23 may be a tribrominated C_3 or C_4 compound having a boiling point somewhere between C_2HBr_3 (Table 2) which boils at 163-4°C and 1,1,2-$C_2H_3Br_3$ which boils at 188-9°C. Peak No. 26 must be a compound with a boiling point

Table 3

Mass Spectra of Ethyl Bromide Spark Discharge
Product Nos. 6, 7 and 8

m/e	Assigned Formulas[b]	Relative Intensities[a] No. 6	No. 7	No. 8
12	C	2.08	0.72	0.35
13	CH	4.33	1.38	0,92
14	CH_2	9.03	1.81	0,76
15	CH_3	78.52		2,57
24	C_2		2.88	1.38
25	C_2H		13,73	7.23
26	C_2H_2		32.18	41.52
27	C_2H_3		100.00	99.97
28	C_2H_4			12.48
29	C_2H_5			100.00
79	Br	29.15	14.09	15.13
81	^{81}Br	28.31	13.70	16.32
91	CBr	10.49	2.26	1.52
92	CHBr	4.08		
93	$CH_2Br, C^{81}Br$	43.38	1.74	5.85
94	$CH_3Br, CH^{81}Br$	100.00		
95	$CH_2{}^{81}Br$			3.72
96	$CH_3{}^{81}Br$	87.93		
103	C_2Br		0.92	
104	C_2HBr		1,87	0,82
106	$C_2H_3Br, C_2H^{81}Br$		37.36	1,19

Table 3 (continued)

m/e	Assigned Formulas[b]	Relative Intensities[a] No. 6	No. 7	No.8
108	C_2H_5Br, $C_2H_3{}^{81}Br$		31.79	50.06
110	$C_2H_5{}^{81}Br$			44.39

[a]Background has been subtracted out of the mass spectra.

[b]BR means ^{79}Br.

Table 4

Mass Spectra of Ethyl Bromide Spark Discharge
Product Nos. 11, 13, 14 and 15

m/e	Assigned Formulas[b]	Relative Intensities[a] No. 11	No. 13	No. 14	No. 15
12	C	1.42			0.41
13	CH	4.69			0.80
14	CH_2	9.19	0.29	1.11	1.92
15	CH_3				0.32
24	C_2			4.57	1.08
25	C_2H		5.50	22.11	6.51
26	C_2H_2	1.75	27.22	59.12	36.89
27	C_2H_3	3.42	100.00	1.01	96.98
28	C_2H_4		3.32		8.18
39	C_3H_3	2.60			
41	C_3H_5	6.78			
79	Br	48.16	21.20	40.02	22.11
81	^{81}Br	45.39	20.97	38.52	23.83
91	CBr	21.26	1.72	3.99	5.64
92	CHBr			2.28	
93	$CH_2Br, C^{81}Br$	100.00	0.88	4.71	14.79
94	$CH^{81}Br$			1.53	
95	$CH_2{}^{81}Br$	67.24			6.95
104	C_2HBr		2.67		
105	$C_2H_2Br, C_2{}^{81}Br$		3.34	100.00	44.32
107	$C_2H_4Br, C_2H_2{}^{81}Br$		64.46	50.49	80.02

Table 4 (continued)

m/e	Assigned Formulas[b]	Relative Intensities[a] No. 11	No. 13	No. 14	No. 15
109	$C_2H_4{}^{81}Br$		55.98		100.00
158	Br_2	2.60		5.04	1.06
160	$Br^{81}Br$	4.44	1.98	9.35	1.76
162	$^{81}Br_2$			3.99	
171	$CHBr_2$		1.90		
172	CH_2Br_2,$CBr^{81}Br$	46.56			
173	$CHBr^{81}Br$		3.07		
174	$CH_2Br^{81}Br$,$C^{81}Br_2$	80.90			
175	$CH^{81}Br_2$		1.37		
176	$CH_2{}^{81}Br_2$	36.52			
184	$C_2H_2Br_2$,$C_2Br^{81}Br$			35.98	
186	$C_2H_4Br_2$,$C_2H_2Br^{81}Br$, $C_2{}^{81}Br_2$		11.04	61.48	7.55
188	$C_2H_4Br^{81}Br$,$C_2H_2{}^{81}Br_2$		18.55	29.30	12.15
190	$C_2H_4{}^{81}Br_2$		8.62		5.72

[a] Background has been subtracted out of the mass spectra.

[b] Br means ^{79}Br.

Table 5

Mass Spectra of Ethyl Bromide Spark Discharge
Product Nos. 19 and 24

m/e	Assigned Formulas[b]	Relative Intensities[a] No. 19	No. 24
12	C	3.56	0.87
13	CH	9.20	1.67
14	CH_2		2.29
24	C_2		2.61
25	C_2H		17.99
26	C_2H_2		73.19
27	C_2H_3		67.70
79	Br	67.31	43.59
81	^{81}Br	62.73	43.65
91	CBr	59.68	6.06
92	CHBr	16.04	
93	$CH_2Br, C^{81}Br$	51.16	8.70
94	$CH_3Br, CH^{81}Br$	18.01	
105	$C_2H_2Br, C_2{}^{81}Br$		100.00
107	$C_2H_4Br, C_2H_2{}^{81}Br$		34.75
158	BrBr	5.03	
160	$Br^{81}Br$	6.61	8.94
171	$CHBr_2$	62.71	1.97
173	$CHBr^{81}Br$	100.00	3.11
175	$CH^{81}Br_2$	46.47	1.43
185	$C_2H_3Br_2, C_2HBr^{81}Br$		85.21

Table 5 (continued)

m/e	Assigned Formulas[b]	Relative Intensities[a] No. 19	No. 24
187	$C_2H_3Br^{81}Br, C_2H^{81}Br_2$		37.83
189	$C_2H_3{}^{81}Br_2$		39.10
250	$CHBr_3$	8.87	
252	$CHBr_2{}^{81}Br$	13.78	
254	$CHBr^{81}Br_2$	13.10	
256	$CH^{81}Br_3$	3.90	
264	$C_2H_3Br_3, C_2HBr_2{}^{81}Br$		4.50
266	$C_2H_3Br_2{}^{81}Br, C_2HBr^{81}Br_2$		8.31
268	$C_2H_3Br^{81}Br_2, C_2H^{81}Br_3$		7.93
270	$C_2H_3{}^{81}Br_3$		2.19

[a] Background has been subtracted out of the mass spectra.

[b] Br means ^{79}Br.

above 200°C as it elutes 20°C after 1,4-$C_4H_8Br_2$, which boils at 197-8°C. Attention should also be drawn to Peak No. 21 whose identification is somewhat ambiguous as its retention time coincides with that of 1,3-$C_3H_6Br_2$ and *racemic*-2,3-$C_4H_8Br_2$. As with the other unknown compounds, it is of minor importance.

All of the compounds observed in the radiolysis occur in the photolysis except Peaks No. 4, 10, 11, 12, 14, 16 and 17. These include C_2H_2, 2-C_4H_9Br, CH_2Br_2, 1-C_4H_9Br, *cis*-1,2-$C_2H_2Br_2$, an unidentified C_3 dibrominated compound and 1,2-$C_3H_6Br_2$.

Compounds that may have eluted on the tail of the ethyl bromide peak, for example 2-C_3H_7Br, would have been obscured.

B. Quantitative Determination of Radiolysis Products

The radiolysis of ethyl bromide was carried out at room temperature over the absorbed dose range of 0.49×10^{20} to 6.35×10^{20} e.v./gram corresponding to the period from 3 to 36 hours. All samples were irradiated at 100 torr except in the case of samples intended for HBr determination, where the pressure was 300 torr. At maximum dosage the amount of ethyl bromide consumed was less than 1%.

Table 6 presents the G values, the number of molecules formed (or consumed) per 100 e.v. absorbed by the system, for the major products formed in the radiolysis. The products are listed according to the shape of their dose-yield plots for reasons discussed in Sec. IV-D. The G values were obtained by the method of least squares. The major product yields are plotted as a function of dose in Figs. 16 through 23 at the end of this section.

Table 6

G Values for Major and Semimajor Radiolysis Products from Ethyl Bromide Vapor at 100 Torr Grouped by Shape of Dose-Yield Plots in the Pure System

Product[a]	Pure System				O_2 Scavenged System[b]			
	Absorbed dose/gram x 10^{-20}				Absorbed dose/gram x 10^{-20}			
	0-0.5	1.0-1.5	3.5-4.0	4.5-5.0	0-0.5	1.0-1.5	3.5-4.0	4.5-5.0
Convex upward								
HBr[c]	≃6.02	3.89	0	0	4.89	4.89	4.89	4.89
Br_2	0	0	0	0	2.4	2.4	0.12	(d)
C_2H_4	0.78	2.17	2.07	0.86	0.78	0.78	0	(d)
C_2H_2	0.16	0.31	0.31	0.13	0.13	≃0.27	0.33	(d)
Concave upward								
CH_4	0.0831	0.0831	0.26	0.26	0.030	0,030	0.06	(d)
CH_3Br	0.080	0.080	0.24	0.24	0.32	≃0.32	1.30	1.30
C_2H_3Br	0.32	0.32	0.75	0.75	0	0	0	0

1,1-$C_2H_4Br_2$	0.88	0.88	≃1.66	0.18	0.028	0.028	0.31	0.31
1,2-$C_2H_4Br_2$	0.12	0.12	0.31	0.31	0.56	≃0.56	1.22	1.22
$CHBr_3$	(e)	0.0078	0.0078	0.03	(e)	0.0034	0.0034	0.02
Linear								
H_2	1.39	1.39	1.39	1.39	1.38	1.38	1.38	1.38
C_2H_6	2.70	2.70	2.70	2.70	0.31	0.31	0.31	0.31

[a]The dose-yield plots for the listed products are found in Figs. 16 through 23. The G values for the minor radiolysis products are given in Table 7.

[b]Oxygen comprised 5% of the total pressure except in the case of samples intended for HBr where it was 12%.

[c]Irradiated ethyl bromide was at 300 torr.

[d]No data points were taken in this absorbed dose regime.

[e]The compound was not detected.

Note: The uncertainty in the G values listed in this table is about 10%.

Hydrogen bromide: HBr production for the pure and scavenged systems is shown in Fig. 16. The initial G value, 6.02, for the pure system may be anomolous because of the difficulties in measuring low HBr concentrations. Discounting this value, the plots show that within the statistical error, the G value is comparable for the oxygenated system, about 4.9 molecules/100 e.v., as compared with about 3.9 molecules/100 e.v. for the unscavenged system. In the scavenged system, the production of HBr varies linearly with dose over the entire dose range measured, extending to 6.5×10^{20} e.v./gram. By contrast, in the pure system HBr production reaches a steady state at approximately 1.7×10^{20} e.v./gram. Beyond that absorbed dose, the net rate of production of HBr decreases to zero with increasing dose.

The G value of HBr given above for the oxygen scavenged system has been corrected for the contribution of bromine in the HBr determination (Sec. II-H-4) using a simple equilibrium calculation. The calculation shows that approximately 15.6% of the bromide yield was due to bromine under an absorbed dose of 1.5×10^{20} e.v./gram. After this dose, the bromine production plateaus (Fig. 17) and contributes less as the hydrogen bromide formation increases linearly with dose over the remaining dose range covered. Before the correction, the G value for hydrogen bromide was 4.95 molecules/100 e.v.

Although not included on the plots, preliminary data indicated the possibility of post-irradiation effects. Specifically, the HBr yield from samples analyzed a few days after irradiation were lower than the corresponding ones obtained from samples analyzed within

2 hours after irradiation. The same effect was observed in the lower yields of unsaturated hydrocarbon products. The precision of the data in subsequent experiments was improved by immersing the vessel immediately after irradiation into a Dewar of liquid nitrogen and analyzing the contents of the vessel as soon as experimentally possible.

Bromine: Although no bromine is observed in the radiolysis of pure ethyl bromide, Fig. 17 shows that a substantial amount of bromine is formed in the oxygen scavenged system. The form of the plot is similar to that for HBr production in the unscavenged system (Fig. 16) in that bromine is produced linearly with dose up to approximately 1.5×10^{20} e.v./gram and then levels off to a constant value. The initial G value estimated from the initial slope of the curve is 2.4 molecules/100 e.v. As alluded to in Sec. II-H-5, the uncertainty of this value may be as large as 20%.

Ethylene: Fig. 20 also shows that ethylene production is non-linear in the total dose range extending to 5.8×10^{20} e.v./gram. In the pure system after the induction period, the 100 e.v. ethylene yield is constant from about 0.8×10^{20} to 3.8×10^{20} e.v./gram. Above the latter dose, the net rate of ethylene production tends toward zero. The linear portion of the curve gives a G value of 2.17. With added O_2 there is no induction period and the initial G value for ethylene production is reduced to 0.78 molecules/100 e.v. Beyond the radiation dose of 3.2×10^{20} e.v./gram, the net G value for the production of additional ethylene is zero.

Acetylene: Acetylene's dose-yield plot in Fig. 18 shows a behavior similar to the curve for ethylene in Fig. 20. After a short induction period, the acetylene production is linear between 0.5 x 10^{20} and 3.9 x 10^{20} e.v./gram and then on larger dose gradually becomes constant. The G value for the linear portion of the curve was 0.31. The addition of 5 mole % O_2 before irradiation essentially leaves the G value for the production of acetylene unchanged.

Methane: Fig. 18 shows that methane production in both the pure and oxygen scavenged systems exhibit a well-defined induction period up to a dose of approximately 1.5 x 10^{20} e.v./gram. The corresponding G values for this period are constant, about 0.08 molecules/100 e.v. in the pure system as compared with about 0.03 molecules/100 e.v. in the oxygenated system. After this induction period, methane is produced linearly with dose over the remaining dose range covered. The slope of the dose-yield plot after this period determines a G value of 0.26 in the unscavenged system and 0.06 in the scavenged system.

Methyl bromide: The methyl bromide plots in Fig. 21 resemble those of methane. In the unscavenged system the G value for the induction period is about 0.08 up to a dose of 1.3 x 10^{20} e.v./gram. Subsequently, the G value increases sharply to 0.24 up to a dose of 5.2 x 10^{20} e.v./gram. The effect of added oxygen on the production of methyl bromide is to enhance both the low-dose and the high-dose 100 e.v. yields to 0.32 and 1.30 respectively.

Vinyl bromide: In Fig. 21 is shown the unscavenged vinyl bromide production as a function of absorbed dose. The presence of

an induction period can be seen. The corresponding G value for this period is 0.32 molecules/100 e.v. up to a dose of 1.9×10^{20} e.v./gram. Thereafter, the G value increases to 0.75 for a dose extending to 5.2×10^{20} e.v./gram. The amount of vinyl bromide in the oxygen scavenged system is one half of that in the pure system at 1×10^{20} e.v./gram. After this dose, however, it is not observed.

1,1-Dibromoethane: Fig. 22 shows the production of 1,1-$C_2H_4Br_2$ in the dose range from 0 to 5.8×10^{20} e.v./gram. 1,1-Dibromoethane is produced with an induction-period G value of 0.88 between the dose of 0 and 1.3×10^{20} e.v./gram. The G value on prolonged irradiation increases to 1.66 for radiation doses up to 3.5×10^{20} e.v./gram. After this dose, the yield of 1,1-$C_2H_4Br_2$ tends to decrease. In the presence of oxygen, the G value for the induction period is reduced to about 0.03 while the G value for prolonged dose decreases to 0.31.

1,2-Dibromoethane: 1,2-$C_2H_4Br_2$ is produced with an induction-period G value of 0.12 up to a dose of 1.5×10^{20} e.v./gram. Thereafter, the G value is 0.31 over the dose range measured as shown in Fig. 17. When oxygen is added to the system, the low-dose and the high-dose 100 e.v. yields increase to 0.56 and 1.22 respectively.

Bromoform: As shown in Fig. 23 the low-dose 100 e.v. bromoform yields in the pure and scavenged systems are 0.0078 and 0.0034 respectively in the dose range between 1.3×10^{20} and 3.8×10^{20} e.v./gram. The high-dose G values are 0.03 and 0.02 respectively. Extrapolation of the linear portion of the long-dose segment intersects the dose axis at 3.2×10^{20} e.v./gram in both the pure and oxygen scavenged systems.

Hydrogen: Fig. 16 also indicates that the 100 e.v. hydrogen yields in ethyl bromide with and without 5 mole % O_2 added are independent of dose and nearly the same, about 1.4, up to a radiation dose of 6.1×10^{20} e.v./gram.

Ethane: Results of the ethane measurements as a function of radiation dose are shown in Fig. 19. The 100 e.v. ethane yield is constant over the investigated region extending to about 4.6×10^{20} e.v./gram. In the oxygen-free system, the G value for ethane production is 2.70 which is approximately 90-fold larger than in the presence of the free radical scavenger oxygen.

Table 7 presents the measured G values for the minor products formed in the radiolysis. Each product is discussed below in the order that it elutes from the gas chromatographic column (Fig. 15).

N-butane: The data for the production of butane as a function of absorbed dose are rather scattered, but the trend indicates that butane is formed rapidly at the beginning and then levels off to a constant value at a dose of 1.5×10^{20} e.v./gram extending to 5.8×10^{20} e.v./gram. The initial slope of the plot corresponds to a G value of 0.002. In the scavenged system, oxygen effectively blocks the butane production.

N-bromopropane: The data for this compound are rather scattered not only because it was in trace amounts, but also because it eluted on the tail of the ethyl bromide peak. In the pure system, the total yield of n-bromopropane increases to a maximum at an absorbed dose of 4.0×10^{20} e.v./gram and then gradually decreases. Its initial

Table 7

G Values of Minor Radiolysis Products
from Ethyl Bromide Vapor at 100 Torr

Product[a]	Pure System		O_2 Scavenged System[b]	
	Initial	Post-Induction Period	Initial	Post-Induction Period
C_4H_{10}	0.002	0.002	0	0
1-C_3H_7Br	≃0.0008	≃0.0005	≃0.002	≃-0.0002
2-C_4H_9Br	0.0012	0.0012	0	0
CH_2Br_2	0.0072	0.0072	0.0040	0.0040
1-C_4H_9Br	0.0018	0.0018	0.0006	0.0006
cis-1,2-$C_2H_2Br_2$	0.0036	0.0036	0.008	0.008
C_3 dibromated at 120°C	0.002[c]	0.002[c]	0.0006[c]	0.0006[c]
1,2-$C_3H_6Br_2$	0.001	0.006	0.0006	0.003
C_3 or C_4 brominated at 128°C	0.0004[d]	0.0004[d]	0.0004[d]	0.0004[d]
meso-2,3-$C_4H_8Br_2$	0.001	0.001	0.0006	0.0006
1,3-$C_3H_6Br_2$ and/or *racemic*-2,3-$C_4H_8Br_2$	0.0006[e]	0.0006[e]	0.005[e]	0.005[e]
1,3-$C_4H_8Br_2$	0.0012	0.0012	0	0
C_3 or C_4 brominated at 140°C	0.006[d]	≃0[d]	0.005[d]	≃0[d]
1,1,2-$C_2H_3Br_3$	0.007	0.007	0.008	0.008
1,4-$C_4H_8Br_2$	0.003	0.008	0.001	0.007
Unknown at 170°C	0.002[d]	0.002[d]	0.005[d]	0.005[d]

Table 7 (continued)

[a]Table 6 presents the G values for the major products.

[b]Oxygen comprised 5% of the total pressure.

[c]The G value is based on the molar response of the flame ionization detector to 1,2-$C_3H_6Br_2$.

[d]The G value is based on the molar response of the flame ionization detector to 1,3-$C_4H_8Br_2$.

[e]The G value is based on the molar response of the flame ionization detector to *racemic*-2,3-$C_4H_8Br_2$.

Note: The uncertainty in the G values listed in this table is about 15%.

G value is approximately 0.0008. When oxygen is added prior to radiolysis, the form of the curve remains essentially unchanged except that the maximum value shifts to a dose of 2.1 x 10^{20}e.v./gram. In this case, the initial G value is about 0.002.

2-Bromobutane: The 2-bromobutane 100 e.v. yield, 0.0012, is nearly independent of dose over the entire dose range extending to 5.3 x 10^{20}e.v./gram. The dose-yield plot extrapolates through the origin. Addition of oxygen prior to radiolysis blocks the production of 2-bromobutane.

Dibromomethane: The amount of methylene bromide produced is a linear function of dose from 1.0 x 10^{20} to 4.0 x 10^{20}e.v./gram with a corresponding G value of 0.0072. After this dose, the net G value for the production of additional CH_2Br_2 is zero. The effect of oxygen is to reduce the initial 100 e.v, yield to 0.0042. As with the pure system, the net rate of production of methylene bromide is zero beyond 4.0 x 10^{20}e.v./gram. Extrapolation of the linear portion of the plots for both the pure and oxygenated systems intersects the dose axis at about 0.7 x 10^{20}e.v./gram.

N-bromobutane: The amount of 1-bromobutane in both the oxygen-free and scavenged system is a linear function of absorbed dose extending to 5.2 x 10^{20}e.v./gram. The G value for the unscavenged system is 0.0018 molecules/100 e.v. and for the scavenged system is 0.0006 molecules/100 e.v.

cis-1,2-dibromoethylene: The *cis*-1,2-$C_2H_2Br_2$ 100 e.v, yields in both the pure and oxygen scavenged systems are nearly constant over the dose range from 0 to 5.1 x 10^{20}e.v./gram. In the pure

system, the G value is 0.0036. The effect of oxygen is to increase the initial yield of *cis*-1,2-$C_2H_2Br_2$ to 0.008.

C_3-Dibrominated compound at 120°C: In both the pure and scavenged systems this compound is produced linearly with dose over the dose range from 0 to 5.2 x 10^{20}e.v./gram. The corresponding G values of the compound are 0.002 and 0.0006 respectively, assuming that the molar response of the ionization detector to it is the same as that to 1,2-$C_3H_6Br_2$.

1,2-Dibromopropane: The data for the formation of 1,2-dibromopropane as a function of dose are scattered, but it is evident that 1,2-dibromopropane varies nonlinearly with dose from 0 to 5.2 x 10^{20} e.v./gram in the presence and absence of oxygen. At an absorbed dose between 0 and 3.0 x 10^{20}e.v./gram the G value is 0.001 for the pure system and 0.0006 for the oxygenated system. On longer irradiation, the G value for each case is 0.006 and 0.003 respectively.

C_3 or C_4-Brominated compound at 128°C: The production of this compound is linear with dose between 2.0 x 10^{20} and 5.0 x 10^{20}e.v./gram. Its G value is 0.0004 based on the flame ionization detector's molar response to 1,3-$C_4H_8Br_2$. Extrapolation of the dose-yield plot to zero yield intersects the dose axis at about 1.4 x 10^{20}e.v./gram. Within experimental error, oxygen has no effect on its production.

Meso-2,3-dibromobutane: Because of the size and the broadness of the chromatographic peak of this compound it was difficult to distinguish from background, particularly at low dose. In the pure system, the plot of *meso*-2,3-dibromobutane is based only on 3 points;

however, the dose-yield plot appears to be linear with dose between 2.0×10^{20} and 5.3×10^{20} e.v./gram and extrapolates through the origin. The corresponding G value is 0.001 molecules/100 e.v. When oxygen is added, the plot is still linear and extrapolates through the origin but the G value decreases to 0.0006 molecules/100 e.v.

Racemic-2,3-dibromobutane and/or 1,3-dibromopropane: The data points are too few and scattered to describe the pure system adequately. The G value, 0.0006, in Table 7, is an estimate only. The addition of oxygen accelerates the production of the compound(s), or some oxygenated compound having the same retention time, to a G value of 0.005. This plot is linear with dose between 2.0×10^{20} and 5.1×10^{20} e.v./gram and extrapolates through the origin. The G values given above are based on the molar response of the flame ionization detector to the *racemic* compound.

1,3-Dibromobutane: The 100 e.v. 1,3-dibromobutane yield is nearly constant, about 0.0012, over the dose range from about 1.76×10^{20} to 5.3×10^{20} e.v./gram and extrapolates through the origin. The formation of 1,3-dibromobutane is completely blocked by the free-scavenger oxygen.

C_3 or C_4-Dibrominated compound at 140°C: In the pure system the initial G value of this unidentified compound is 0.006 from an absorbed dose of 1.0×10^{20} to 4.0×10^{20} e.v./gram based on the molar response of the ionization detector to 1,3-dibromobutane. After this dose, the production of the compound decreases rapidly. Extrapolation of the initial dose-yield plot to zero yield intersects the dose axis at about 0.45×10^{20} e.v./gram. The addition of oxygen reduces the G value to 0.005 but leaves the form of the plot unchanged.

1,1,2-Tribromoethane: The results of the measurements are somewhat scattered; however, over the dose range of 1.7×10^{20} to 5.3×10^{20} e.v./gram, the production of 1,1,2-tribromoethane appears linear with dose. The corresponding G value for its formation is 0.007 molecules/100 e.v. in the unscavenged system. The effect of oxygen is to increase the G value to 0.008.

1,4-Dibromobutane: The 1,4-dibromobutane production is a non-linear function of the input energy in the dose range extending to 5.2×10^{20} e.v./gram. In the pure system, its G value is constant, 0.003, between 0 and 1.5×10^{20} e.v./gram and then increases to 0.008 over the rest of the range covered. In the scavenged system, its initial G value is 0.001 up to a dose of 1.8×10^{20} e.v./gram and then on longer irradiation increases to 0.007.

Unknown compound at 170°C: In both the pure and scavenged system, the dose-yield plot of this compound is linear from a dose of 1.0×10^{20} to 5.0×10^{20} e.v./gram and extrapolates at zero yield to 0.6×10^{20} e.v./gram. The G values for the two cases are 0.002 and 0.005 respectively. These G values are based on the response of the flame ionization detector to 1,3-dibromobutane.

Ignoring the negligible contribution of the minor products, the material balance of the products in the pure system can be estimated with the enlistment of Table 6.

$$G_H(-C_2H_5Br) = G(HBr) + 2[G(H_2)+G(C_2H_2)] + 3[G(CH_3Br)+G(C_2H_3Br)] + 4[G(CH_4)+G(C_2H_4)+G(1,1\text{-}C_2H_4Br_2)+G(1,2\text{-}C_2H_4Br_2)] + 6G(C_2H_6)$$

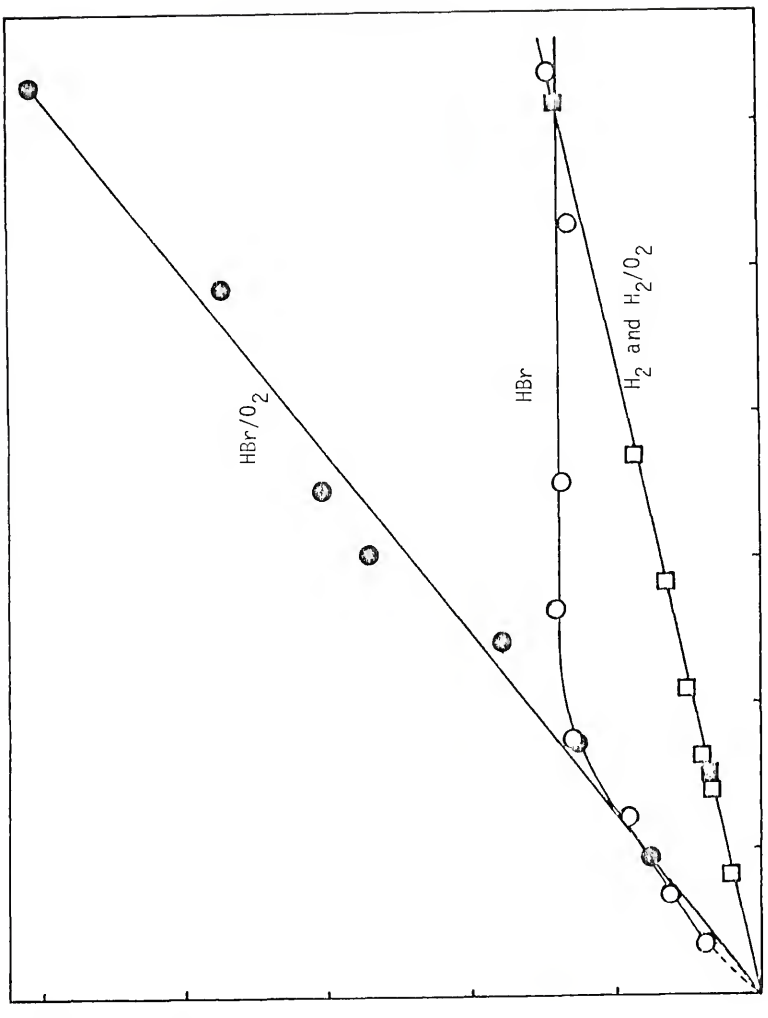

Fig. 16 Production of hydrogen bromide (pure, ○; 12% O_2, ●) and hydrogen (pure, □ ; 5% O_2, ■) as a function of dose.

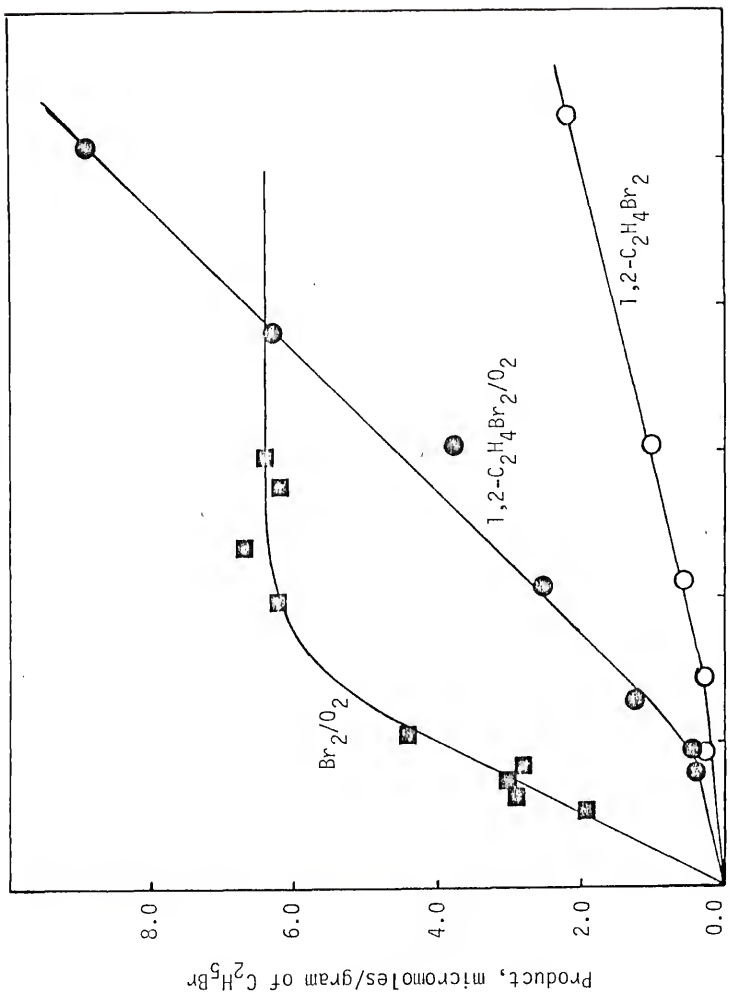

Fig. 17 Production of bromine (5% O_2, ■) and 1,2-dibromoethane (pure, O; 5% O_2, ●) as a function of dose.

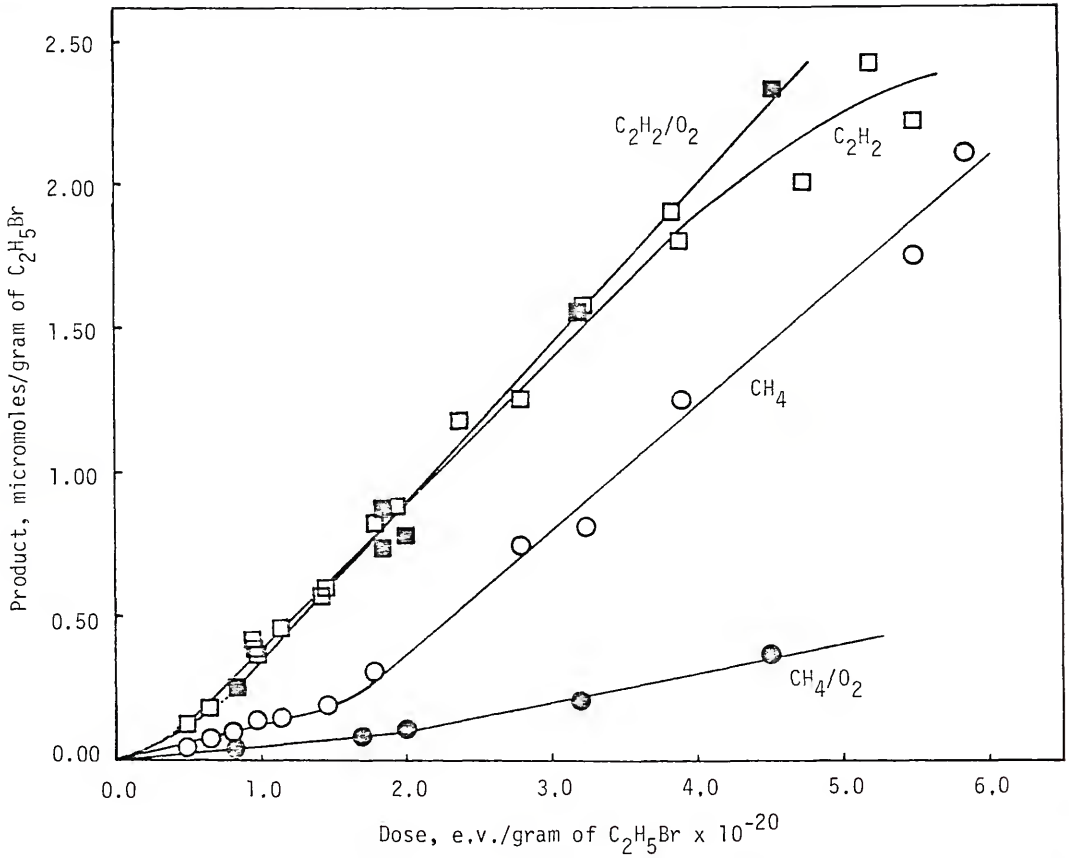

Fig. 18 Production of methane (pure, ○; 5% O_2, ●) and acetylene (pure, □; 5% O_2, ■) as a function of dose.

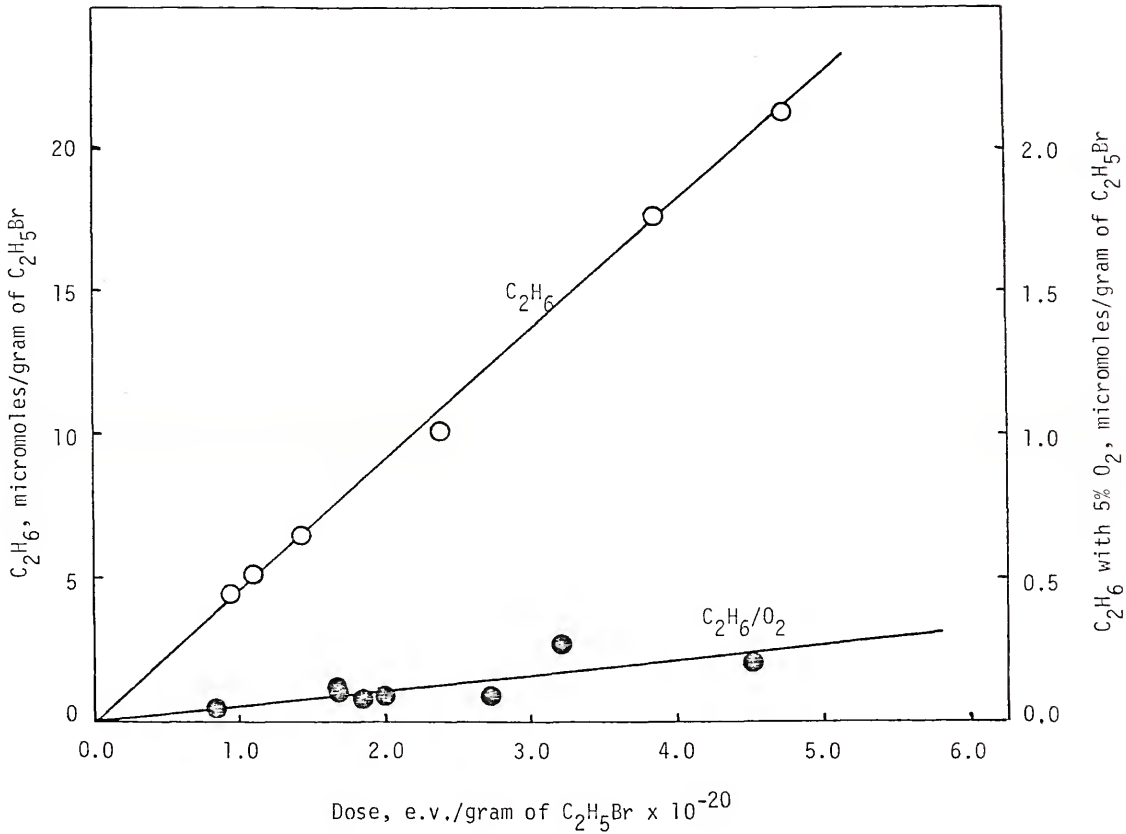

Fig. 19 Production of ethane (pure, ○; 5% O_2, ●) as a function of dose.

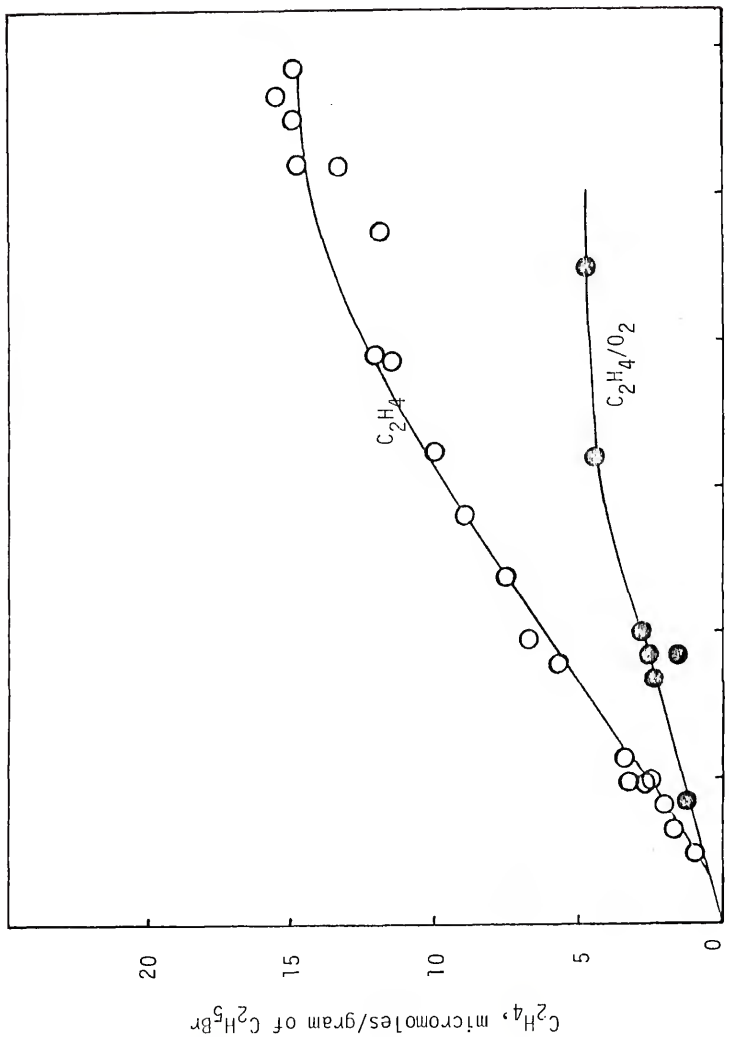

Fig. 20 Production of ethylene (pure, O; 5% O_2, ●) as a function of dose.

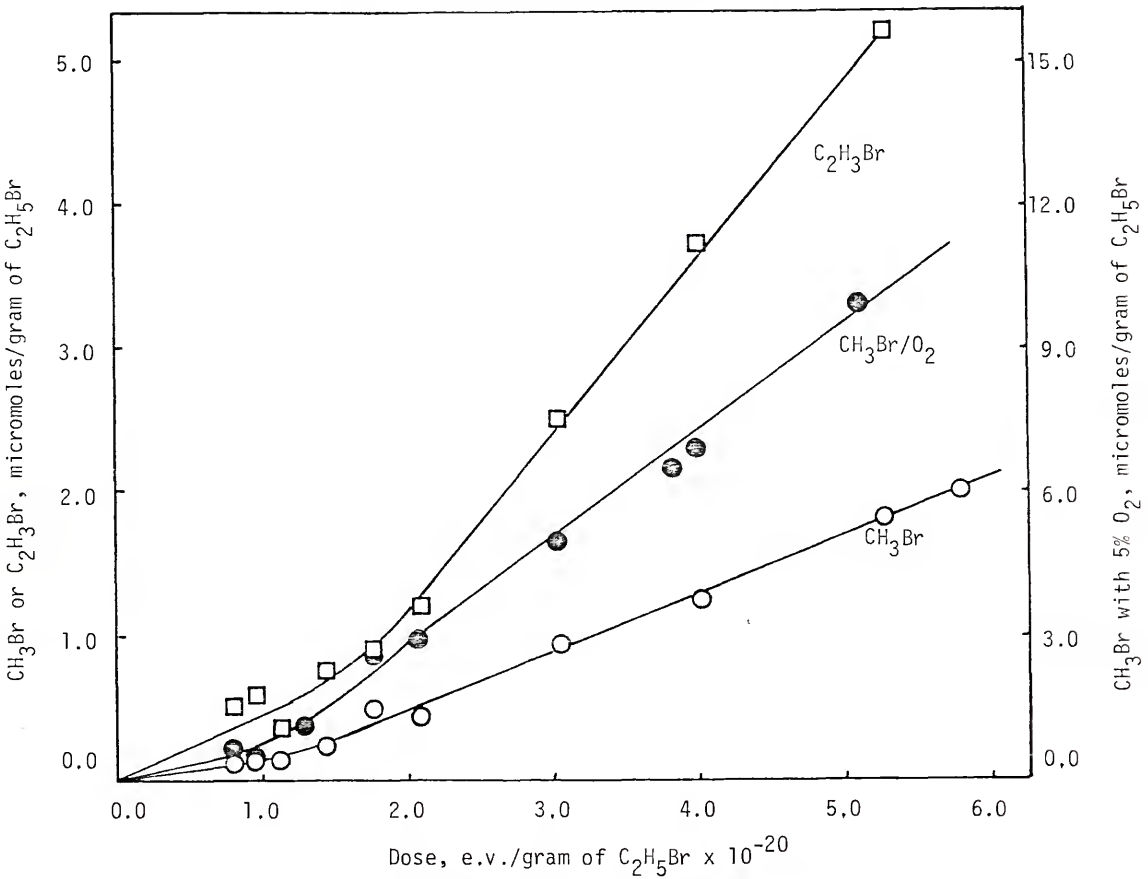

Fig. 21 Production of methyl bromide (pure, ○; 5% O_2, ●) and vinyl bromide (pure, □) as a function of dose.

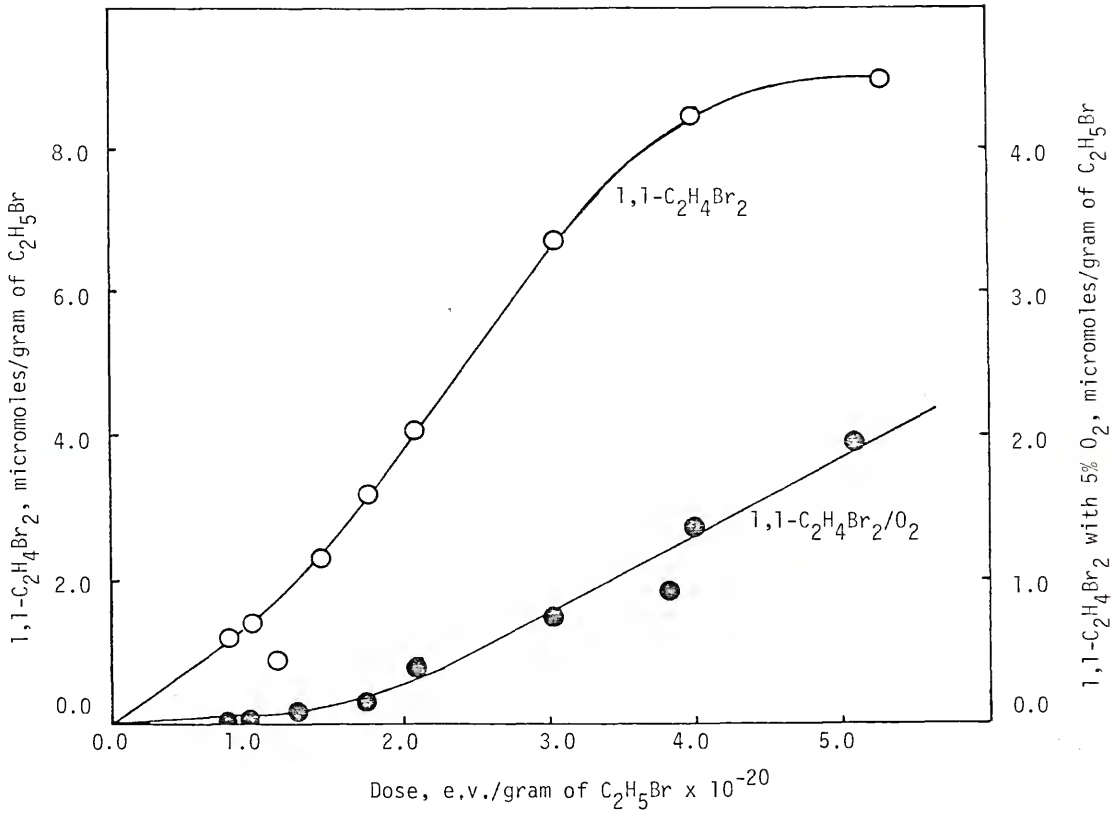

Fig. 22 Production of 1,1-dibromoethane (pure, ○; 5% O_2, ●) as a function of dose.

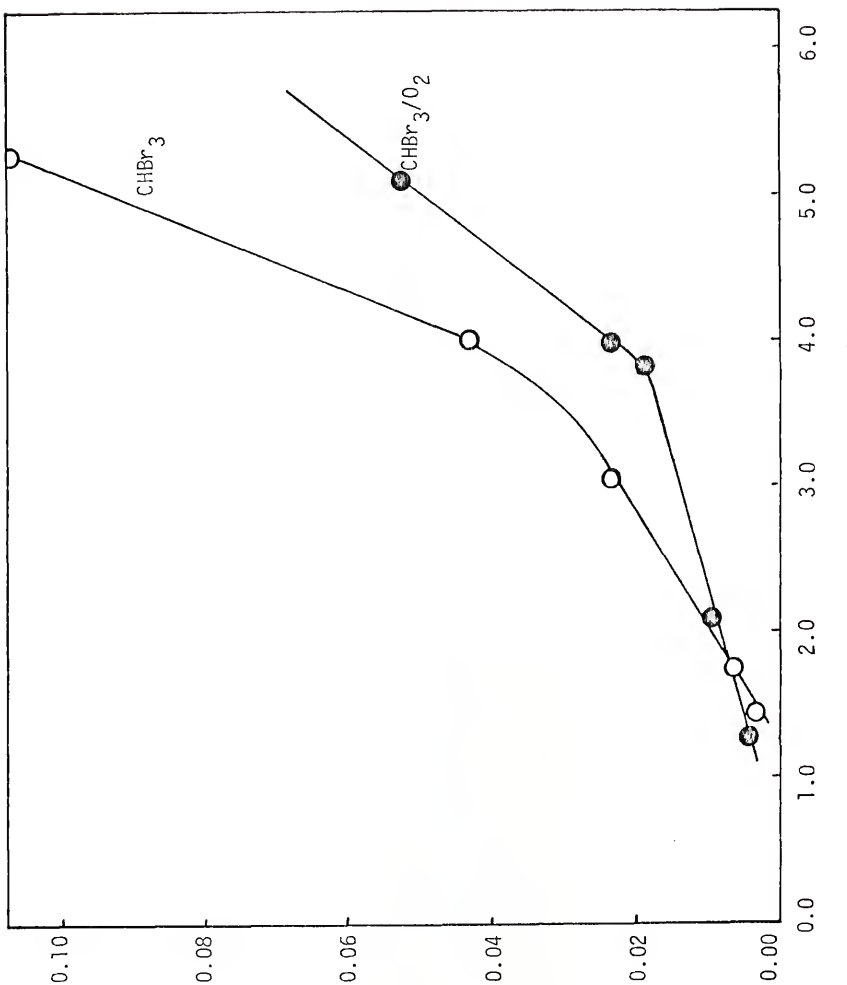

Fig. 23 Production of bromoform (pure, ○; 5% O_2, ●) as a function of dose.

Similar equations for carbon and bromine atoms lead to the ratio C/H/Br equal to 1.75/5.00/0.84 and 2.02/5.00/0.62 within the dose ranges of 1.0×10^{20} to 1.5×10^{20} e.v./gram and 3.0×10^{20} to 3.5×10^{20} e.v./gram respectively.

C. Quantitative Determination of Photolysis Products

The photolysis of ethyl bromide was studied at 100 torr and 23 $\pm$ 1°C using radiation of 253.7 nm emitted by a 15 watt General Electric germicidal lamp for periods between 0.5 to 10 minutes. As discussed in Sec. II-F-2, the number of quanta absorbed per second at this pressure corresponded to $7.7 \pm 0.2 \times 10^{15}$ for the large reaction vessel and $2.7 \pm 0.1 \times 10^{15}$ for the small vessel. At the longest irradiation time, the amount of ethyl bromide consumed was less than 1%.

In the pure photolysis, there are five major products of the decomposition: hydrogen bromide, ethane, ethylene, 1,1-dibromoethane and 1,2-dibromoethane. In the presence of oxygen, bromine is formed in substantial yield. Table 8 presents the summary of quantum yields, the number of molecules formed (or consumed) per quantum of light absorbed, for these major products. For reasons discussed in Sec. IV-B, the products are grouped according to the shape of their dose-yield curves. The quantum yields were calculated using the least squares determined slopes of the curves in Figs. 24 through 30. A brief description of these results follows:

Table 8

Quantum Yields for Major and Semimajor Photolysis Products from Ethyl Bromide Vapor at 100 Torr Grouped by Shape of Dose-Yield Plots in the Pure System

Product[a]	Pure System				O_2 Scavenged System			
	Photolysis time (minutes)				Photolysis time (minutes)			
	0-0.5	1.0-1.5	3.5-4.0	6.0-7.0	0-0.5	1.0-1.5	3.5-4.0	6.0-7.0
Convex upward								
HBr	0.36	0.26	0.13	≈0	0.55	0.47	0.29	0.29
Br_2	0	0	0	0	0.22	0.22	0.19	0.12
C_2H_6	0.40	0.40	0.24	0.24	0.00032	0.00032	0.00032	0.00032
C_2H_4	0.028	0.028	0.017	≈0	0.0081	0.0081	0.0033	0.0032
C_2H_3Br	0.015	0.009	0.0008	-0.004	0	0	0	0
1,1,2-$C_2H_3Br_3$	(b)	0.0027	0.0016	0.0016	0	0	0	0

Concave upward								
$1,1\text{-}C_2H_4Br_2$	0.102	0.102	0.169	0.169	0.0040	0.0040	0.0091	0.0091
$1,2\text{-}C_2H_4Br_2$	0.0012	0.0092	0.014	0.016	0.0073	0.022	0.041	(c)
CH_4	0.00052	0.00052	0.0031	0.0031	0.00010	0.0001	0.00018	0.00018
CH_3Br	(b)	0.00091	0.0024	0.0031	(b)	0.091	0.21	0.21

[a]The dose-yield plots for the listed products are found in Figs. 24 through 30. The quantum yields for the minor photolysis products are given in Table 9.

[b]The compound was not detected.

[c]There are insufficient data in this time regime.

Note: The uncertainty in the quantum yields listed in this table is about 10%.

Hydrogen bromide: Hydrogen bromide data for the pure and scavenged systems are graphically displayed as a function of photolysis time extending to 10 minutes in Fig. 24. In the unscavenged system, the hydrogen bromide yield is nearly constant, 0.36 molecules/quantum, up to a photolysis time of one minute and then gradually decreases to zero by 6.0 minutes. The effect of 5% oxygen is to augment the initial quantum yield to 0.55 molecules/quantum. After about 1.5 minutes, the quantum yield for hydrogen bromide production drops to a constant value of 0.29. As with the radiolysis data, the quantum yield for hydrogen bromide with added oxygen has been corrected for the presence of bromine in the HBr determination (Sec. II-H-4). According to the equilibrium calculations, the bromine contributes about 11.7% of the bromide ion concentration at 1 minute and thereafter slowly increases to 13% at 9 minutes. The uncorrected quantum yield is 0.62 molecules/quantum.

Bromine: No bromine is detected in the pure system. In the oxygen scavenged system, as Fig. 25 shows, the bromine yield is fairly constant, 0.22 molecules/quantum, between a photolysis time of 0 and 1.5 minutes. After this point, the net rate of bromine production decreases with photolysis.

Ethane: As in the radiolysis, ethane is the main product; however, in contrast to the radiolysis, the ethane yield is dependent on the dose as shown in Fig. 26. The quantum yield is 0.40 up to 1.5 minutes and then becomes 0.24 throughout the rest of the close range covered. When 5 mole % oxygen is added prior to irradiation, the

ethane production is independent of dose, although its quantum yield is reduced to 0.1% of its previous value.

Ethylene: The ethylene production shows no induction period in contrast to the radiolysis. Fig. 27 shows that the net rate of ethylene production is constant for the first 1,5 minutes and then tends rather abruptly to zero at approximately 4.5 minutes. In the oxygenated system, ethylene production is effectively blocked but not completely eliminated as in the radiolysis. Specifically, its quantum yield is reduced from 0.028 in the pure system to 0,0081 in the system with added oxygen.

1,1,2-Tribromoethane: The plot for the production of 1,1,2-tribromoethane as a function of photolysis time consists of two linear segments as shown in Fig. 28. The first segment, between 0,5 and 2 minutes, indicates a quantum yield of 0,0027. Extrapolation of this segment to zero yield intersects the time axis at 0.4 minutes. The second segment, extending to 6 minutes, gives a quantum yield of 0.0016. Addition of oxygen prior to photolysis blocks the production of 1,1,2-tribromoethane.

Vinyl bromide and methyl bromide: The resolution of the methyl and vinyl bromide chromatographic peaks in the photolysis was characteristically poor. Quantitative determination was further complicated by the variation in the relative size of their peak areas as a function of photolysis time. At photolysis times less than 2 minutes, vinyl bromide is the dominant peak whereas after 4 minutes, methyl bromide is considerably larger. The combined effects make it difficult to proportion the peak areas between them, especially

since methyl bromide tails substantially. Consequently, there is a rather large uncertainty attached to their respective quantum yields given below.

The behavior of the vinyl bromide production as a function of energy input differs markedly from its counterpart in the radiolysis. Fig. 29 shows that the vinyl bromide yield goes through a maximum at about 4 minutes and then decreases towards zero. The initial quantum yield for its formation is 0.015 ± 0.004. In the oxygen scavenged system, vinyl bromide is only observed at a photolysis time of 0.5 minutes and at a corresponding amount of approximately 0.5 its value in the pure system.

Methyl bromide in the pure system is undetected below 1 minute as shown in Fig. 28. Its dose-yield plot is linear between 1 and 2 minutes with a corresponding quantum yield of 0.0009l; on longer irradiation extending to 8 minutes, the quantum yield increases to 0.0031 ± 0.0008. When 5 mole % oxygen is added, methyl bromide is observed at a photolysis time of 0.5 minutes. The quantum yield of methyl bromide is nearly constant, about 0.09l, between 0.5 and 2 minutes and then on longer doses dramatically increases to 0.21.

1,1-Dibromoethane: Fig. 25 shows that 1,1-dibromoethane exhibits an induction period as in the radiolysis. In the pure system the yield during the induction period is about 0.102 molecules/quantum up to a photolysis time of 1,5 minutes. After this period, the quantum yield for 1,1-dibromoethane production increases to 0.169 over the rest of the dose range measured. With 5 mole % O_2, the induction-period quantum yield is 0,0040; thereafter, the yield is 0.009l molecules/quantum.

1,2-Dibromoethane: Fig. 30 shows the production of 1,2-dibromoethane as a function of photolysis time. In both the pure and oxygenated systems, the quantum yields for the production of 1,2-$C_2H_4Br_2$ increase rather markedly for about the first 4 minutes. After this period, the yields become approximately constant, at 0.015 and 0.041 respectively. Extrapolation of the linear portion of the curve to the time axis in each case indicates an induction period of about 1.6 minutes.

Methane: Results of the methane measurements parallel those in the radiolysis as shown in Fig. 29. After a short induction period, the methane production is linear between approximately 1.75 and 9 minutes. In the unscavenged system, the quantum yield for the induction period is 0.00052 and for longer irradiation is 0.0031. The addition of 5 mole % O_2 before irradiation reduces the methane quantum yield for these periods to 0.00010 and 0.00018 respectively.

A compilation of the quantum yields for the minor products is presented in Table 9. Although these products are easily detected with the flame ionization detector, their quantum yields are small and do not appreciably affect the material balance. The following discussion will deal with these products.

Hydrogen: No hydrogen is detected using either thermal conductivity gas chromatography or the Toepler-McLeod combination. Amounts of hydrogen less than about 0.1 micromoles would be undetectable using these techniques.

Table 9

Quantum Yields of Minor Photolysis Products at 253.7 nm from Ethyl Bromide Vapor at 100 Torr

Product[a]	Pure System		O_2 Scavenged System[b]	
	Initial	Post-Induction Period	Initial	Post-Induction Period
C_4H_{10}	0.0001	0.0000007	0.000008	0.000004
$1\text{-}C_3H_7Br$	0.0002	0.000013	0.00007	≃0
$CHBr_3$	0.00026	0.00026	0	0
C_3 or C_4-brominated at 128°C	≃0.00001[c]	≃0.0002[c]	0	0
meso-$2,3\text{-}C_4H_8Br_2$	0.00001	0.00001	0.00052	0.00052
$1,3\text{-}C_3H_6Br_2$ and/or *racemic*-$2,3\text{-}C_4H_8Br_2$	0.00001	0.00001	0	0
$1,3\text{-}C_4H_8Br_2$	0.0005	0.00003	0	0
C_3 or C_4-brominated at 140°C	0.0003[c]	0.0002[c]	0.0004[c]	0.0004[c]
$1,4\text{-}C_4H_8Br_2$	0.00013	0.00013	0	0
Unknown at 170°C	0.0002[c]	0.0002[c]	0.0002[c]	0.0001[c]

[a]Table 8 presents the quantum yields for the major products.

[b]Oxygen comprised 5% of the total pressure.

[c]The quantum yield is based on the molar response of the flame ionization detector to $1,3\text{-}C_4H_8Br_2$.

Note: The uncertainty in the quantum yields listed in this table is about 15%.

N-butane: Measurements of butane are scattered throughout the entire 8 minute duration of the photolysis experiments, but it appears that the total amount of butane produced increases rapidly with photolysis time and then reaches a nearly constant value, 0.2 nanomoles, after about 1.5 minutes. The initial yield corresponds to 0.0001 molecules/quantum. The effect of oxygen is to reduce the net rate of butane production by a factor of 12.5 and to improve the reproducibility of the data while leaving the form of the curve the same.

N-bromopropane: The initial quantum yield of n-bromopropane is nearly constant, about 0.0002, up to a photolysis time of 1.5 minutes. Although the data are scattered, it appears that after this point the total yield reaches a maximum and then begins to decrease. The effect of oxygen is to reduce the initial quantum yield to 0.00007 and leave the form of the curve unchanged.

Bromoform: Six measurements for bromoform were carried out between 1 and 8 minutes. In the pure system, bromoform is produced linearly as a function of photolysis time and extrapolation of the straight line to zero yield intersects the time axis at 0.5 minutes. No bromoform is detected when oxygen is added prior to photolysis.

C_3 or C_4-Brominated compound at 128°C: The formation of this compound is dependent on the energy input over the range measured, extending to 8 minutes. The initial quantum yield is nearly constant, 0.0001, from 0 to 2 minutes, assuming the same molar response of the ionization detector to 1,3-$C_4H_8Br_2$. Subsequently, the total yield increases from 0.03 nanomoles at 2 minutes to 0.56 nanomoles at 8 minutes. The production of this compound is completely blocked by oxygen.

Meso-2,3-dibromobutane, 1,3-dibromopropane and *racemic*-2,3-dibromobutane: These products in the pure system are all difficult to determine and their quantum yields in Table 9 are estimates only. In the presence of oxygen, only one peak occurs in this region of the chromatogram. This peak has the same retention time as *meso*-2,3-dibromobutane and is observed to increase linearly with photolysis time between 0 and 8 minutes. Based on the molar response of the ionization detector to the *meso*-compound, its quantum yield is 0.00052.

1,3-Dibromobutane: In the pure system, the quantum yield for 1,3-dibromobutane is constant, 0.0005, up to a photolysis time of 1.5 minutes and then gradually decreases with prolonged irradiation. Although the data are scattered, it appears that between 6 and 8 minutes the net quantum yield for additional 1,3-dibromobutane is zero. In the presence of the free radical scavenger oxygen, the compound is not observed.

C_3 or C_4-Brominated compound at 140°C: The plot for this compound resembles that of vinyl bromide. Its total yield reaches a maximum at about 5 minutes and thereafter decreases with photolysis time. Its initial yield is about 0.0003 molecules/quantum. The addition of 5 mole % O_2 does not alter the form of the plot but does augment the quantum yield to 0.0004.

1,4-Dibromobutane: The dose-yield plot for 1,4-dibromobutane is linear over the entire dose range and extrapolates through the origin. The quantum yield for 1,4-dibromobutane is 0.00013 molecules/quantum. In the scavenged system, the production of 1,4-dibromobutane is entirely inhibited.

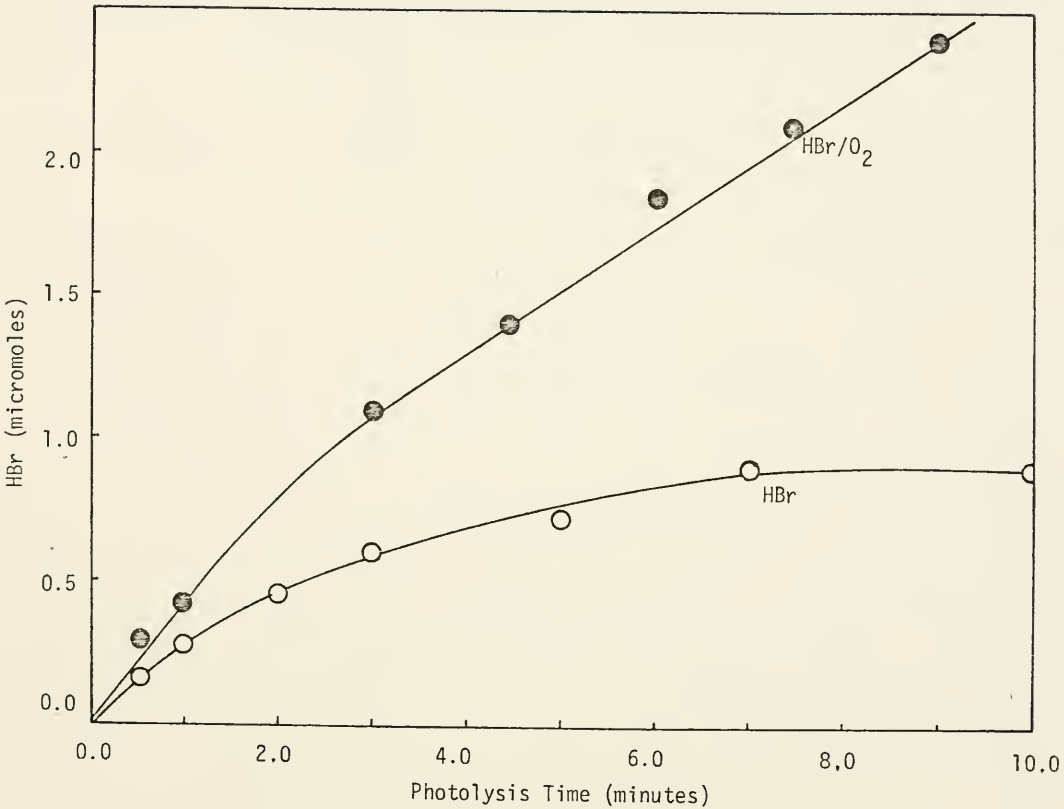

Fig. 24 Production of hydrogen bromide (pure, ○; 5% O_2, ●) as a function of photolysis time.

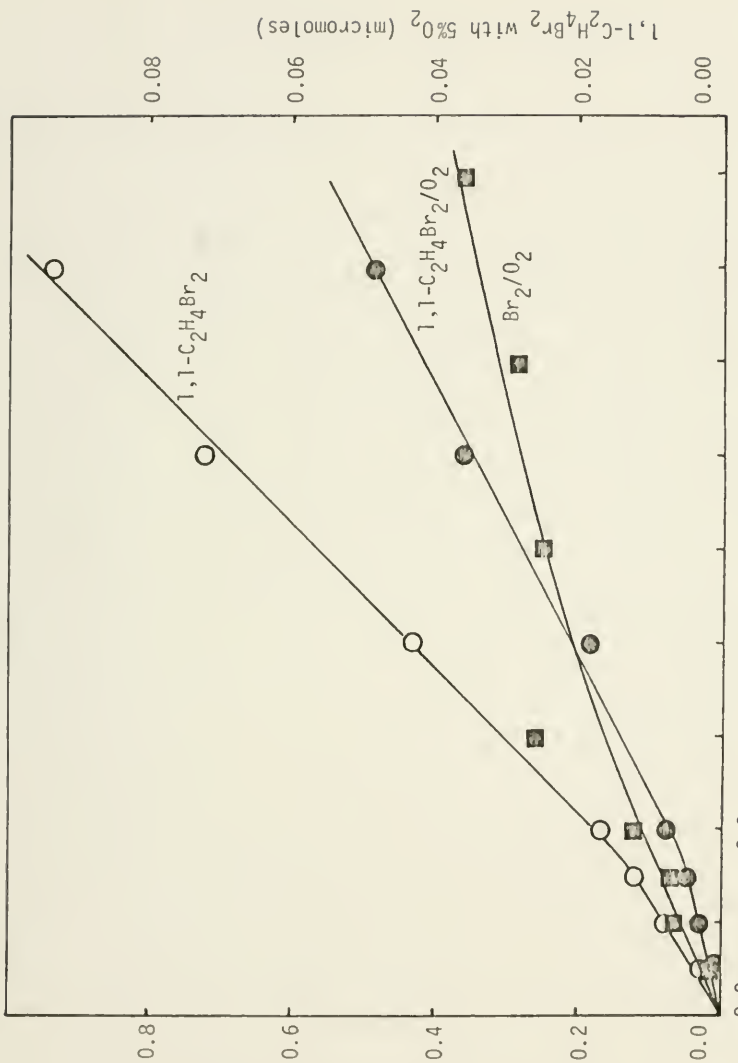

Fig. 25 Production of bromine (5% O_2, ■) and 1,1-dibromoethane (pure, ○; 5% O_2, ●) as a function of photolysis time.

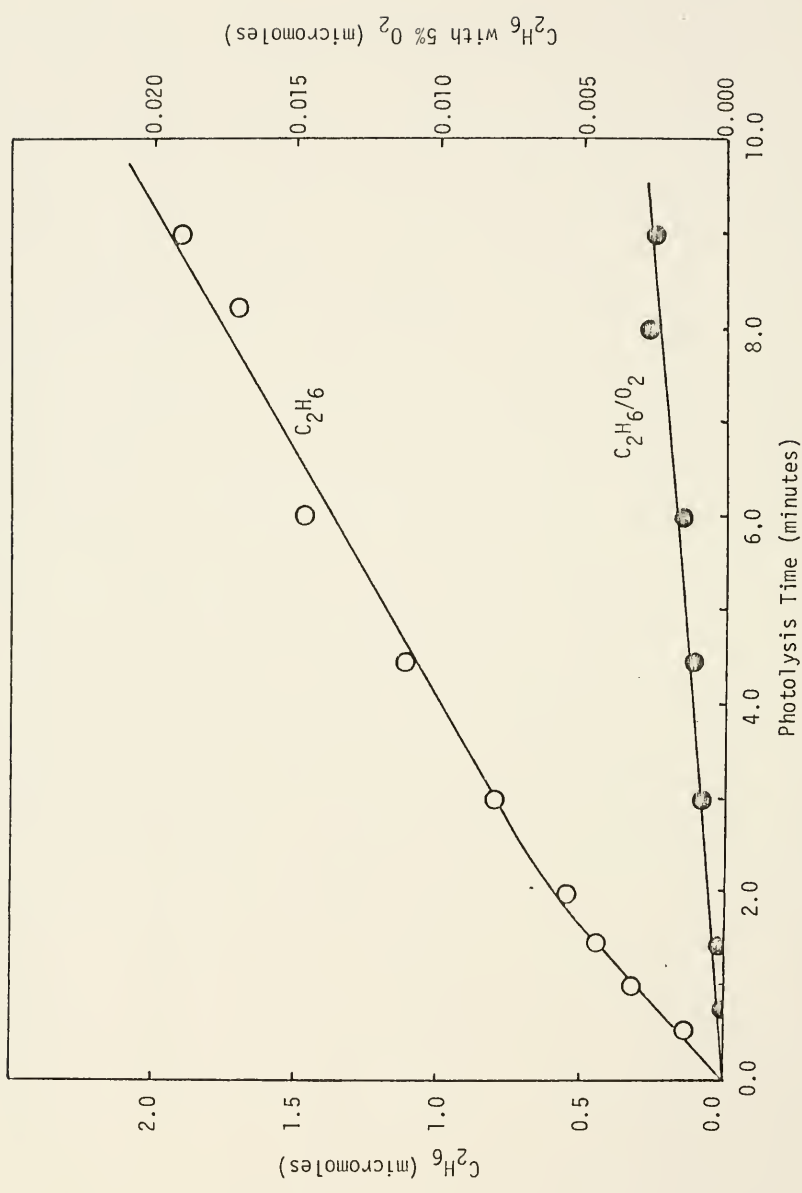

Fig. 26 Production of ethane (pure, O; 5% O_2, ●) as a function of photolysis time.

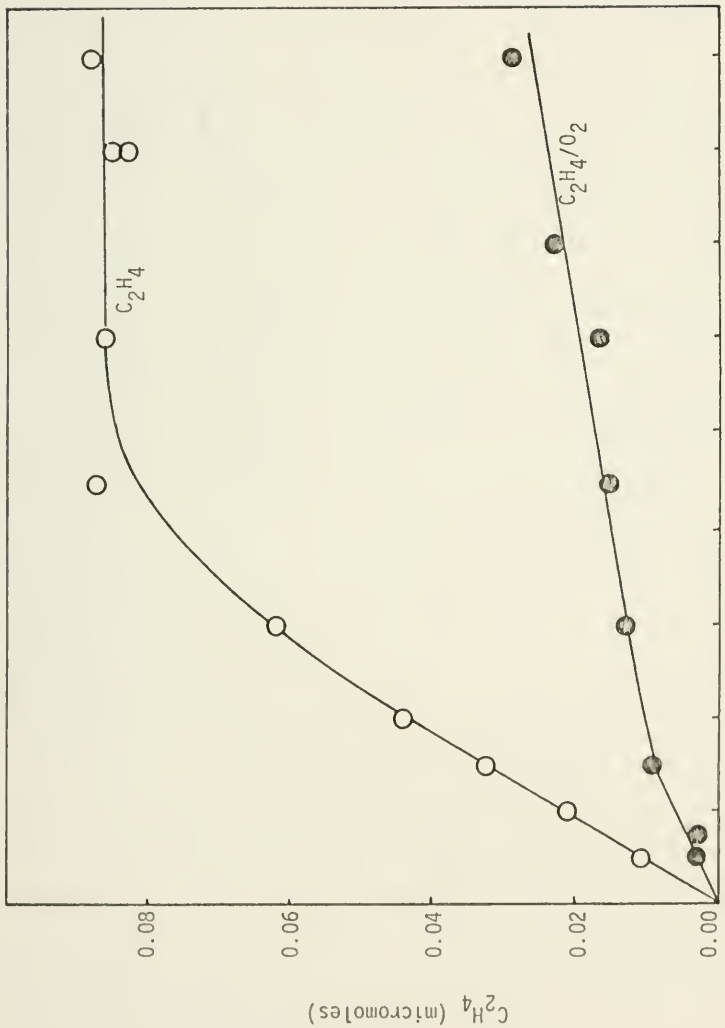

Fig. 27 Production of ethylene (pure, ○; 5% O_2, ●) as a function of photolysis time.

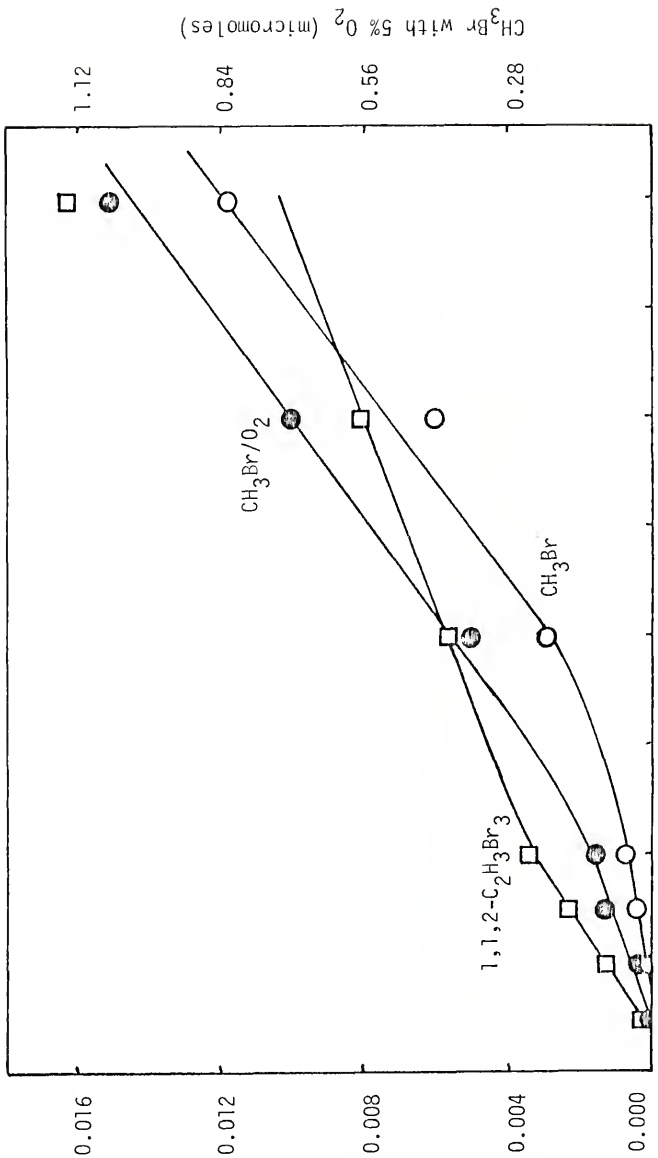

Fig. 28 Production of methyl bromide (pure, ○; 5% O_2, ●) and 1,1,2-tribromoethane (pure, □) as a function of photolysis time.

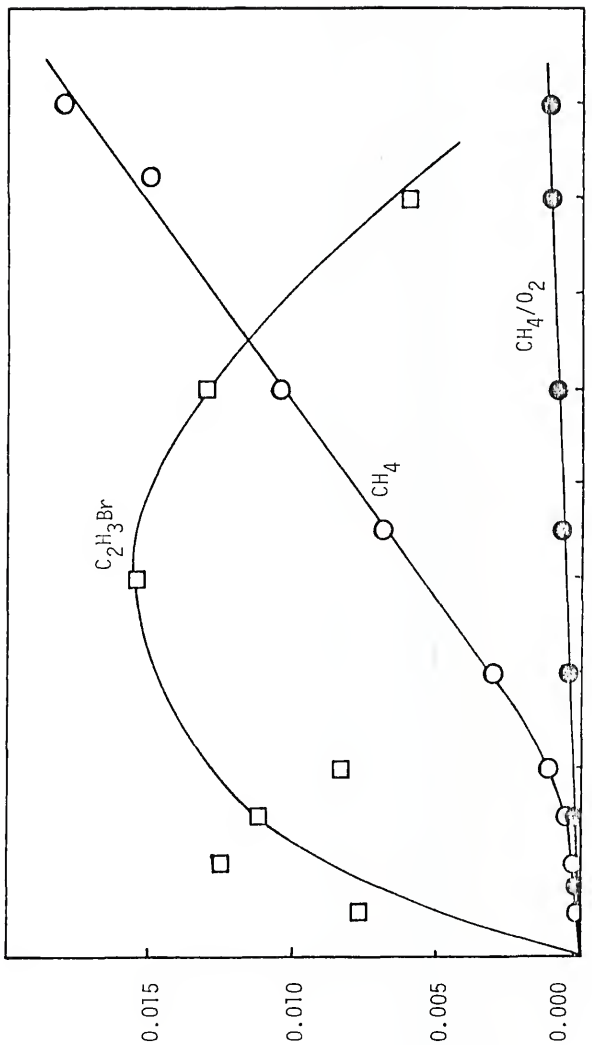

Fig. 29 Production of methane (pure, O; 5% O_2, ●) and vinyl bromide (pure, □) as a function of photolysis time.

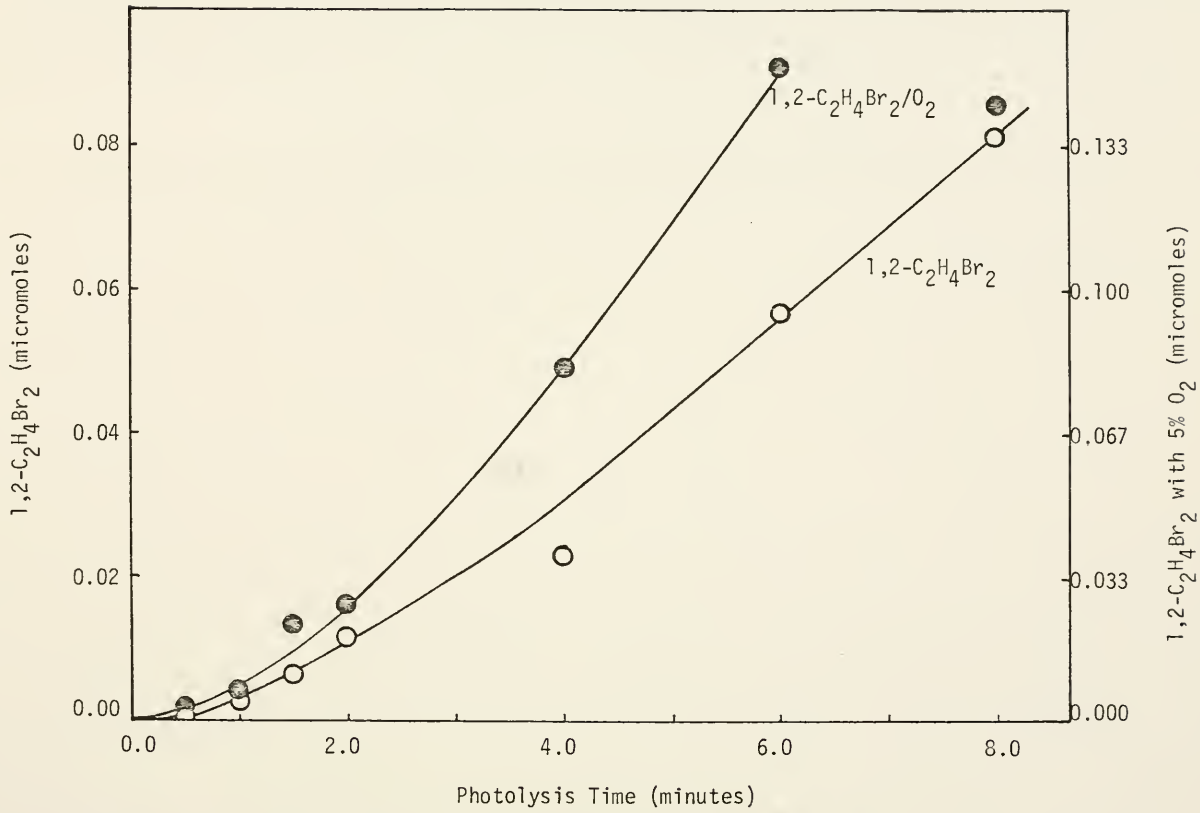

Fig. 30 Production of 1,2-dibromoethane (pure, ○; 5% O_2, ●) as a function of photolysis time.

Unknown compound at 170°C: In both the unscavenged and scavenged systems, the total yields of this compound reach a maximum value at about 6 minutes and then decrease. The plot is similar in form to that of vinyl bromide. The initial yields of this compound for the pure and oxygenated systems are the same, about 0.0002, assuming the same molar response of the detector to 1,3-$C_4H_8Br_2$. However, in the scavenged system the maximum yield at 6 minutes is about 0.5 times that of the unscavenged system.

Using the quantum yields in Table 8, the material balances of the products in the pure system are estimated to be C/H/Br = 1.69/5.00/0.77 and 1.86/5.00/1.05 for the dose ranges of 1.0 to 1.5 minutes and 3.5 to 4.0 minutes respectively.

D. Ion-Molecule Reactions

Since the ion-molecule reactions in ethyl bromide have been investigated previously (15, 16, 17, 18) and no new results have developed in this work, the discussion that follows will be brief.

The ionic reactions in ethyl bromide were examined to pressures as high as 296 microns, using a Bendix Model 14-107 mass spectrometer with an ion source modified for high pressure work. In addition to the major ions $C_2H_5Br^+$, $C_2H_5^+$, $C_2H_3^+$ and Br^+ present in the low pressure mass spectrum, Fig. 31 shows the variation with pressure of the intensities of the ion-molecule reaction products $C_2H_6Br^+$, $(C_2H_5)_2Br^+$ and $C_4H_{10}Br_2^+$. The most intense ion in the spectrum above 140 microns is $(C_2H_5)_2Br^+$, which is consistent with the observation of other

workers (16, 17). As the pressure is elevated, the dimer ion $C_4H_{10}Br_2^+$ becomes increasingly more important. At pressures greater than 170 microns it is second in intensity only to $(C_2H_5)_2Br^+$; however, above 210 microns its ion abundance curve plateaus and gradually falls with pressure. It is interesting to note that $C_4H_{10}Br_2^+$ represents one of the first examples of a persistent ion-molecule collision complex observed by mass spectrometry (15). The ion $C_2H_6Br^+$ corresponds to the protonated parent ion. The measurement of this ion is difficult as it falls within one mass unit of the parent ion which at times overlaps with it.

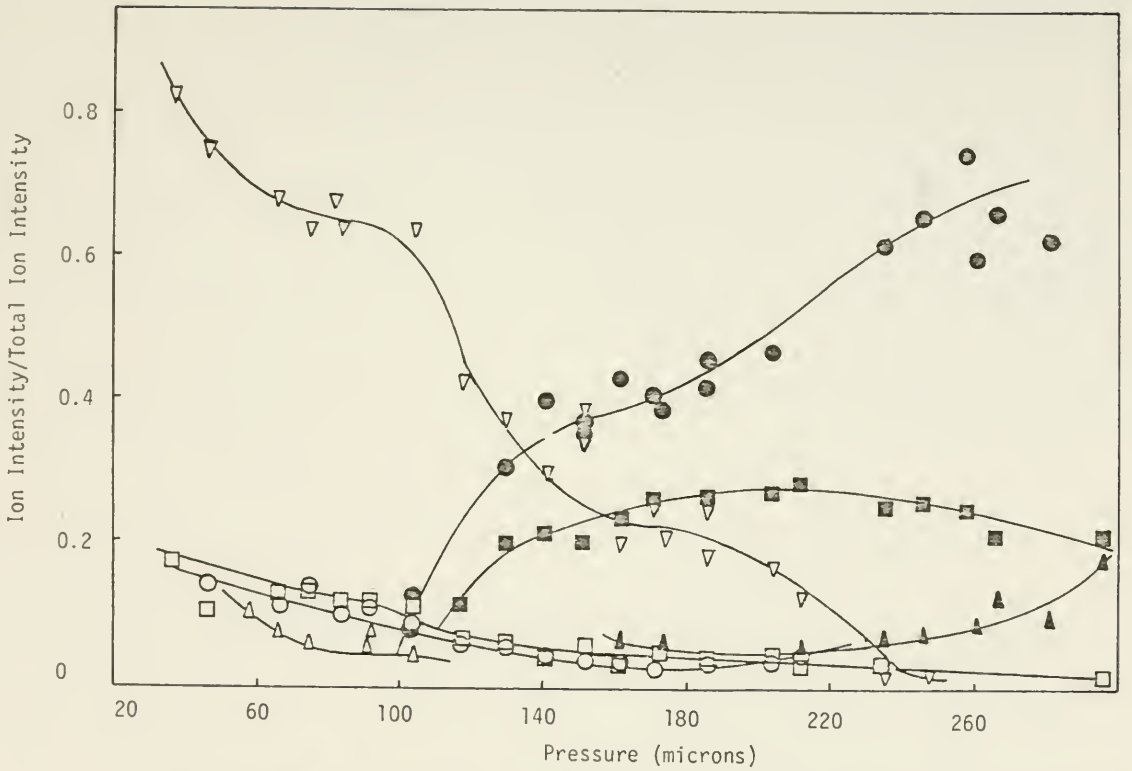

Fig. 31 The relative intensities of $C_2H_5Br^+$ (▽), $C_2H_5^+$ (○), $C_2H_3^+$ (□), $C_2H_6Br^+$ (▲), $C_4H_{10}Br^+$ (●) and $C_4H_{10}Br_2^+$ (■) as a function of pressure.

IV. DISCUSSION AND INTERPRETATION

A. Introduction

In this chapter the gamma radiolysis of ethyl bromide is discussed in light of the information derived from the photochemical and ion-molecule studies of the system. Since there are fewer distinct activated species in the photochemical and ion-molecule systems than in the radiolysis these will be dealt with first.

B. Photolysis

The near ultraviolet absorption band of ethyl bromide probably originates from the transition of the non-bonding p electrons on the bromine atom to the lowest σ^* antibonding orbital involving the carbon and bromine atoms (55). Since there is no evidence of structure in the absorption spectrum of ethyl bromide between 300 and 185 nm (30), the σ^* orbital is likely to be purely dissociative.

It was seen in Chapter III that the dose-yield plots of the major and semimajor products had three general forms: concave upward, linear and convex upward. The shapes of these curves are indicative of the types of reactions that are occurring in the system. For this reason the quantum yields for the products are arranged in Table 8 according to the shape of their dose-yield plots.

Three primary steps are suggested to account for the observed photolysis products. These are included in the kinetic scheme postulated in Table 10. It should be noted that all reactions relating to the photolytic mechanism are indexed with a P for the purpose of identifying them in later sections of this chapter,

Although a substantial amount of bromine is observed in the oxygen scavenged system, none is detected in the pure system. Nevertheless, it can be seen in Table 10 that bromine is assumed to be present and to play a significant role in the kinetic scheme. Even though formation of molecular bromine was not postulated in the high temperature photolysis of ethyl bromide, it would not be expected to occur under those circumstances, since more energy is available to drive the bromine atom abstraction reaction from the substrate at elevated temperatures. Evidence from a computer simulation of the photolysis mechanism (Sec. IV-C) indicates not only that bromine is a necessary part of the mechanism, but also that it would be below the detection limit of the analytical method employed. Bromine in amounts less than 10^{-5} moles/liter would be spectrophotometrically unobservable in the reaction cell used. The simulation also indicates that bromine atoms cannot be ignored; they are assumed to take part in abstraction type reactions. For simplicity the mechanistic steps have been written generally in terms of Br_2; however, the Br· atom is energetically capable of undergoing the same reactions.

Table 10

Photolysis Mechanism

$h\nu + C_2H_5Br \longrightarrow C_2H_5\cdot + Br\cdot$	P-1
$\longrightarrow C_2H_4 + HBr$	P-2
$\longrightarrow CH_3\cdot + CH_2Br\cdot$	P-3
$Br\cdot + Br\cdot + M \longrightarrow Br_2 + M$	P-4
$C_2H_5\cdot + C_2H_5Br \longrightarrow C_2H_6 + CH_3\dot{C}HBr$	P-5
$C_2H_5\cdot + HBr \longrightarrow C_2H_6 + Br\cdot$	P-6
$C_2H_5\cdot + Br_2 \longrightarrow C_2H_5Br + Br\cdot$	P-7
$C_2H_5\cdot + Br\cdot \longrightarrow C_2H_4 + HBr$	P-8
$Br\cdot + C_2H_4 \rightleftharpoons \cdot CH_2CH_2Br$	P-9, P-9'
$\cdot CH_2CH_2Br + C_2H_5Br \longrightarrow CH_3\dot{C}HBr + C_2H_5Br$	P-10
$\cdot CH_2CH_2Br + HBr \longrightarrow C_2H_5Br + Br\cdot$	P-11
$\cdot CH_2CH_2Br + Br_2 \longrightarrow BrCH_2CH_2Br + Br\cdot$	P-12
$Br\cdot + C_2H_5Br \rightleftharpoons HBr + CH_3\dot{C}HBr$	P-13, P-13'
$CH_3\dot{C}HBr + Br_2 \longrightarrow CH_3CHBr_2 + Br\cdot$	P-14
$CH_3\dot{C}HBr + Br\cdot \longrightarrow C_2H_3Br + HBr$	P-15
$Br\cdot + C_2H_3Br \longrightarrow BrCH_2\dot{C}HBr$	P-16
$BrCH_2\dot{C}HBr + HBr \longrightarrow BrCH_2CH_2Br + Br\cdot$	P-17
$BrCH_2\dot{C}HBr + Br_2 \longrightarrow BrCH_2CHBr_2 + Br\cdot$	P-18
$CH_3\cdot + HBr \longrightarrow CH_4 + Br\cdot$	P-19
$CH_3\cdot + Br_2 \longrightarrow CH_3Br + Br\cdot$	P-20
$HBr + Wall \longrightarrow HBr - Wall$	P-21

Products with convex upward dose-yield plots: The rates of formation of ethane, ethylene, vinyl bromide and 1,1,2-tribromoethane (Figs. 26, 27, 29 and 28) are assumed to be intimately dependent on the relative concentrations of hydrogen bromide and bromine in the system.

The major primary event in the photolysis of ethyl bromide is presumed to be process P-1. Since the rupture of the C-Br bond consumes 68 kcal/mol (56) following the absorption of 253.7 nm radiation, a maximum of 44.6 kcal/mol of excess energy is available for partition between the fragments. If the bromine atom is excited to the $^2P_{1/2}$ state or the ethyl radical is internally excited, the amount available as translational energy will be less than the maximum. In any event, the ethyl radical will carry off a minimum of 70% of the excess translational energy because of the disparity of the masses.

Since the addition of oxygen reduces the quantum yield of ethane to 0.1% of its value in the pure system, the role of hot ethyl radicals is negligible in this system. Therefore, a process with the same stoichiometry as reaction P-5 but involving hot ethyl radical abstraction from the substrate is not considered important under the conditions of the experiments reported here. Reaction P-5 has an estimated activation energy of 8 to 10 kcal/mol (57) based on the analogous thermal reaction: $CH_3\cdot + CH_3Br \longrightarrow CH_4 + CH_2Br\cdot$ and would therefore be rather slow for thermal ethyl radicals at room temperature. Reaction P-6 has an activation energy of about

2 kcal/mol and must contribute substantially to the ethane yield, 0.40 molecules/quantum.

Ethane formation arising from the disproportionation reactions of ethyl radicals must be negligible since the concomitant butane yield is 10^{-4} molecules/quantum and the ratio of $k_{disproportionation}/k_{combination}$ is 0.12 (58). The total quantum yield for all combination reactions leading to C_4 compounds is only about 10^{-3}.

Step P-7 accounts for the back reaction involving the ethyl radical. This step competes with reactions P-5, P-6 and P-8 for the destruction of the radical. Reaction P-8 is taken up in more detail when ethylene is discussed.

The convex shape of the dose-yield plot for ethane is presumed to represent the competition of the reactions of ethyl radicals with Br· atoms, Br_2 and HBr on the one hand and with the substrate on the other. The latter reaction yields ethane directly whereas the former set of reactions leads to both ethane and reformed parent. In agreement with expectation, the computer simulation shows that the HBr and bromine concentrations build slowly during the early stages of the experiment (Br atoms reach steady state in a fraction of a second). After HBr and Br_2 have built up and attained a plateau value, the net rate of ethane production is constant but lower.

The ethylene yield is very small, 0.028 molecules/quantum, and as in the liquid phase photolysis of ethyl bromide (6) represents only about 3% of the total product yield. Addition of 5% oxygen prior to photolysis reduces the ethylene yield by about 71%. Since

in the radiolysis of ethyl bromide, the ethylene yield is suppressed to about the same extent while the acetylene yield is unaffected, it is suggested that oxygen is not interfering with the primary process. However, there is some evidence that oxygen may be effecting the reduction of ethylene other than by scavenging radicals. In ethyl chloride radiolysis (11, Fig. 1 in ref 10) the ethylene yield is markedly reduced by oxygen while other free radical scavengers (I_2 and NO) have much less effect; in spite of this, HCl elimination is considered to be a major primary process. It was postulated in the gas phase (12) and liquid phase (59) photolysis of ethyl iodide that ethylene is formed in a primary photolytic event similar to step P-2. The radical processes producing ethylene proceed through steps P-8 and P-9'. The lower activation energy for hydrogen abstraction by bromine compared with iodine (17) makes step P-8 in ethyl bromide more favorable than in ethyl iodide (12, 60). Step P-8 is quite exoergic, about 48.9 kcal/mol (61), and may be viewed as a simple disproportionation reaction.

Step P-9' has been invoked in several mechanisms including the high temperature photolytic decomposition of ethyl bromide (3) and the radiation induced addition of HBr to C_2H_4 (62). The activation energy for the unimolecular decomposition reaction is sufficiently low, about 11.1 kcal/mol (5), that with its high frequency factor, $10^{12.9}$ sec^{-1} (5), the reaction can compete with steps P-10, P-11 and P-12.

Ethylene is consumed in reaction P-9 to form the 2-bromo-1-ethyl radical which can then either go on to form the 1,2-dibromoethane in step P-12 or decay back to ethylene and Br· atom in step P-9', It is significant that there is a reciprocity between the ethylene and 1,2-dibromoethane dose-yield plots as seen in Figs. 27 and 30.

The amount of hydrogen bromide produced by molecular elimination in step P-2 is not sufficient to account for the large hydrogen bromide yield of 0.36 molecules/quantum. On the basis of the unscavengeable ethylene yield in the oxygenated system, a minimum of 2.3% of the HBr is formed in step P-2. Hydrogen bromide is, therefore, proposed to occur mainly through radical processes involving steps P-8, P-13 and P-15. Step P-15 like step P-8 is very exoergic. Both steps involve the interaction of the three predominant radicals in the system. In the high temperature photolysis (3, 5) HBr has been assumed to arise from hydrogen abstraction by bromine atom from either the α or the β position of ethyl bromide. The activation energy of these steps has been estimated to be about 13 kcal/mol (3, 63). However, Semenov (64) considers abstraction from the α position to be 3 kcal/mol more exoergic than from the adjacent carbon atom. In the radiolysis of ethyl alcohol vapor (65), α-hydrogen abstraction rather than β-hydrogen abstraction has been found to be the predominant effect. In the room temperature photolysis of ethyl bromide, therefore, only the abstraction from the α position is assumed to be significant. Even if the activation energy were ca. 3 kcal/mol lower for the removal of the α-hydrogen, it would

still be slow at room temperature for the $Br(4^2P_{3/2})$. However, the energy barriers to $Br(4^2P_{1/2})$ are only 2.5 kcal/mol and if this state is formed, it is sufficiently long lived, 1.1 seconds (66), to undergo these reactions. Donovan and Husain (7) attributed the absence of the absorption signal from the $^2P_{1/2}$ state following the flash photolysis of ethyl bromide in a kinetic spectroscopy experiment to be due to the rapid electronic quenching of the excited state by ethyl bromide.

Irrespective of the high activation energy of step P-13, it is necessary to account for the large HBr yield in view of the low ethylene yield. Evidence that this reaction may be important at room temperature comes from the investigation of the liquid phase radiolysis of n-propyl bromide (9). The initial HBr yield was found to be strongly dependent on temperature indicating that the elementary steps involved in its production have an appreciable activation energy which was estimated to be between 15 and 22 kcal/mol. In addition, in the computer simulation (Sec. IV-C) the omission of this reaction leads to a substantial decrease in both the HBr and 1,1-dibromoethane yields relative to the experimental measurements.

Hydrogen bromide is consumed in reactions P-6, P-11, P-13', P-17, P-19 and P-21. The activation energies for steps P-11 and P-13' are 2 and 6 kcal/mol respectively (61). Steps P-19 and P-17 are estimated to have approximately the same activation energies as steps P-11 and P-13'. Reaction P-21 accounts for an observation

noted in the early stages of this research before the post-irradiation precaution of placing the reaction vessel in liquid nitrogen immediately following irradiation was taken. Namely, it was observed that over a long period of time the walls of the reaction vessels used in gamma radiolysis became etched. The same type of behavior would presumably have occurred in the photolysis if the above precaution had not been taken.

In the scavenged system, the enhanced bromine and hydrogen bromide yields may be due to oxygen reacting with free radicals that would otherwise consume these species. Alternatively, oxygenated radicals formed may react with HBr to liberate bromine atoms. These Br· atoms could then recombine according to step P-4 or interact with the oxygenated compounds formed in the scavenged system. Although there are only sparse kinetic data in the literature on oxygen and alkyl halide mixtures to guide speculation, one series of steps leading to an increase in HBr which involves the main radicals produced in this system is

$$C_2H_5\cdot + O_2 \longrightarrow C_2H_5O_2\cdot \qquad \text{P-22}$$

$$C_2H_5O_2\cdot \longrightarrow CH_3CHO + HO\cdot \qquad \text{P-23}$$

$$HO\cdot + C_2H_5O_2\cdot \longrightarrow C_2H_5OH + O_2 \qquad \text{P-24}$$

$$Br\cdot + CH_3CHO \longrightarrow CH_3CO\cdot + HBr \qquad \text{P-25}$$

$$Br\cdot + C_2H_5OH \longrightarrow CH_3\dot{C}HOH + HBr \qquad \text{P-26}$$

Steps P-22 and P-23 are estimated to have activation energies of about 0 and 20 kcal/mol respectively (67) and are currently part of the accepted interpretation (67, 68) of the induced chain oxygenation of hydrocarbons. With step P-24 these account for the primary products, ethanol and acetaldehyde, in the oxidation of ethyl iodide (68). Steps P-25 and P-26 involve the removal of the relatively weak α-hydrogen atom. The former step is about 1 kcal/mol exoergic, while step P-26 has an activation energy of about 2.6 ± 2.0 kcal/mol (58). Another possible sequence to account for the increase in HBr which is based on the important 1-bromo-1-ethyl radical is

$$CH_3\dot{C}HBr + O_2 \longrightarrow CH_3CHBrO_2\cdot \qquad \text{P-27}$$

$$CH_3CHBrO_2\cdot \longrightarrow CH_3\dot{O} + CHBrO \qquad \text{P-28}$$

$$\begin{matrix} & O & \\ & C\text{-}H & \longrightarrow CO + HBr \\ Br & & \end{matrix} \qquad \text{P-29}$$

An analogue of step P-28 (cf step P-23) has been assumed in the mechanism of hydrocarbon oxidations (67). In the present case, the effect of the bromine and oxygen on the same carbon atom should make C-C bond fission more favorable than in the hydrocarbon system. Step P-29 accounts for the rapid decomposition of CHBrO which is expected to be quite thermodynamically unstable.

The data for the vinyl bromide dose-yield plot are rather scattered for reasons discussed in Sec. III-C. Vinyl bromide production is attributed to the hydrogen abstraction in step P-15. This step is obviously exoergic and should compete with steps P-13'

and P-14 for the 1-bromo-1-ethyl radical. Another possible mechanism for vinyl bromide production is step P-30.

$$h\nu + C_2H_5Br \longrightarrow C_2H_3Br + H_2 \qquad \text{P-30}$$

However, there seems to be little evidence in the chemical literature for a four step branching scheme as part of the primary photolytic event in the 253.7 nm energy regime for a molecule as simple as ethyl bromide. If vinyl bromide were only formed in a primary event and then consumed by bromine atom in step P-16, the quantum yield of vinyl bromide would be independent of dose. The data seem to indicate, however, that vinyl bromide production reaches a maximum and then decreases. In light of the proposed mechanism the reason for the decrease in vinyl bromide with time could be that the 1-bromo-1-ethyl radical is being diverted to form 1,1-$C_2H_4Br_2$ or C_2H_5Br. Ultimately, it would be expected that the dose-yield plot for vinyl bromide should plateau. The form of the dose-yield plot seems to suggest that vinyl bromide is produced mainly by the secondary process.

In step P-16 vinyl bromide is converted into the 1,2-dibromoethyl radical which in turn forms 1,2-dibromoethane and 1,1,2-tribromethane in competing steps P-17 and P-18. The rapid diminution of vinyl bromide is in agreement with the observation of Leitch and Morse (69) who investigated the photolysis of acetylene and hydrogen bromide in the gas phase. It was noted in this study that acetylene and hydrogen bromide react rapidly even in the dark to form

1,2-dibromoethane. Certainly the course of the reaction must proceed through a vinyl bromide intermediate.

In the presence of 5% oxygen, vinyl bromide and 1,1,2-tribromoethane are essentially eliminated; only a trace amount of vinyl bromide may be present at 0.5 minutes. In view of the sensitivity of the vinyl bromide to large concentrations of hydrogen bromide or bromine, the addition of oxygen cannot indicate whether there is any contribution to the vinyl bromide yield by process P-30.

Products with concave upward dose-yield plots: 1,1-$C_2H_4Br_2$, 1,2-$C_2H_4Br_2$, CH_4 and CH_3Br all have dose-yield plots (Figs. 25, 30, 29, and 28) that exhibit an induction period.

The yield of 1,1-$C_2H_4Br_2$ is about 11 times larger than that of 1,2-$C_2H_4Br_2$ in the oxygen-free system over the dose range covered. The difference in yields is attributed in part to the inertness of the 1-bromo-1-ethyl radical to unimolecular decay relative to the 2-bromo-1-ethyl radical and the ease of removing from ethyl bromide the α-hydrogen as compared with the β-hydrogen. In addition, the computer simulation of the reaction mechanism (Sec. IV-C) indicates the necessity of hypothesizing reaction P-10 to keep the calculated 1,1-dibromoethane and 1,2-dibromoethane yields close to the experimentally measured values.

The 1-bromo-1-ethyl radical disappears in reactions P-13', P-14 and P-15 to form ethyl bromide, 1,1-dibromoethane and vinyl bromide respectively. The 2-bromo-1-ethyl radical is consumed in reactions P-10, P-11 and P-12 to form the 1-bromo-1-ethyl radical,

ethyl bromide and 1,2-dibromoethane. 1,2-$C_2H_4Br_2$ is also formed from the 1,2-dibromoethyl radical which arises in step P-16. It is doubtful that HBr can directly add to vinyl bromide to form the 1,2-dibromoethane. Such four-centered addition reactions tend to have high activation energies. For example, $HI + C_2H_4 \longrightarrow C_2H_5I$ has an activation energy of 28.9 kcal/mol (70). In any event, it can be seen from a comparison of the dose-yield curves of vinyl bromide (Fig. 29) and 1,2-dibromoethane (Fig. 30) that there is an apparent reciprocity between the compounds as would be required for C_2H_3Br to be the precursor to 1,2-$C_2H_4Br_2$.

In the scavenged system, oxygen effectively competes with bromine and hydrogen bromide for the 1-bromo-1-ethyl radical. The 1,1-dibromoethane yield is reduced 94% while the 1,2-dibromoethane yield is increased 188%. The mechanism as formulated in this work does not account for the large increase in the 1,2-dibromoethane yield or for that matter the 100-fold enhancement of the methyl bromide yield in the presence of oxygen. This latter observation, however, points to an enhanced amount of carbon-carbon bond breakage in the presence of oxygen. Possibly $CH_3\dot{C}O$ formed in step P-25 reacts with bromine to form methyl bromide in step P-31.

$$CH_3\dot{C}O + Br_2 \longrightarrow CH_3Br + CO + Br\cdot \qquad \text{P-31}$$

This step was postulated to occur in the acetyl bromide system (71). In that system, 1,2-dibromoethane was assumed to be formed in step P-32.

$$2\dot{C}H_2COBr \longrightarrow BrCH_2CH_2Br + 2CO \qquad P\text{-}32$$

where $\cdot CH_2COBr$ results from a hydrogen abstraction reaction. Alternatively, CH_3Br may be formed by a molecular rearrangement reaction which would not be scavengeable by oxygen. Evidently, oxygen has opened up a pathway for the formation of 1,2-$C_2H_4Br_2$, which may or not have been there in the pure system, while concurrently closing the route leading to the 1,1-$C_2H_4Br_2$. Perhaps this is occurring by radical reactions sensitized by oxygenated radicals.

It is difficult to sort out reactions that are induced by oxygen from those that are directly related to the mechanism in the pure system. Without a more detailed analysis of the products formed in the ethyl bromide-oxygen system further speculation of mechanistic steps would be moot. The fact remains that the catalytic effect of oxygen has now been observed in the pyrolysis (72), photolysis and, as will be seen later, in the radiolysis of ethyl bromide.

The amounts of methane and methyl bromide produced in the pure system are extremely small as their combined yields contribute only about 0.6% to the total product yield. Steps P-3, P-19 and P-20 are suggested to account for their formation. The activation energies for steps P-19 and P-20 are reported to be 1.5 $\pm$1 and about 0 kcal/mol respectively (64). Another reaction that might occur to some extent is

$$CH_3\cdot + C_2H_5Br \longrightarrow CH_4 + C_2H_4Br\cdot \qquad P\text{-}33$$

The activation energy of 6.6 kcal/mol (64) for this reaction does not

exclude it from consideration; however, the pronounced induction period exhibited by the methane dose-yield plot suggests that this reaction can only account for part of the methane yield. The bromomethyl radical would also be expected to react according to steps P-34 and P-35.

$$CH_2Br^{\cdot} + C_2H_5^{\cdot} \longrightarrow C_3H_7Br \qquad \text{P-34}$$

$$CH_2Br^{\cdot} + Br_2 \longrightarrow CH_2Br_2 + Br^{\cdot} \qquad \text{P-35}$$

Although 1-bromopropane was observed in trace amounts, no dibromomethane was detected possibly due to the low sensitivity of the flame ionization detector to the C_1-brominated compounds.

Since the methyl radicals produced in step P-3 should carry off about 86% of the excess translational energy, some would be expected to react hot. The results of the oxygen scavenging experiments suggest that approximately 6% of the methane is produced in hot reactions. The interpretation of the effect of oxygen on the production of methyl bromide is included as part of the discussion of 1,2-dibromoethane.

C. Computer Simulation of the Photolysis Mechanism

A computer program designed to deal with steady state kinetics was used to test the validity of the proposed mechanism. The program was written in Fortran II by DeTar (73) and has been converted to Fortran IV for use on the IBM 370 computer at the University of

Florida. The Fortran IV version of the program has been included in the Appendix.

The input to the program includes the mechanistic steps, their rate constants, the identification of each radical and the initial concentration of each reactant. With this information as well as the choice of several parameters which control the progress of the computation, the program furnishes the concentration of each chemical species as a function of time. The algorithm used to perform the calculations is trapezoidal integration of the set of simultaneous rate equations. To limit the complexity of the calculation, the reactions involving the C_1 compounds and several other less significant products were omitted. The general computer simulated mechanism is presented in Table 11. The elementary steps listed therein are indexed with a C for identification with this section.

The mechanism was tested using various values for the rate constants. From the results of the calculations it has become quite evident that the analysis of the reaction mechanism and the estimation of the rate constants are two problems that cannot be separated. Only a few kinetic data are available in the literature pertinent to the reaction mechanism and some of these are contradictory. For example, the activation energy for step C-13 is estimated to be 2.3 kcal/mol (57) or greater than 5 kcal/mol (57). A more extreme example is the data on the reaction $C_2H_4Cl\cdot \longrightarrow C_2H_4 + Cl\cdot$ which were needed in the comparison of the radiolysis of the ethyl halides (Sec. IV-G). An activation energy for this unimolecular decay

Table 11

General Photolysis Mechanism Used in Computer Simulations A, B and C

$C_2H_5Br \longrightarrow C_2H_5 + Br\cdot$	C-1
$C_2H_5Br \longrightarrow C_2H_4 + HBr$	C-2
$Br\cdot + Br\cdot \longrightarrow Br_2$	C-3
$C_2H_5\cdot + C_2H_5Br \longrightarrow C_2H_6 + CH_3\dot{C}HBr$	C-4
$C_2H_5\cdot + HBr \longrightarrow C_2H_6 + Br\cdot$	C-5
$C_2H_5\cdot + Br_2 \longrightarrow C_2H_5Br + Br\cdot$	C-6
$C_2H_5\cdot + Br\cdot \longrightarrow C_2H_5Br$	C-7
$Br\cdot + C_2H_5\cdot \longrightarrow C_2H_4 + HBr$	C-8
$Br\cdot + C_2H_4 \longrightarrow \cdot CH_2CH_2Br$	C-9
$\cdot CH_2CH_2Br \longrightarrow Br\cdot + C_2H_4$	C-10
$\cdot CH_2CH_2Br + C_2H_5Br \longrightarrow CH_3\dot{C}HBr + C_2H_5Br$	C-11
$\cdot CH_2CH_2Br + HBr \longrightarrow Br\cdot + C_2H_5Br$	C-12
$\cdot CH_2CH_2Br + Br_2 \longrightarrow BrCH_2CH_2Br + Br\cdot$	C-13
$\cdot CH_2CH_2Br + Br\cdot \longrightarrow BrCH_2CH_2Br$	C-14
$Br\cdot + C_2H_5Br \longrightarrow CH_3\dot{C}HBr + HBr$	C-15
$CH_3\dot{C}HBr + HBr \longrightarrow Br\cdot + C_2H_5Br$	C-16
$CH_3\dot{C}HBr + Br_2 \longrightarrow CH_3CHBr_2 + Br\cdot$	C-17
$CH_3\dot{C}HBr + Br\cdot \longrightarrow CH_3CHBr_2$	C-18
$Br\cdot + CH_3\dot{C}HBr \longrightarrow C_2H_3Br + HBr$	C-19
$Br\cdot + C_2H_3Br \longrightarrow Br\dot{C}HCH_2Br$	C-20
$Br\dot{C}HCH_2Br + HBr \longrightarrow Br\cdot + BrCH_2CH_2Br$	C-21

of 8 $\pm$ 5 kcal/mol is found in Steacie's monograph (57) in contrast to 22.2 kcal/mol in Benson and O'Neal's tabulation (5). The 14.2 kcal/mol difference in activation energies means that the respective rate constants differ by a factor of 2.7×10^{10}. Accordingly, there is a great deal of uncertainty in the estimation of some of the 21 rate constants used in the computer simulations. For this reason approximately 40 computer runs were carried out in order to optimize the rate constants. The computer simulations represent a reasonable approximation of the experimental results; however, more time and money might produce results somewhat closer to the measured values. Despite the difficulty, the program provided insight into the mechanism that could not otherwise be attained. For instance, reaction C-11 is proposed to enhance the 1,1-dibromoethane yield while at the same time to prevent the 1,2-dibromoethane yield from becoming several orders of magnitude larger than its experimental value. Reaction C-11 seems quite plausible on the basis of energetic considerations.

In Figs. 32 through 38, presented at the end of this section, are plotted the results of the calculated product distributions as well as the experimental curves. The experimental curves are drawn to fit the actual data although these are not displayed. The fact that the simulated results do not always reproduce the shapes of the experimental dose-yield plots probably reflects both the difficulty of estimating the rate constants and the simplicity of the mechanism. Elementary steps P-3, P-18, P-19 and P-20 in Table 10 have been omitted from consideration in Table 11. The rate constants used in the computer-simulated mechanism are given in Table 12.

Table 12

Rate Constants Used in Computer Simulations A, B and C

Reaction No.	A	B	C
1	2.09×10^{-5}[a]	2.09×10^{-5}[a]	2.09×10^{-5}[a]
2	5.2×10^{-6}[a]	5.2×10^{-6}[a]	5.2×10^{-6}[a]
3	2.2×10^{11}	2.2×10^{11}	5.0×10^{10}
4	1.0×10^{5}	8.0×10^{6}	7.7×10^{4}
5	1.1×10^{11}	1.1×10^{11}	1.1×10^{11}
6	1.8×10^{11}	1.8×10^{11}	1.8×10^{11}
7	5.0×10^{13}	8.0×10^{13}	0.0
8	5.0×10^{13}	1.0×10^{14}	0.0
9	2.0×10^{10}	2.0×10^{10}	4.0×10^{9}
10	5.5×10^{4}[a]	5.5×10^{4}[a]	5.5×10^{4}[a]
11	2.0×10^{9}	2.0×10^{9}	7.7×10^{9}
12	1.1×10^{11}	1.1×10^{11}	1.1×10^{11}
13	1.8×10^{11}	1.8×10^{11}	4.2×10^{11}
14	5.0×10^{13}	6.0×10^{13}	0.0
15	1.8×10^{4}	1.0×10^{6}	1.0×10^{5}
16	1.2×10^{8}	9.0×10^{10}	1.3×10^{8}
17	2.0×10^{8}	1.0×10^{11}	2.1×10^{8}
18	2.0×10^{13}	3.0×10^{13}	0.0
19	1.0×10^{13}	6.0×10^{11}	1.0×10^{12}
20	4.0×10^{8}	1.3×10^{9}	4.0×10^{8}
21	1.0×10^{10}	1.0×10^{10}	1.0×10^{7}

Note: Units are in cc/mol-sec, unless otherwise indicated.

[a]Units are in sec^{-1}.

The A mechanism incorporates all the elementary steps listed in Table 11. The rate constants used in the calculations are based on values found in the literature.

A number of assumptions were made in estimating the rate constants for the A mechanism. Also because of limitations of the program, termolecular reactions had to be treated as pseudo-second order with the substrate concentration incorporated into the rate constant.

The quantum yield for reaction C-2 was taken as 0.20 rather than the 0.02 estimated on the basis of the oxygen scavenging experiments. The larger quantum yield was assumed since it has been shown that oxygen decreases the ethylene yield more than other types of free radical scavengers (I_2 and NO) in the ethyl chloride system (11, Fig. 1 in ref 10). Accordingly, the quantum yield for reaction C-1 was taken as 0.80. The rate constants for reactions C-1 and C-2 were then selected to correspond to ethyl bromide under actual experimental conditions: 100 torr pressure, 91.2 cc. volume reaction vessel, 297°K and an absorbed light intensity of 8.5×10^{13} quanta/cc.-sec.

The rate constant for reaction C-3 is pseudo-second order since it includes the ethyl bromide concentration. The value is based on the termolecular rate constant for the reaction $Br\cdot + Br\cdot + CO_2 \longrightarrow Br_2 + CO_2$ (74) multiplied by a factor of 3 to account for the higher third body efficiency of ethyl bromide. Reaction C-4 is expected to have an activation energy of 8 to 10 kcal/mol and a preexponential factor of about $10^{11.5}$ mol/cc.-sec. The rate constant for reaction

C-5 should be about the same magnitude as reaction C-12. Benson (61) estimates the rate constant for the bimolecular reaction with hydrogen bromide (step C-12) to be $10^{12.5-2/\theta}$ cc./mol-sec. where θ is 2.303 R T in kcal/mol. Furthermore, reaction C-6 has been determined to be about 1.7 times faster than reaction C-5 (58). Similarly reactions C-13 and C-17 are estimated to have rate constants that are approximately twice that of elementary steps C-12 and C-16 respectively. Since steps C-7, C-8, C-14, C-18 and C-19 are radical-radical recombination or disproportionation reactions, they are generally given rate constants on the order of 5×10^{13} mol/cc.-sec.

The rate constant for bromine addition (step C-9) was estimated from the unimolecular rate constant for reaction C-10 and the ratio of 3.3×10^{-6} mol/cc. for k_{C-10}/k_{C-9} at 25°C (62). Since no kinetic data were available for reaction C-11, the rate constant was adjusted to keep the concentration of the 1,2-$C_2H_4Br_2$ within the range of the experimental value. The rate constant for reaction C-15 was obtained from the equilibrium constant $10^{1.3-7/\theta}$ for the reaction $Br\cdot + C_2H_5Br \rightleftharpoons HBR + CH_3\dot{C}HBr$ and the rate constant $10^{12.5-6/\theta}$ cc./mol-sec. for the back reaction in step C-16 (61). Step C-20 is estimated to have a rate constant between 0.01 and 0.1 of that for reaction C-9. Since bromine is an electron-withdrawing group it will tend to inhibit the addition of bromine atom to the double bond of vinyl bromide. Reaction C-21 should be slower than reaction C-16 because there are two electron-withdrawing groups as well as possible steric hindrance. This reaction has been given a rate constant of approximately 0.01 of that of reaction C-16.

In view of the approximate nature of some of the rate constants used several were varied to produce simulations B and C. The results of all three simulations show that with a realistic rate constant for step C-3 a substantial amount of Br_2 is produced which strongly suggests that the presence of Br_2 cannot be ignored in this system. In Table 13 it may be observed that the radical concentrations at steady state in general are not unreasonable with the exception of that for the $BrCH_2\dot{C}HBr$ radical in simulation C. Even here, however, it is not a serious problem since the reactions producing and consuming the radical are of minor importance to the mechanism.

D. Ion-Molecule Reactions

The following ion-molecule reactions are found to take place in the high pressure mass spectrometry of ethyl bromide with 100 e.v. electrons between 30 and 296 torr.

$$C_2H_5Br^+ + C_2H_5Br \longrightarrow (C_2H_5Br)_2^+ \qquad \text{I-1}$$

$$\longrightarrow C_2H_5Br^+C_2H_5 + Br \qquad \text{I-2}$$

$$Br^+ + C_2H_5Br \longrightarrow C_2H_5Br^+ + Br \qquad \text{I-3}$$

$$C_2H_3^+ + C_2H_5Br \longrightarrow C_2H_5Br^+H + C_2H_2 \qquad \text{I-4}$$

$$C_2H_5^+ + C_2H_5Br \longrightarrow C_2H_5Br^+H + C_2H_4 \qquad \text{I-5}$$

$$C_2H_5Br^+H + C_2H_5Br \longrightarrow C_2H_5Br^+C_2H_5 + HBr \qquad \text{I-6}$$

Table 13

Radical Concentrations at Photolysis Time 5 Minutes for Computer Simulations A, B and C

Radical	A (micromoles)	B (micromoles)	C (micromoles)
$Br^{\cdot}$	5.3577×10^{-4}	4.7803×10^{-4}	3.7557×10^{-3}
$C_2H_5^{\cdot}$	7.8989×10^{-6}	7.1462×10^{-6}	3.2216×10^{-5}
$^{\cdot}CH_2CH_2Br$	4.3938×10^{-7}	5.4785×10^{-7}	6.0649×10^{-8}
$CH_3\dot{C}HBr$	2.6887×10^{-5}	1.7025×10^{-5}	6.0641×10^{-5}
$BrCH_2\dot{C}HBr$	1.2910×10^{-5}	1.2344×10^{-6}	3.4328×10^{-1}

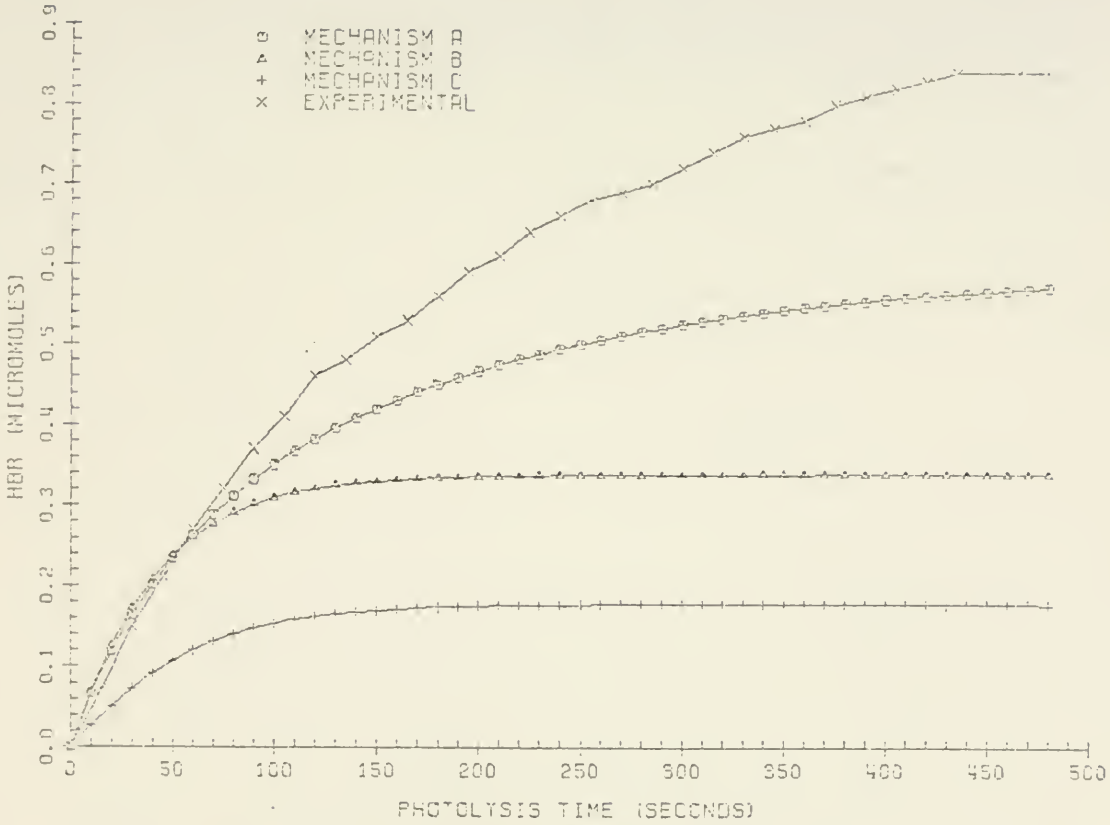

Fig. 32 Computer simulation of photolysis mechanism compared with experimental data: Production of hydrogen bromide as a function of photolysis time.

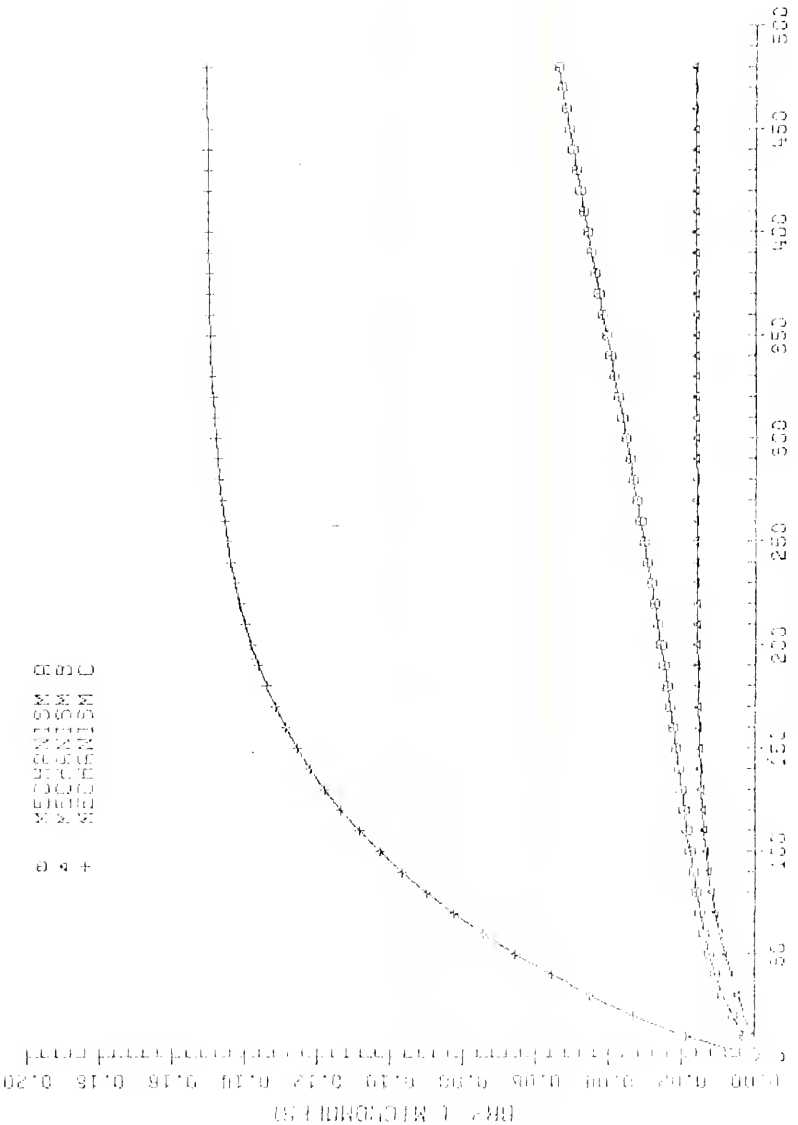

Fig. 33 Computer simulation of photolysis mechanism; Production of bromine as a function of photolysis time.

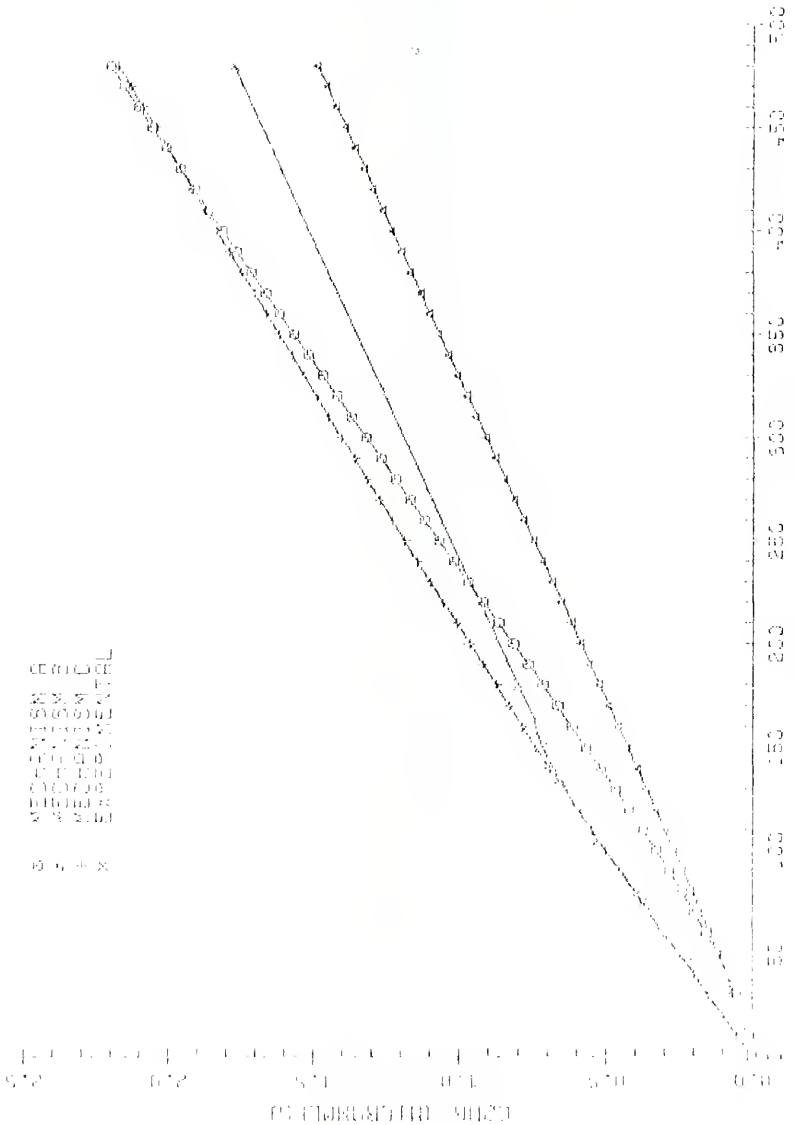

Fig. 34 Computer simulation of photolysis mechanism compared with experimental data: Production of ethane as a function of photolysis time.

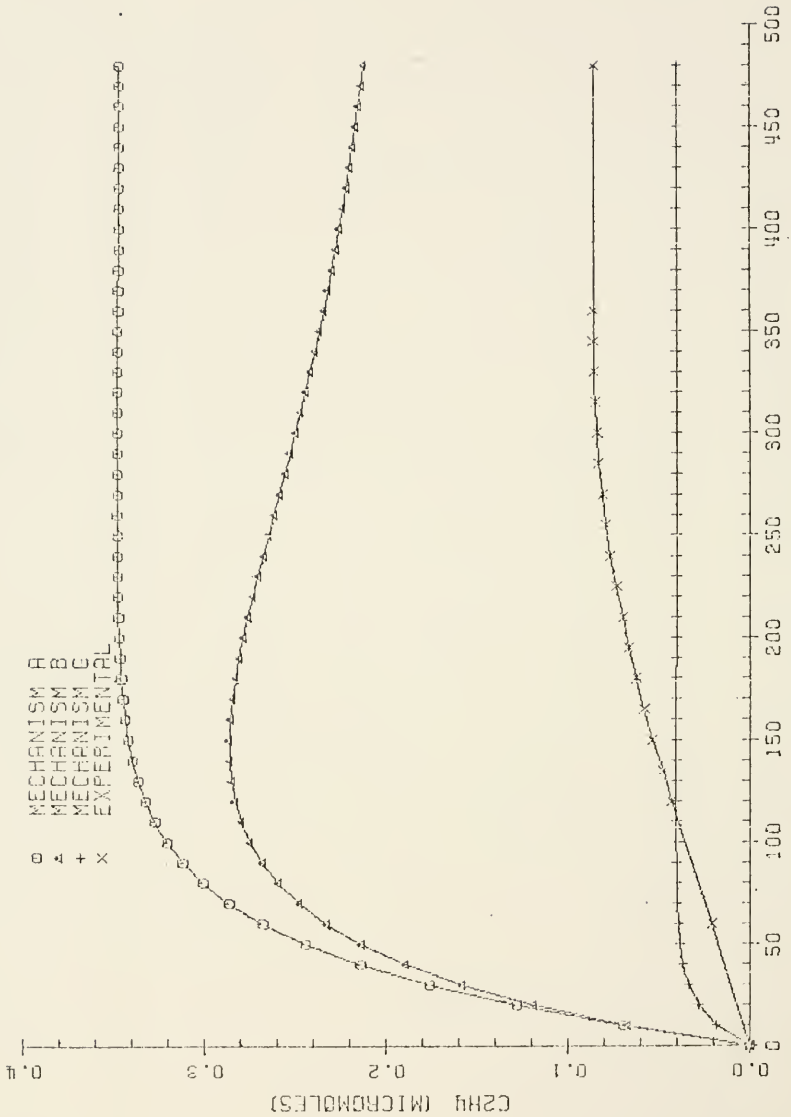

Fig. 35 Computer simulation of photolysis mechanism compared with experimental data: Production of ethylene as a function of photolysis time.

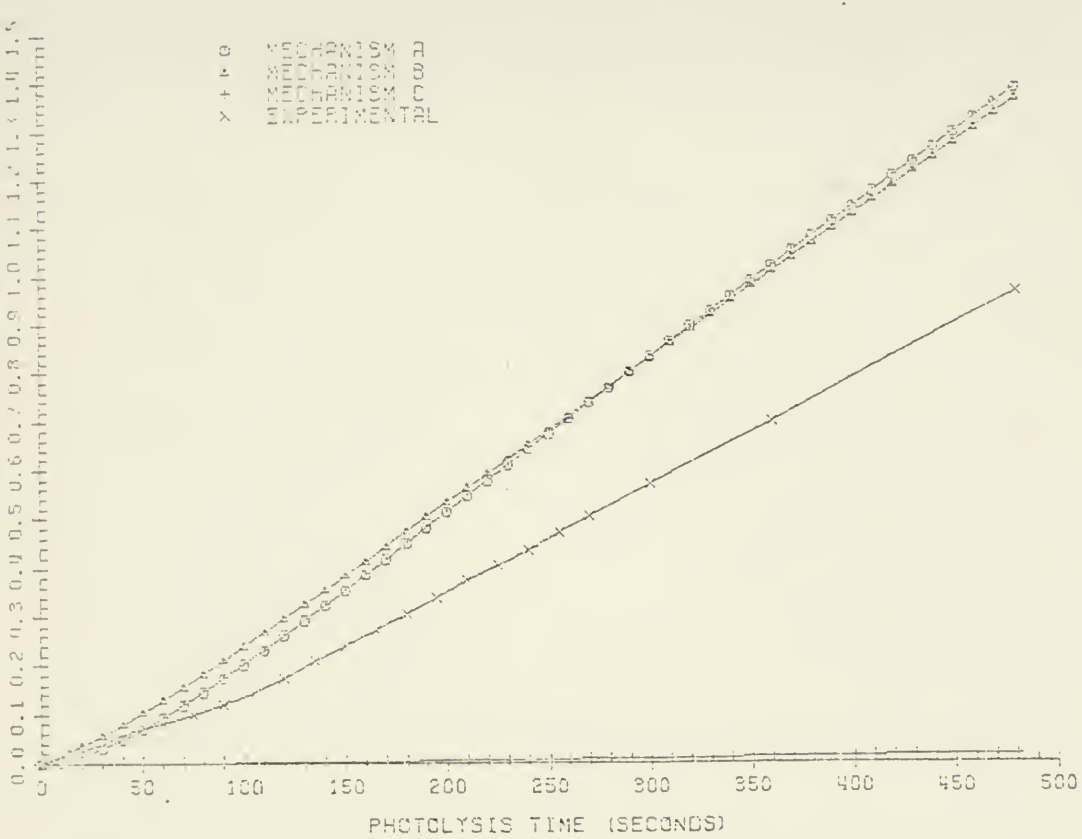

Fig. 36 Computer simulation of photolysis mechanism compared with experimental data: Production of 1,1-dibromoethane as a function of photolysis time.

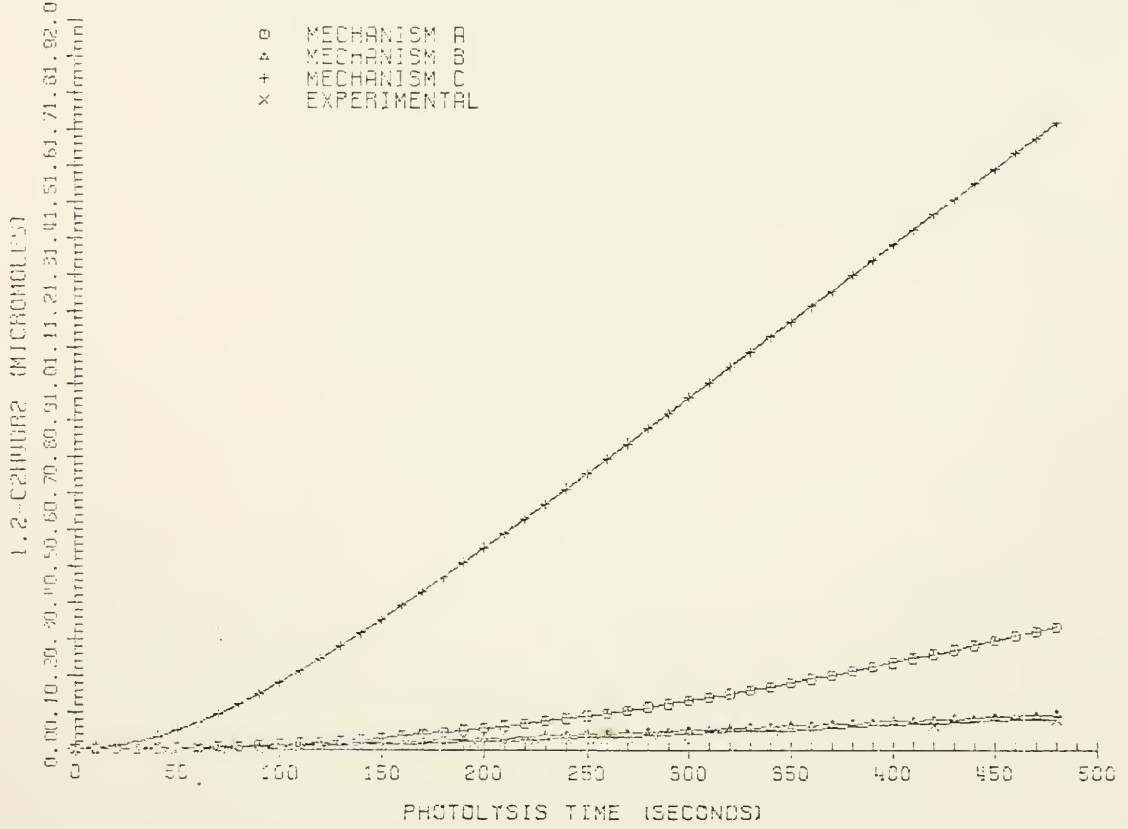

Fig. 37 Computer simulation of photolysis mechanism compared with experimental data: Production of 1,2-dibromoethane as a function of photolysis time.

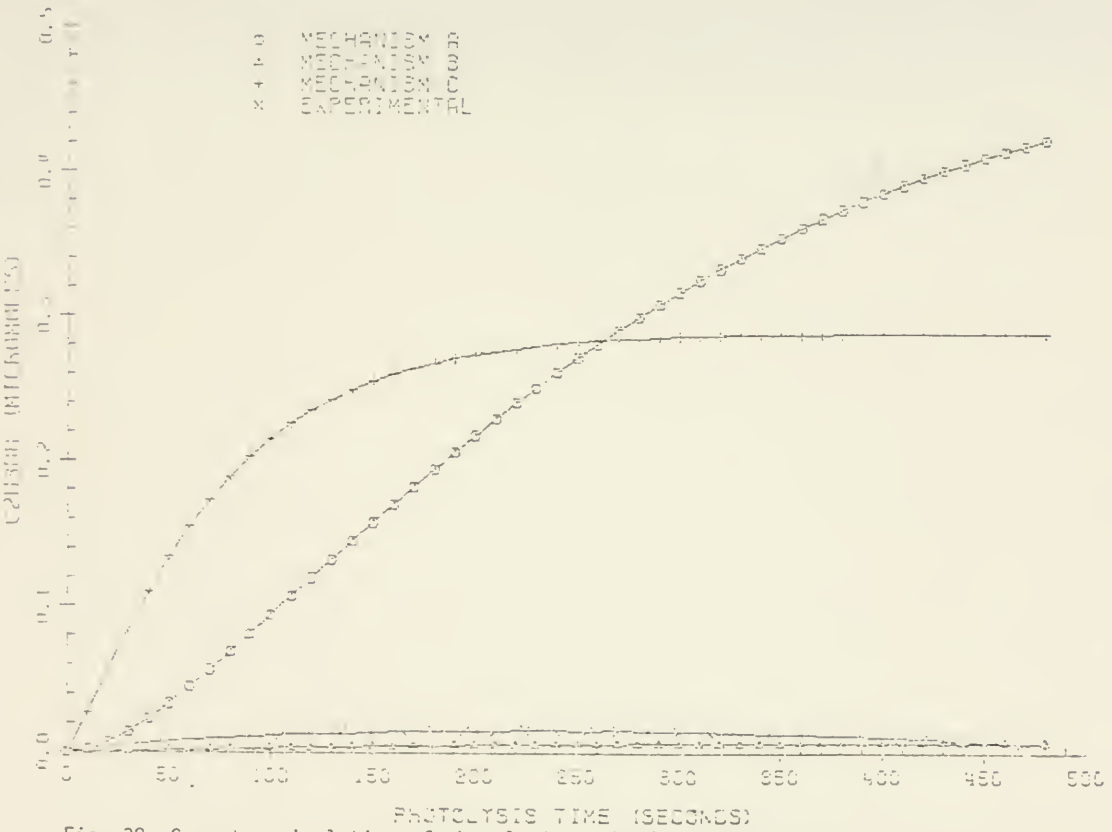

Fig. 38 Computer simulation of photolysis mechanism compared with experimental data: Production of vinyl bromide as a function of photolysis time.

Since these ionic reactions have been investigated by others (17, 15, 16, 18), the results of this work will only be dealt with briefly.

At pressures less than 100 microns only primary $C_2H_5Br^+$, Br^+, $C_2H_3^+$ and $C_2H_5^+$ are observed (Fig. 31). From 50 to 120 microns Br^+ is consumed in the charge transfer reaction, I-3. As the pressure is elevated above 100 microns, the condensation reactions I-1 and I-2 take place through a common collision complex $[C_4H_{10}Br_2^+]$. The dissociative lifetime of the collision complex has been estimated to be at least 5.4 microseconds (18). The stability of the complex is associated with the endothermicity of the proton transfer reaction leading to $C_2H_5Br_2H^+ + C_2H_4$ and the relatively inefficient and complex transfer of the ethyl cation leading to reaction I-2 (17, 18). The Br atom comes with equal probability from $C_2H_5Br^+$ and C_2H_5Br (17). The most intense ions above 140 microns are the dimeric parent ion and the diethylbromonium ion. Above 140 microns the hydrocarbons $C_2H_3^+$ and $C_2H_5^+$ undergo proton transfer reactions with C_2H_5Br in steps I-4 and I-5 to form the protonated parent ion $C_2H_5BrH^+$. The reactions appear to proceed through a transient dialkylbromononium ion (17). The protonated parent ion then reacts in step I-6 to form the diethylbromonium ion.

E. Radiolysis

The photochemical and ion-molecule studies of ethyl bromide have each provided a partial view of the chemical events which follow the passage of high energy radiation through the system. The low,

nearly monoenergetic photolysis experiments emphasized the interaction of neutral fragments while the high pressure mass spectrometry investigation considered only the role of (positively) charged fragments. The radiolytic system, however, is a diverse mixture of both ions and neutrals in various energy states.

It will be informative to correlate the elementary processes in the radiolysis with those in the photolysis and ion-molecule systems. The appropriate reaction steps which have already been discussed are post-indexed with a P for photolysis and I for ion-molecule. In the radiolysis only products whose G values are greater than 0.02 are considered significant to the radiolytic mechanism. These G values are summarized in Table 6 according to the shape of their dose-yield plots (cf Table 8).

The primary events in the photolysis are assumed to be operative in the radiolysis. In addition, it is necessary to postulate a number of competing primary reactions to account for the products observed in the radiolysis.

$C_2H_5Br \rightsquigarrow C_2H_5^{\cdot} + Br^{\cdot}$ R-1-P

$\rightsquigarrow C_2H_4 + HBr$ R-2-P

$\rightsquigarrow C_2H_2 + H_2(\text{or } 2H^{\cdot})$ R-3

$\rightsquigarrow C_2H_3Br + H_2$ R-4

$\rightsquigarrow C_2H_4Br^{\cdot} + H^{\cdot}$ R-5

$$\sim\!\!\sim\!\!\sim\!\!\rightarrow CH_3^{\cdot} + CH_2Br^{\cdot} \qquad \text{R-6-P}$$

$$\sim\!\!\sim\!\!\sim\!\!\rightarrow CH_4 + {}^{\cdot}CHBr^{\cdot} \qquad \text{R-7}$$

Some ionic fragmentation of ethyl bromide is also possible in the radiolysis. The major ions formed in the low pressure mass spectrum (75) and their relative abundances are $C_2H_5Br^+$, 100; $C_2H_5^+$, 79; $C_2H_3^+$, 69; $C_2H_2^+$, 23; $C_2H_4^+$, 16; and Br^+, 7. Only those primary ions that appear in both the low and the high pressure mass spectra are considered to be formed in the primary radiolytic events. Other ionic species seen by high pressure mass spectrometry are thought to be important as secondary processes in the radiolysis system, as discussed later.

$$C_2H_5Br \sim\!\!\sim\!\!\sim\!\!\rightarrow C_2H_5Br^+ + e^- \qquad \text{R-8}$$

$$\sim\!\!\sim\!\!\sim\!\!\rightarrow C_2H_5^+ + Br + e^- \qquad \text{R-9}$$

$$\sim\!\!\sim\!\!\sim\!\!\rightarrow C_2H_3^+ + (H_2 + Br) + e^- \qquad \text{R-10}$$

$$\sim\!\!\sim\!\!\sim\!\!\rightarrow Br^+ + C_2H_5 + e^- \qquad \text{R-11}$$

$$\sim\!\!\sim\!\!\sim\!\!\rightarrow C_2H_5^+ + Br^- \qquad \text{R-12}$$

Pair production step R-12 is very important in the region near onset (14).

Formation of negative ions and excitation of the substrate by slow electrons are also postulated in this system.

$$e^- + C_2H_5Br \longrightarrow C_2H_5\cdot + Br^- \qquad \text{R-13}$$

$$\longrightarrow C_2H_5Br^- \qquad \text{R-14}$$

$$\longrightarrow C_2H_5Br^* + e^- \qquad \text{R-15}$$

The cross section for dissociative electron capture in step R-13 is a maximum for 0.76 e.v. electrons (19, 21). Step R-13 proceeds through a compound negative ion state having a lifetime less than 10^{-13} sec. (19). As the electron affinity of ethyl bromide is 3.36 e.v. (20), the dissociative process is 9.5 kcal/mol exoergic. The non-dissociative process R-14 leading to an ion with a lifetime much greater than bond-vibration times and the autoionization process R-15 have also been observed (19, 20).

Neutralization of the positive ions $C_2H_5Br^+$, $C_2H_5^+$ and $C_2H_3^+$ by electrons, Br^- and $C_2H_5Br^-$ should produce several radicals which will be different for each species. These radicals will take part in the secondary reactions postulated below.

As in the photolysis, bromine is not observed in the pure system although it is present in the oxygenated system. Nevertheless, it is postulated to play a role in the radiolysis of the pure system in light of the results of the computer simulation of the photolysis mechanism.

Products with linear dose-yield plots: Hydrogen and ethane (Figs. 16 and 19) are produced linearly over the entire dose range investigated.

The G value for H_2 production is 1.38 in the pure system and, within experimental error, unchanged in the presence of oxygen. On

this basis, hydrogen is assumed to originate mainly by the molecular and ionic processes in steps R-3, R-4, R-5 and R-10. Some molecular hydrogen is formed in an α, β-elimination reaction (10). However, more significant may be the hydrogen elimination from a single carbon atom in an α,α- or β,β- elimination. This was the case in the far ultraviolet investigations of ethylene (76). Although it cannot be demonstrated from this study, hydrogen is assumed to arise from the unimolecular decomposition of ethylene in step R-3 rather than as part of a single primary decomposition into three fragments.

$$C_2H_5Br \rightsquigarrow C_2H_2 + HBr + H_2 \qquad \text{R-16}$$

It is relevant that acetylene and hydrogen are the major products in the ultraviolet photolysis of ethylene (76). Hydrogen is also formed in step R-10 along with bromine. Although there are no experimental data to distinguish between H_2 + Br and HBr + H, formation of the H-H bond is energetically more favorable than the H-Br bond.

Step R-5 is also proposed to contribute to the observed hydrogen yield. Although H· atoms are produced in this step, it is not incompatible with the unscavengeability of hydrogen by oxygen. In ethyl iodide the hydrogen yield was not reduced by the addition of free radical scavengers. Mass spectrometric isotope studies were interpreted to show that roughly 15% of the hydrogen was formed from translationally hot H· atoms (12). In ethyl chloride approximately 20% of the hydrogen yield was ascribed to non-thermal radical processes (10). If it is assumed, as it is probable, that the

excess translational energy of the hot H· atoms is converted within the first few collisions into vibrational energy of the substrate, which represents about 95% of the species in the oxygenated system, then there must be a thermal yield of hydrogen atoms which is commensurate with the hot yield. The fate of such thermalized hydrogen atoms is expected to be reaction with the substrate, since bond strength considerations suggest that ethyl bromide should be a good hydrogen atom scavenger.

$$H\cdot + C_2H_5Br \longrightarrow C_2H_5\cdot + HBr \qquad \text{R-17}$$

$$\longrightarrow C_2H_4Br\cdot + H_2 \qquad \text{R-18}$$

It is consistent with the above interpretation that addition of oxygen does not reduce the H_2 yield in this system. The relative importance of steps R-17 and R-18 has been determined in the liquid phase radiolysis of the alkyl bromides (77). Assuming the same H· atom reactivity in the gas phase, the ratio of the rates of hydrogen to bromine abstraction is about 0.27 for $k_{R\text{-}18}/k_{R\text{-}17}$.

In view of the results of the isotope labeling experiments in the ethyl chloride (10) and ethyl iodide (12) systems and the arguments regarding the contribution of thermal hydrogen to the hydrogen yield, it is estimated that roughly 30 to 40% of the hydrogen yield is due to radical processes. It is thus possible to assign G values to both reactions R-17 and R-18. In step R-18 the G value for hydrogen production is approximately 0.35 times the total hydrogen yield or 0.49 and the G value for step R-17 is 1.81 based on the ratio of the

rates of hydrogen to bromine abstraction, k_{R-18}/k_{R-17}. Since the sum of the acetylene and vinyl bromide yields (Table 6) in steps R-3 and R-4 must balance the corresponding hydrogen yield, the contribution of the molecular processes is 0.63 molecules/100 e.v. The amount of hydrogen formed in step R-10 must be the residual yield after the radical and molecular portions have been taken into account. Therefore, the molecular, ionic and radical contributions to the hydrogen yield are estimated to be in the ratio of 0.63 : 0.27 : 0.49 or 45% to 19% to 35%. Because the predominant hydrogen scavenger in the system is the substrate, scavenging by ethylene should not be important in the system.

Ethane is produced with a constant G value of 2.70 in the pure system and is almost completely scavenged by oxygen. In addition to the primary events and step R-17, the same secondary reactions that formed ethane in the photolysis are assumed to be occurring in the radiolysis.

$$C_2H_5^{\cdot} + HBr \longrightarrow C_2H_6 + Br^{\cdot} \qquad \text{R-19-P}$$

$$C_2H_5^{\cdot} + C_2H_5Br \longrightarrow C_2H_6 + CH_3\dot{C}HBr \qquad \text{R-20-P}$$

Ethane formation by hydrogen abstraction from the substrate in reaction R-20-P is not expected to be as important as step R-19-P at room temperature since it has an estimated activation energy of 8 to 10 kcal/mol. Hot ethyl radicals do not contribute substantially to the ethane yield, since only about 1% of the ethane was nonscavengeable by 5% added oxygen.

The butane yield is small, less than 0.02 molecules/100 e.v. Since the ratio of $k_{disproportionation}/k_{combination}$ is 0.12 (58), it

follows that the ethane yield arising from the disproportionation reaction is insignificant. Indeed, the G value for all the combination reactions leading to the C_4-compounds is only about 0,02 as calculated from the data of the minor products in Table 7. It is proposed that the butane yield is due to the back reaction of ethyl radicals with bromine.

$$C_2H_5' + Br_2 \longrightarrow C_2H_5Br + Br' \qquad \text{R-21-P}$$

It is notable that the ethane curve is linear under radiolytic conditions, but slightly convex upward in the photolysis. Presumably, the explanation must lie in the radical-scavenger reaction dynamics, but the exact interpretation is not obvious. It may be relevant that the gross rate of energy input is about 10^3 times greater in the photolysis than in the radiolysis; radical production rates and steady state concentrations would be comparably greater in the photolysis as well.

Products with convex upward dose-yield plots: Ethylene, acetylene, hydrogen bromide and bromine have dose-yield plots (Figs. 20, 18, 16 and 17) that are convex upward.

The G value for ethylene is 2,17 over most of the dose range. A short induction period is observed initially and on long dose the ethylene production gradually decreases. The effect of oxygen is to reduce the G value to 0.78 and to eliminate the induction period. The G value for acetylene is 0,31 in the pure system and nearly the same with added oxygen. A short induction period is present with

and without oxygen. Besides the molecular processes in steps R-2-P and R-3, ethylene and acetylene may be formed in ion-molecule reactions.

$$C_2H_3^+ + C_2H_5Br \longrightarrow C_2H_5Br^+H + C_2H_2 \qquad \text{R-22-I}$$

$$C_2H_5^+ + C_2H_5Br \longrightarrow C_2H_5Br^+H + C_2H_4 \qquad \text{R-23-I}$$

Since oxygen reduces the ethylene yield by 64%, radical processes must also be occurring.

$$C_2H_5\cdot + Br\cdot \longrightarrow C_2H_4 + HBr \qquad \text{R-24-P}$$

$$\cdot CH_2CH_2Br \longrightarrow C_2H_4 + Br\cdot \qquad \text{R-25-P}$$

Reaction R-24-P is 48.9 kcal/mol exoergic (61) while step R-25-P has an activation energy of 11.1 kcal/mol (5). Most of the scavengeable yield of ethylene may be attributed to these reactions.

The induction periods seen in the yields of both ethylene and acetylene may be related to the fact that both of these species are labile in the presence of bromine atoms.

$$Br\cdot + C_2H_2 \longrightarrow C_2H_2Br\cdot \qquad \text{R-26}$$

$$Br\cdot + C_2H_4 \longrightarrow C_2H_4Br\cdot \qquad \text{R-27-P}$$

However, none of the many computer simulation calculations performed for the photolysis mechanism suggested that the free radical reaction dynamics would lead to an induction period in the ethylene yield. (Acetylene is not formed in the photolysis.) In agreement with experimental results, the computations did show that the ethylene

yield should fall off as an experiment proceeds. In fact, all of the important unsaturated species show an induction period under radiolysis since the effect is also seen for vinyl bromide. In general, the induction period effect would require a production process which grows in importance as an experiment continues, or a consumption which falls off. In the case of the olefin yields, the relevant processes must be unique to the radiolysis since neither vinyl bromide nor ethylene shows induction periods under photolysis. Since none of the primary or secondary processes which occur only in the radiolysis appear to have the necessary consequences on the olefin yields, it is tentatively concluded that these induction effects are due to traces of reactive species (possibly OH· or O·) ejected from the vessel walls under gamma radiolysis.

With a low-dose G value of 3.89 in the pure system, hydrogen bromide is the major product in the radiolysis. Oxygen augments G(HBr) to 4.89. In addition to the molecular elimination process in step R-2-P, and the secondary radical reactions in steps R-17 and R-24-P, hydrogen bromide is assumed to arise from radical and ion-molecule reactions in steps R-28-P and R-29-I.

$$Br\cdot + CH_3\dot{C}HBr \longrightarrow C_2H_3Br + HBr \qquad \text{R-28-P}$$

$$C_2H_5Br^+H + C_2H_5Br \longrightarrow C_2H_5Br^+C_2H_5 + HBr \qquad \text{R-29-I}$$

It is also expected that Br· atom attack on the substrate occurs in the radiolysis as well as in the photolysis.

$$Br^{\cdot} + C_2H_5Br \longrightarrow \dot{C}H_3CHBr + HBr \qquad \text{R-30-P}$$

As discussed in the photolysis, hydrogen bromide is assumed to interact with the wall through a process similar to reaction R-31-P.

$$HBr + \text{wall} \longrightarrow HBr\text{-wall} \qquad \text{R-31-P}$$

Again as in the photolysis, the hydrogen bromide production reaches steady state (Fig. 16). Added oxygen prevents the radicals from reacting with HBr and so its dose-yield plot is linear. Additional HBr may be produced by oxygen containing compounds as described in the photolysis.

Although bromine was not observed in the pure system, it is assumed to be present.

$$Br^{\cdot} + Br^{\cdot} + M \longrightarrow Br_2 + M \qquad \text{R-32-P}$$

Evidence in support of this assumption in part comes from the computer simulation of the photolysis mechanism (Sec. IV-C) and is in addition discussed in Sec. IV-B. In the oxygenated system, the initial G value for bromine production, 2.4, is substantial for reasons similar to those mentioned in Sec. IV-B.

Ion-molecule reactions such as step R-33-I also contribute to the supply of bromine atoms.

$$Br^{+} + C_2H_5Br \longrightarrow C_2H_5Br^{+} + Br \qquad \text{R-33-I}$$

Products with concave upward dose-yield plots; Methane, methyl bromide, bromoform, 1,1-dibromoethane, 1,2-dibromoethane and vinyl bromide have dose-yield plots (Figs. 18, 21, 22, and 17) that are concave upward. It is assumed that the production of all of these products are directly or indirectly dependent on the relative concentrations of hydrogen bromide and bromine.

The formation of methane is assumed to occur in steps R-34-P and R-35-P.

$$CH_3\cdot + C_2H_5Br \longrightarrow CH_4 + CH_3\dot{C}HBr \qquad \text{R-34a-P}$$

$$\longrightarrow CH_4 + \cdot CH_2CH_2Br \qquad \text{R-34b-P}$$

$$CH_3\cdot + HBr \longrightarrow CH_4 + Br\cdot \qquad \text{R-35-P}$$

The activation energies for these reactions are estimated to be about 6.6 and 1.5 $\pm$ 1 kcal/mol respectively (64). Since the shape of the dose-yield curve of methane exhibits an induction period, reaction R-35-P must be of substantial importance compared to reaction R-34-P. Some methyl radicals must be formed in hot reactions since 30% of the methane yield is unscavenged by 5% oxygen. However, since ethyl radicals are almost completely scavenged in both the radiolysis and photolysis, whereas there is a much larger amount of nonscavengeable methane in the radiolysis, some methane must also be formed in reaction R-7.

Methyl radicals are depleted in reaction R-36-P to form methyl bromide.

$$CH_3\cdot + Br_2 \longrightarrow CH_3Br + Br\cdot \qquad \text{R-36-P}$$

Some $CH_2Br\cdot$ is converted to methylene bromide in a reaction analogous to 36-P. The G value of this product is quite small, about 0.007. It is assumed that the concave upward form of the methane and methyl bromide dose-yield plots is due to the importance of reactions R-35-P and R-36-P in that the rate of methane and methyl bromide formation depend upon the relative concentrations of HBr and Br_2.

Bromoform probably comes about via reaction R-37.

$$\cdot CHBr\cdot + Br_2 \longrightarrow CHBr_3 \qquad \text{R-37}$$

Since about 56% of bromoform is scavenged by oxygen, it must be formed in part by hot processes.

The G value of C-C bond breakage may be roughly estimated to be 0.09 from one half of the sum of the 100 e.v. C_1 yields in the dose range of 1.0×10^{20} to 1.5×10^{20} e.v./gram. Since $G(-C_2H_5Br)$ is 6.31 in this dose range, about 1.4% of all ethyl bromide molecules consumed undergo C-C bond fission.

The G value of 1,1-dibromoethane is about 6 times larger than that of 1,2-dibromoethane presumably as a result of the same set of reactions as discussed for the photolysis.

$$CH_3\dot{C}HBr + HBr \longrightarrow CH_3CH_2Br + Br\cdot \qquad \text{R-38-P}$$

$$\cdot CH_2CH_2Br + HBr \longrightarrow CH_3CH_2Br + Br\cdot \qquad \text{R-39-P}$$

$$CH_3\dot{C}HBr + Br_2 \longrightarrow CH_3CHBr_2 + Br\cdot \qquad \text{R-40-P}$$

$$\cdot CH_2CH_2Br + Br_2 \longrightarrow CH_2BrCH_2Br + Br\cdot \qquad \text{R-41-P}$$

In the gas phase radiolysis of ethylene and hydrogen bromide, ethyl bromide is formed with an ion-pair yield of 10^5. The high ethyl bromide yield is accounted for in part by reaction R-39-P (62).

Oxygen inhibits almost completely the 1,1-dibromoethane formation in accordance with the proposed radical mechanism. In contrast to this effect, for reasons detailed in the discussion of 1,2-dibromoethane and methyl bromide in the photolysis, oxygen amplifies their yields dramatically.

Because of the shape of the vinyl bromide dose-yield plot and the large concentration of the nonpropagating radical $CH_3\dot{C}HBr$, this radical is assumed to be the precursor to vinyl bromide.

$$CH_3\dot{C}HBr + Br\cdot \longrightarrow CH_2CHBr + HBr \qquad \text{R-42-P}$$

There are no data on the activation energy for reacton R-42-P; however, it is evidently quite exoergic.

The existence of a large hydrogen yield suggests that vinyl bromide is also formed directly from ethyl bromide in step R-4. Because of the sensitivity of vinyl bromide to high concentrations of HBr and bromine, the suppression of vinyl bromide by oxygen does not exclude the possibility of step R-4.

Steps R-48-P and R-44-P compete, as in the photolysis, for the 1-bromo-1-ethyl radical. Step R-44-P leads to 1,2-dibromoethane.

$$CH_3\dot{C}HBr + Br_2 \longrightarrow CH_3CHBr_2 + Br\cdot \qquad \text{R-43-P}$$

$$CH_2Br\dot{C}HBr + HBr \longrightarrow CH_2BrCH_2Br + Br\cdot \qquad \text{R-44-P}$$

F. Comparison of Photolysis and Radiolysis

Table 14 presents the relative yields of the major and semi-major products formed in the radiolysis and photolysis of ethyl bromide at 100 torr. Ethane and hydrogen bromide are clearly the two main products in both systems. A comparison of the relative yields of hydrogen, ethylene, acetylene and vinyl bromide will indicate that the processes that lead to their formation in the radiolysis play only a minor or negligible role in the photolysis. It may also be concluded from the relative yields of methane and methyl bromide that the carbon-to-carbon bond rupture in the radiolysis is significantly more probable, approximately 10-fold, than in the photolysis. In the radiolysis, the ratio of the yields of 1,1-$C_2H_4Br_2$ to 1,2-$C_2H_4Br_2$ is approximately 6, while in the photolysis it is about 12. As is apparent from their small yields, bromoform and 1,1,2-tribromoethane play only a secondary role in both systems.

There are several primary processes postulated in the radiolysis which could also be primary processes in the photolysis; however, theory does not support complex primary processes in the photochemistry of "simple" molecules such as ethyl bromide. Thus in the photolysis the unscavengeable methane yield and the vinyl bromide production were attributed only to secondary processes. Traditionally in radiation chemistry such processes may be postulated as primary events. Even with a molecule as "simple" as ethyl bromide, a vertical transition may lead to a state where there are many complex crossings of energy surfaces. The parallel behavior between the radiolysis

Table 14

Relative Product Distribution of the Major and Semimajor Products from the Radiolysis and Photolysis of Ethyl Bromide Vapor at 100 Torr

Products[a]	Pure Radiolysis				Pure Photolysis			
	Absorbed dose/gram x 10^{-20}				Photolysis time (minutes)			
	0-0.5	1.0-1.5	3.5-4.0	6.0-7.0	0-0.5	1.0-1.5	3.5-4.0	6.0-7.0
Convex upward								
HBr[b]	1.64	1.64	≃0	≃0	0.90	0.65	0.54	≃0
C_2H_4	0.45	0.80	0.77	0.32	0.07	0.07	0.07	≃0
C_2H_4	0.06	0.11	0.11	0.05	(c)	(c)	(c)	(c)
1,1,2-$C_2H_3Br_3$	0.00	0.00	0.00	0.00	(c)	0.01	0.01	0.01
Concave upward								
CH_4	0.03	0.03	0.10	0.10	0.00	0.00	0.01	0.01
CH_3Br	0.03	0.03	0.09	0.09	(c)	0.00	0.01	0.01
C_2H_3Br[d]	0.12	0.12	0.28	0.28	0.04	0.02	≃0	-0.02

1,1-$C_2H_4Br_2$	0.33	0.33	0.61	0.07	0.26	0.26	0.70	0.70
1,2-$C_2H_4Br_2$	0.04	0.04	0.11	0.11	0.00	0.02	0.06	0.07
$CHBr_3$	(c)	0.00	0.00	0.01	0.00	0.00	0.00	0.00
Linear								
H_2	0.51	0.51	0.51	0.51	(c)	(c)	(c)	(c)
C_2H_6[e]	1.00	1.00	1.00	1.00	1.00	1.00	1.00	1.00

[a]All values given in Table 14 were determined from the yields listed in Tables 6 through 8. The relative yields of all products not included in this table are less than 0.01.

[b]The gamma irradiated ethyl bromide was at 300 torr.

[c]The compound was not detected.

[d]C_2H_3Br is concave upward in the radiolysis but convex upward in the photolysis.

[e]C_2H_6 is linear in the radiolysis but convex upward in the photolysis.

and photolysis seems to suggest many independent reaction channels common to both. Within the format of radiation chemical interpretation, the results strongly suggest a diversity of primary processes in the radiolysis and the same evidence exists for the photolysis and points to a diversity of primary processes there too.

All secondary processes occurring in the photolysis must also occur in the radiolysis. Indeed, the forms of the photolysis and radiolysis dose-yield plots are analogous with the exception of vinyl bromide and ethane. However, there may be ionic secondary processes in the radiolysis which are not possible in the photolysis.

In view of the results of the computer simulation work, it seems probable that the difference between the linear dose-yield plot seen in the radiolysis and the convex upward form seen in the photolysis is adequately accounted for by secondary reactions involving HBr, Br_2, ethyl bromide substrate, labile olefinic products, and various free radical intermediates, as shown in Figs. 32 through 38 and listed in Table 13. With certain choices of rate constants and primary yields, curved graphs resembling the photolysis results were seen. Many other combinations of parameters gave straight-line plots, as in the radiolysis.

G. Comparison of the Gas Phase Radiolysis of Ethyl Chloride, Ethyl Bromide and Ethyl Iodide

A comparison of the radiation chemistry of ethyl chloride, ethyl bromide and ethyl iodide is of interest in understanding the

effects of the different halogens on the chemical kinetics. G values for the ethyl halide systems are presented in Table 15. Pertinent kinetic data on activation and bond energies are compiled in Table 16 for convenience.

On the basis of bond energy arguments, it is possible to predict the relative amounts of C-X (X=Cl, Br or I), C-H and C-C bond rupture in the primary event for the three alkyl halide systems. The probability of C-X bond fission is smallest for ethyl chloride and largest for ethyl iodide because of the differences in the carbon-halogen bond energies. To the extent that the C-X bond is much weaker than the C-H bond, the C-X bond breaks preferentially. Thus there is more C-I than C-H bond breakage. In ethyl chloride the C-Cl and C-H bond energies are much closer than in ethyl iodide and so the probabilities of C-Cl and C-H bond fission are expected to be more nearly equal. Thus more C-H bond rupture is anticipated in ethyl chloride than in ethyl bromide and still less in ethyl iodide. The probability of C-C bond scission is greatest in ethyl chloride and least in ethyl iodide. The C-Cl bond is energetically equivalent to a C-C bond, whereas in ethyl iodide the C-C bond is substantially stronger, by about 30 kcal/mol, than the C-I bond.

From the experimental data (Table 6) it is possible to estimate the amount of single bond rupture in the primary event in ethyl bromide. The G value for C-C bond rupture is about 0.09 as determined earlier. Ignoring the contribution of possible secondary reactions, an upper limit for the G value of the primary C-H bond fission is

Table 15

Comparison of G Values in Radiolysis of Pure Ethyl Chloride, Ethyl Bromide and Ethyl Iodide

Product	Ethyl Chloride		Ethyl Bromide	Ethyl Iodide
	Hughes & Tiernan[a]	Schindler[b]	This Work[c]	Schindler[d]
HX	(0.37(?))[e]	4.5± 10%	4.42	(f)
X_2	(f)	(f)	(g)	(f)
H_2	4.41	2.44	1.39	0.73
CH_4	1.09	0.24	0.26(0.08)	0.02
CH_3X	(f)	0.05	0.24(0.08)	≃0.02
CH_2X_2	(f)	0.06	≃0.01	≃0.05
CHX_3	(f)	(f)	0.03(0.01)	(f)
C_2H_6	2.40	2.11(1.4)	2.70	1.34
C_2H_4	4.08	2.06	2.17	1.57
C_2H_2	1.72	0.75	0.31	0.48
C_2H_3X	(f)	0.66	0.75(0.32)	≃0.04
1,1-$C_2H_4X_2$	(f)	(f)	1.66(0.88)	0.2
1,2-$C_2H_4X_2$	(f)	(f)	0.31(0.12)	"negligible"
1,1,2-$C_2H_3X_3$	(f)	(f)	≃0.01	(f)
1,2-$C_3H_6X_2$	(f)	{0.05}	0.01	(f)
1,3-$C_3H_6X_2$	(f)		<0.01	(f)
C_4H_{10}	(f)	0.10±0.03	<0.01	(g)
1-C_4H_9X	(f)	0.05	<0.01	(f)
2-C_4H_9X	1.44	0.49	<0.01	(f)
meso-2,3-$C_4H_8X_2$	{3.00}	0.76	<0.01	(f)
racemic-2,3-$C_4H_8X_2$		0.80	<0.01	(f)

Table 15 (continued)

Product	Ethyl Chloride		Ethyl Bromide	Ethyl Iodide
	Hughes & Tiernan[a]	Schindler[b]	This Work[c]	Schindler[d]
1,3-$C_4H_8X_2$	0.47	0.35	<0.01	(f)
1,4-$C_4H_8X_2$	(f)	0.03	<0.01	(f)

[a]Reference 11.

[b]Reference 10

[c]The major products are listed in Table 6 and the minor ones are presented in Table 7.

[d]Reference 12

[e]This G value for HCl was not experimentally determined but was calculated using the material balance relationship given on page 433 in the reference listed in a.

[f]The G value is not reported.

[g]The product was not observed in the pure system.

Table 16

Bond and Activation Energies for the Ethyl Halides

Bond Energies (kcal/mol)[a]

E(bond) X=	Cl	Br	I
$E(C_2H_5\text{-}X)$	83	68	52
E(H-X)	103.1	87.4	71.4
E(X-X)	57.87	46.08	46.06

$E(CH_3CHX\text{-}H) \simeq 95$[b]

$E(CH_3\text{-}CH_3) \simeq 83$[a]

Activation Energies (kcal/mol)

Reactions X=	Cl	Br	I
$X^{\cdot}+C_2H_5X \longrightarrow C_2H_4X^{\cdot}+HX$	<1[c]	13[d]	20[e]
$HX+C_2H_5^{\cdot} \longrightarrow C_2H_6 + X^{\cdot}$	3 ± 2[c]	2[f]	1 ± 1[e]
$^{\cdot}CH_2CH_2\text{-}X \longrightarrow C_2H_4 + X^{\cdot}$	22.2[g]	11.1[g]	6 ± 2[e]

[a]Reference 56.

[b]Estimated value for the ethyl halides.

[c]Reference 10.

[d]Reference 61.

[e]Estimated value on the basis of the reactions involving the $Br^{\cdot}$ and $Cl^{\cdot}$ radicals.

[f]Reference 57.

[g]Reference 5.

$G(1,1\text{-}C_2H_4Br_2) + G(1,2\text{-}C_2H_4Br_2) = 1.00$. Also assuming that all ethyl radicals formed in the primary event are converted to ethane, a lower limit for the G value of the primary C-Br bond scission is $G(C_2H_6) = 2.70$. Similar estimates have been made in the ethyl chloride (10) and ethyl iodide (12) systems. The probability of single bond rupture in the primary event can be represented roughly by the ratios:

	$C_2H_5\text{-}X$	:	$C_2H_4X\text{-}H$	:	$CH_3\text{-}CH_2X$
Cl	1.00		1.3		0.2
Br	1.00		0.4		0.03
I	1.00		0.06		0.01

The trends of these ratios are in agreement with the predictions based on bond energies.

Also because of the difference in the bond energies of H-X and C-X, hydrogen abstraction from $C_2H_4X\text{-}H$ is exoergic for the Cl· radical, slightly endoergic for the Br· radical and very endoergic for the I· atom. At room temperature the activation energy for hydrogen abstraction by I· is too high for thermal reaction and so the I· atom recombines as I_2 via the reaction $I\cdot + I\cdot + M \longrightarrow I_2 + M$. To a lesser extent, Br· accumulates as Br_2. Thus it is expected that for a given amount of sample, $[I_2] > [Br_2] > [Cl_2]$.

On the basis of only C-X bond fission in the primary event, the G value for the formation of ethane might be expected to be largest for ethyl iodide compared with the other systems; however, the efficient back reaction of the ethyl radical with I_2 results

in ethyl iodide having the smallest ethane yield in the ethyl halides. Back reactions in ethyl iodide are more important than in ethyl bromide and still more important than in ethyl chloride. Because of the larger number of ethyl radicals produced in the primary event and the lower activation energy for the reaction : $HX + C_2H_5^{\cdot} \longrightarrow C_2H_6 + X^{\cdot}$ in ethyl bromide, the ethane yield is larger in this system than in ethyl chloride.

For the same reasons that the primary $H^{\cdot}$ atom yield is larger in ethyl chloride than in ethyl bromide and ethyl iodide, the H_2 elimination is also expected to be more important. Furthermore, because of the relative magnitudes of the C-X bond strengths in the alkyl halides, halogen abstraction by thermal hydrogen is most prevalent in ethyl iodide and least likely in ethyl chloride. Consequently, the ratio of the rate of halogen to hydrogen abstraction from the substrate by thermal $H^{\cdot}$ atoms is in the direction $C_2H_5I > C_2H_5Br > C_2H_5Cl$. Thus, both the primary and secondary hydrogen yields are largest in ethyl chloride and smallest in ethyl iodide.

Relative to ethyl bromide and ethyl iodide, the number of $C_2H_4X^{\cdot}$ radicals formed in the primary event and in secondary reactions, due to the ability of $Cl^{\cdot}$ to abstract $H^{\cdot}$ atom from the substrate, are larger in ethyl chloride. Furthermore, because of the relatively low concentrations of the $Cl^{\cdot}$ and/or Cl_2 species and the high activation energy to unimolecular decomposition, the chloroethyl radicals will mainly recombine either with themselves or with ethyl radicals to produce the large quantities of C_4-chlorinated compounds. In ethyl iodide, the yields of C_4-halogenated compounds are expected to

be less than in the other two systems because of the relatively large concentration of I_2 molecules and the low probability of H· atom abstraction from the substrate by I· atoms. Thus, as would be anticipated the G values for the C_4-chlorinated compounds are larger than the G values for the C_4-brominated and iodated compounds. The total G value for recombination of monochloroethyl radicals is about 194 times greater than for the recombination in the brominated system. Again, because of the low concentrations of Cl· and/or Cl_2, butane is observed in the ethyl chloride system and is only minor or negligible in the ethyl bromide and ethyl iodide systems.

On the basis of the amount of C-C bond fission and the concentrations of X and/or X_2 and C_2H_4X· radicals, the G values for the C_3-compounds are expected to be largest in ethyl chloride and smallest in ethyl iodide.

As the yields of the C_4-halogenated compounds are large in ethyl chloride, so are the G values for the C_2-dihalogenated compounds in ethyl bromide and ethyl iodide. Because of the larger number of X and/or X_2 species in ethyl bromide and ethyl iodide, they can react with C_2H_4X· and C_2H_5· before the radicals can recombine to form C_4 compounds. The G values for the C_2-dihalogenated compounds are larger in ethyl bromide than in ethyl iodide because of the greater number of C_2H_4X· radicals formed in the primary and secondary reactions and the higher activation energy for $HX + C_2H_4X\cdot \longrightarrow C_2H_5X + X\cdot$ in the brominated system.

On the basis of the difference in the C-X and C-H bond energies, H-X elimination is expected to be greatest in ethyl chloride and least in ethyl iodide. The primary ethylene yield should parallel the trend occurring with HX elimination. It should be pointed out, however, that it may not be possible to correlate the molecular HX yield with the unscavengeable ethylene yield in light of the work on the radiolysis of ethyl chloride (10, 11). The effect of added oxygen is to reduce the C_2H_4 yield relatively more than other free radical scavengers (11, Fig. 1 in ref 10). Thus the G value for the unscavengeable ethylene yield represents only a lower limit to the splitting out of molecular HX.

The contribution of molecular processes in the primary event can be estimated from the results of free radical scavenger experiments. In ethyl bromide, the G value for methane formed from nonradical processes is approximately the same as for bromoform, 0.01. Similarly the G value for vinyl bromide arising from molecular processes is 0.32. Since the ethylene yield in the presence of O_2 is 0.78 molecules/100 e.v., the total G value for molecular processes is roughly $G(C_2H_4) + G(C_2H_2) + G(CH_4) + G(C_2H_3Br) + G(H_2) \geq 2.32$. Also in this dose range, 1.0×10^{20} to 1.5×10^{20} e.v./gram, the G value for the ethyl bromide consumption is 6.31. Thus, approximately 37% or more of all primary events are molecular. Schindler estimates that 50% of the processes in ethyl chloride (10) are molecular whereas in ethyl iodide (12) only about 33% are molecular.

H. Summary

The results of this study and the conclusions drawn from them are summarized as follows:

1. Photolysis

The photolysis of ethyl bromide was studied at 100 torr and 23°C using 253.7 nm radiation. In the pure system between 60 and 90 sec. at an absorbed light intensity of 7.7×10^{15} quanta/sec. the major photolytic products and their respective quantum yields are as follows: hydrogen bromide, 0.26; ethane, 0.40; ethylene, 0.028; 1,1-dibromoethane, 0.102; 1,2-dibromoethane, 0.0092; vinyl bromide, 0.009; 1,1,2-tribromoethane, 0.0027; methane, 0.0052; and methyl bromide, 0.00091. When 5 mole % oxygen is added, the quantum yields in this time period become the following: hydrogen bromide, 0.47; ethane, 0.00032; ethylene, 0.0081; 1,1-dibromoethane, 0.0040; 1,2-dibromoethane, 0.022; vinyl bromide, 0; 1,1,2-tribromoethane, 0; methane, 0.0001; and methyl bromide, 0.091. In addition, bromine is observed in the presence of oxygen and has a quantum yield of 0.22.

Ethane, hydrogen bromide and 1,1-dibromoethane are the three main products in the photolysis of the pure compound. Ethylene represents only about 3% of the total product yield.

The product distribution indicates that the major primary event is carbon-halogen bond rupture. Also some ethylene is formed during the molecular elimination of HBr. However, it may not be possible to quantitatively correlate the yield of unscavengeable ethylene with the

extent of HBr elimination in light of radical scavenging work carried out in the ethyl chloride system (10, 11). In that system oxygen was found to decrease ethylene more than other free radical scavengers (11, Fig. 1 in ref 10). Accordingly, the yield of unscavengeable ethylene in ethyl bromide probably represents a lower limit for the yield of the molecular process. Carbon-carbon bond rupture is of minor importance in the primary event.

The 1,1-dibromoethane yield is about 12 times larger than the 1,2-dibromoethane yield and is almost completely scavenged by oxygen. The radical precursor to the 1,1-dibromoethane is proposed to be the 1-bromo-1-ethyl radical. This radical probably originates from α-hydrogen abstraction from the substrate by several species including the ethyl radical and the bromine atom.

Computer simulation of the photolysis reaction mechanism indicates that the 2-bromo-1-ethyl radical can adequately be accounted for by the addition of bromine atoms to ethylene. Because this reaction produces an excess of the 2-bromo-1-ethyl radical, it is proposed that the 2-bromo-1-ethyl radical isomerizes to form the 1-bromo-1-ethyl radical.

Furthermore, the computer simulation strongly supports the assumption that bromine is present at steady state in the pure system and is playing an important role in the reaction mechanism.

The vinyl bromide yield is essentially eliminated in the presence of oxygen. Although this result could be due either to oxygen scavenging or to reaction involving Br_2, which is formed in the presence of oxygen, it is proposed that vinyl bromide does arise from secondary

radical processes. The 1,1,2-tribromoethane is presumed to result from the bromination of vinyl bromide through radical processes.

2. Ion-Molecule Studies

In the high pressure mass spectrometry of ethyl bromide with 100 e.v. electrons, the dimeric parent ion and the diethylbromonium ion are the principal ionic species. The secondary ionic reactions studied under conditions of high pressure mass spectrometry are presumed to occur in the radiolysis as well.

3. Radiolysis

The gamma radiolysis of ethyl bromide was studied at 100 torr and 23°C. In the pure system between an absorbed dose of 1.0×10^{20} and 1.5×10^{20} e.v./gram the major products and their respective G values are as follows: hydrogen bromide, 3.89; ethane, 2.70; ethylene, 2.17; acetylene, 0.31; hydrogen, 1.39; 1,1-dibromoethane, 0.88;1,2-dibromoethane, 0.12; vinyl bromide, 0.32; methane, 0.0831; methyl bromide, 0.080; and bromoform, 0.0078. When oxygen is added, the G values in this dose range become the following: hydrogen bromide, 4.89; ethane, 0.31; ethylene, 0.78; acetylene, 0.27; hydrogen, 1.38; 1,1-dibromoethane, 0.028; 1,2-dibromoethane, 0.56; vinyl bromide, 0; methane, 0.03; methyl bromide, 0.32; and bromoform, 0.0034. In addition, bromine is observed in the presence of oxygen and has a G value of 2.4.

The presence of hydrogen and acetylene in the radiolysis indicates that they must be formed from higher energy processes not

accessible in the photolysis, On the basis of the product distribution, the probability of single bond rupture in the primary event can be represented roughly by the ratio: C_2H_5-Br; C_2H_4Br-H;CH_3-CH_2Br = 1.00: 0.40: 0.06.

Under the assumption that the unscavengeable ethylene yield can be correlated with the HBr elimination reaction, it is possible to estimate that roughtly 37% of the primary processes are molecular. This is compatible with estimates of molecular processes in ethyl chloride, about 50% (10), and ethyl iodide (12), about 33%.

The similarity of the forms of the dose-yield plots suggest that all secondary processes in the photolysis occur in the radiolysis as well.

Differences in the gas phase radiolysis of the ethyl chloride, ethyl bromide and ethyl iodide systems can largely be explained by differences in the energetics of analogous elementary processes in the respective reaction systems.

APPENDIX

```
C       REACTION MECHANISM PROGRAM WITH STEADY STATE ROUTINES
        DIMENSION AK(30),C(20),CPDNAM(20),D(30),DATE(2) ,HEADER(10)
        DIMENSION ISS(9),JRE(30,4),JSS(9,30),JTENTY(8),TDLCPD(8)
        DIMENSION TBLH(8),DL(30),EQUAT(6),PROBLM(12)
C       TO CHANGE DIMENSIONS-
C       AK(MXR),C(MXCPDS),CPDNAM(MXCPDS),D(MXR),ISS(MXSTST),
C       JSS(MXSTST,MXAPP),JTENTY(MXTUNT),JRE(MXR,4)
C       TDLCPD(MXTBNT),TBLH(MXTBNT),DL(MXR)
C       DEFINITIONS OF VARIABLES
C       AK(N)    RATE CONSTANT FOR EQUATION N (LATER CONST*DT)
C       C(K)    CONCENTRATION OF COMPOUND K
C       CPDNAM(K)  NAME OF COMPOUND K
C       CSSTOT   IF A NUMBER IS PUNCHED HERE, SS CONCS. ARE HELD CONSTANT
C       D(N)    REACTION DECREMENT
C       DAMP     STEADY STATE CALCULATION DAMPING FACTOR
C       DL       VALUE OF D AT PREVIOUS INTERVAL
C       DT       INCREMENT OF TIME
C       EQUAT    TEMPORARY ARRAY FOR WRITING EQUATIONS
C       ISS(K)  NUMBER OF APPEARANCES OF SS K
C       JRE(N,J)    C-ARRAY INDEX FOR REACTIONS AND PRODUCTS
C       JTENTY(I)   COMPOUND INDEX FOR ITH TABLE ENTRY
C       JSS(K,I)    EQUATION NUMBER FOR ITH APPEARANCE OF SS
C                   COMPOUND. JSS IS + IF K IS PRODUCT, -IF REACTANT
C       NCPCAT      INDEX NO. OF CPD. THAT CATALYZES REACT. NRCAT
C       NCPDS       TOTAL NUMBER OF COMPOUNDS
C       NI          NUMBER OF ITERATIONS PER PRINT INTERVAL
C       NP          NUMBER OF PRINT INTERVALS
C       NR          NUMBER OF REACTIONS
C       NRCAT       REACTION CATALYZED BY NCPCAT
C       NREPSS      NO. OF ITERATIONS IN STEADY STATE ADJUSTMENT
C       NSS         NUMBER OF STEADY STATE COMPOUNDS
C       NTENT       NUMBER OF TABLE ENTRIES (MAX.MXTBNT)
C       TDLCPD(I)   CONCENTRATION ENTRY FOR ITH TABLE ENTRY
C       TBLH(I)     HEADER FOR ITH COMPOUND IN TABLE
        MXAPP = 30
        MXCPDS = 20
        IQ79=0
        MXR = 30
        MXSTST = 9
        MXTBNT = 8
        DAMP = 0.7
        READ (5,7000) BL
 7000 FORMAT ( A4)
C       ZERO JRE, ISS, JSS, AND BLANK TBLH
     5  DO 10 N=1,MXR
        DO 10 J = 1,4
    10  JRE(N,J) = 0
    12  DO 15 J=1,MXSTST
    13  ISS(J) = 0
    14  DO 15 I = 1,MXAPP
    15  JSS(J,I) = 0
        DO 17 J=1,MXTBNT
    17  TBLH(J) = BL
C       THERE ARE 10 READ STATMENTS, SOME REQUIRE MORE THAN
C       ONE CARD. ALL ARE MARKED WITH ASTERISKS.
C       ********1
    20  READ (5,8000) DATE, HEADER
  8000  FORMAT (12A4)
    25  WRITE (6,9000) HEADER, DATE
  9000  FORMAT ('1',///////////,12A4,/)
C       READ THE INDEX TOTALS AND CATALYZED REACTION SPECS.
C       ********2
    30  READ (5,8010) NCPDS, NSS, NR, NRCAT, NCPCAT
  8010  FORMAT (14(I3,3X))
C       CHECK NCPS, NSS, NR, TO PREVENT OVERRUN OF DIMENSIONS
    31  IF (NCPDS-MXCPDS) 35,35,32
    32  NCPDS = MXCPDS
    33  WRITE (6,9001)
  9001  FORMAT (' ',' TOO MANY COMPOUNDS')
    35  IF (NSS-MXSTST) 39,39,36
    36  NSS = MXSTST
    37  WRITE (6,9002)
  9002  FORMAT (' ',' TOO MANY SS COMPOUNDS')
    39  IF (NR-MXR) 45,45,40
    40  NR=MXR
    41  WRITE (6,9003)
  9003  FORMAT (' ',' TOO MANY REACTIONS')
C       READ COMPOUND NAMES
C       ********3
    45  READ (5,8020) (CPDNAM(K),K=1,NCPDS)
  8020  FORMAT (7(A4,4X))
C       ** BE SURE TO LIST STEADY STATE COMPOUNDS FIRST **
C       READ THE JRE(N,I) VALUES JRE(N,1), JRE(N,2), ARE C IN-
```

```
C       DEXES OF REACTANTS (0 OR BLANK FOR JRE(N,2) IF JUST
C       ONE REACTANT) WHILE JRE(N,3) AND JRE(N,4) REFER TO
C       PRODUCTS. NO PROVISION FOR MORE THAN 2 REACTANTS OR
C       PRODUCTS.
   50 DO 77 N = 1,NR
C       IF THERE ARE SS COMPOUNDS, SET UP CALCULATION ARRAY.
C       ******* A
   52 READ (5,8010) (JRE(N,I),I=1,4)
   53 IF (NSS) 77,77,54
   54 DO 75 I = 1,4
   55 IF (JRE(N,I)) 75,75,56
C       FIRST DETERMINE WHETHER THE COMPOUND IS SS
   56 IF (JRE(N,I) - NSS) 58,58,75
   58 J = IABS (JRE(N,I))
C       NEXT DETERMINE HOW MANY TIMES THIS SS HAS APPEARED
C       BEFORE AND ASSIGN SERIAL NO. FOR PRESENT APPEARANCE.
   60 IS = ISS(J) +1
   61 ISS(J) = IS
C       TEST TO PREVENT OVERRUNNING DIMENSIONS OF JSS
   63 IF (IS - MXAPP) 67,67,64
   64 ISS(J) = ISS(J) - 1
   65 WRITE (6,9005) CPDNAM(J)
 9005 FORMAT (' ', ' TOO MANY APPEARANCES OF ', A4)
   66 IS = MXAPP
C       THE ISTH APPEARANCE OF SS COMPOUND J OCCURS IN REACT-
C       ION N. IF REACTANT, JSS IS-
   67 JSS(J,IS) = N
C       JRE IS SET - TO IDENTIFY REFERENCE TO SS COMPOUND.
   68 JRE(N,I) = -JRE(N,I)
   70 IF (I-3) 72,75,75
   72 JSS(J,IS) = -N
   75 CONTINUE
   77 CONTINUE
   80 NSS1 = NSS + 1
   85 IF (NSS) 110,110,100
  100 WRITE (6,9010) (CPDNAM(K),K=1,NSS)
 9010 FORMAT (' ', 3X,' STEADY STATE INTERMEDIATES-',1X,7( A4,2X))
  110 WRITE (6,9020) (CPDNAM(K),K=NSS1,NCPDS)
 9020 FORMAT (' ', 'REACTANTS AND PRODUCTS-',5X,7( A4,2X)/31X,
     17( A4,2X))
C       SET UP EQUATIONS LISTING
  120 DO 200 N=1,NR
      JJ = IABS (JRE(N,1))
      EQUAT(1)=CPDNAM(JJ)
C       IT IS ASSUMED THAT FIRST REACTANT IS ALWAYS JRE(N,1)
C       AND FIRST PRODUCT ALWAYS JRE(N,3) SO THAT TEST ON
C       JRE(N,2) OR JRE(N,4) SUFFICES TO IDENTIFY THAT THERE
C       IS JUST ONE.
  130 IF (JRE(N,2)) 140,150,140
  140 JJ=IABS (JRE(N,2))
      EQUAT(3) = CPDNAM(JJ)
      GO TO 160
  150 EQUAT (2)=BL
      EQUAT(3)=BL
  160 JJ = IABS (JRE(N,3))
      EQUAT(4)=CPDNAM(JJ)
      IF(JRE(N,4)) 170,180,170
  170 JJ = IABS (JRE(N,4))
      EQUAT(6)=CPDNAM(JJ)
      GO TO 182
  180 EQUAT(5)=BL
      EQUAT(6)=BL
  182 IF (JRE(N,2) .EQ. 0) GO TO 184
      IF (JRE(N,4) .EQ. 0) GO TO 188
      WRITE (6,9030) N,EQUAT(1),EQUAT(3),EQUAT(4),EQUAT(6)
      GO TO 200
 9030 FORMAT (' ',I3,1X,A4,' + ',A4,2X,'=',2X,A4,' + ',A4)
  184 IF (JRE(N,4) .EQ. 0) GO TO 186
      WRITE (6,9031) N,EQUAT(1),EQUAT(3),EQUAT(4),EQUAT(6)
      GO TO 200
 9031 FORMAT (' ',I3,1X,A4,3X,A4,2X,'=',2X,A4,' + ',A4)
  186 WRITE (6,9032) N,EQUAT(1),EQUAT(3),EQUAT(4),EQUAT(6)
      GO TO 200
 9032 FORMAT (' ',I3,1X,A4,3X,A4,2X,'=',2X,A4,3X,A4)
  188 WRITE (6,9033) N,EQUAT(1),EQUAT(3),EQUAT(4),EQUAT(6)
 9033 FORMAT (' ',I3,1X,A4,' + ',A4,2X,'=',2X,A4,3X,A4)
  200 CONTINUE
  230 IF (NCPCAT*NRCAT) 240,240,235
  235 WRITE (6,9045) NRCAT,CPDNAM(NCPCAT)
 9045 FORMAT (' ','REACTION ',I2,1X,'IS CATALYZED BY', A4)
C
C       READ IN THE NUMBER OF PROBLEM SETS AND THE DESIRED
C       NO. OF SS REPEATS. (20-40 USUALLY OK)
C
```

```
C       ******** K
  240 READ (5,8010) NPROB,NREPSS
C
C       NEXT FOLLOWS THE MAIN LOOP FOR PROBLEM SETS
C
  260 DO 900 NPRB = 1,NPROB
C       READ IN PROBLEM SETS
C       FIRST THE HEADER
C       ******** 6
  270 READ (5,8000) PROBLM
C       NEXT THE RATE CONSTANTS
C       ******** 7
  280 READ (5,8050) (AK(N),N=1,NR)
 8050 FORMAT (7E10.5)
  285 WRITE (6,9000) HEADER, DATE
  290 WRITE (6,9060) PROBLM
 9060 FORMAT (' ',' ',12A4)
C       THEN THE CALCULATING PARAMETERS
C       ******** 8
  300 READ (5,8060) NP,N1,DT,T,IWRITE,NTENT
 8060 FORMAT (I5,3X,I3,3X,2E10.5,I2,4X,I3)
  305 IF (NTENT-MATBNT) 307,307,306
  306 NTENT = MATBNT
C       READ IN COMPOUND INDEX NUMBERS FOR TABLE ENTRIES.
C       ******** 9
  307 READ (5,8010) (JTENTY(I),I=1,NTENT)
  310 WRITE (6,9070) DT,(N,AK(N),N=1,NR)
 9070 FORMAT (' ',' DT =',1PE13.5,/,' RATE CONSTANTS-',1X,5(I2,1X,
     1E11.5,3X)/17X,5(I2,1X,E11.5,3X),/,17X,5(I2,1X,E11.5,3X)*/,
     217X,5(I2,1X,E11.5,3X),/,17X,5(I2,1X,E11.5,3X))
C       NON INITIAL CONCENTRATIONS. LOCATION MAY BE BLANK IF 0
C       ******** 10 ** END OF READ STATEMENTS
  315 READ (5,8050) (C(I),I=1,NCPDS),CSSTOT
  317 DO 319 I=1,NTENT
  318 J=JTENTY(I)
  319 TBLNM(I)=CPDNAM(J)
  320 WRITE (6,9080) (TBLNM(I),I=1,NTENT)
 9080 FORMAT (' ',/,6X,'TIME',10X,8( A4, 9X))
C       IF INITIAL CONCENTRATION OF SS HAVE NOT BEEN ENTERED,
C       THEY ARE SET TO 1.E-20
  322 IF (NSS) 332,332,323
  323 DO 326 I=1,NSS
  324 IF (C(I)) 325,325,326
  325 C(I)=1.0E-20
  326 CONTINUE
  332 DO 334 I=1,NTENT
  333 J = JTENTY(I)
  334 TBLCPD(I)=C(J)
  340 WRITE (6,9090) T, (TBLCPD(I),I=1,NTENT)
 9090 FORMAT (' ',1P9E13.4)
      DO 350 N=1,NR
  345 DL(N)=0
  350 AK(N)=AK(N)*DT
C       START PRINT INTERVAL LOOP
  360 DO 850 IP=1,NP
C       START ITERATION LOOP
  370 DO 800 IT=1,N1
  375 IF (NSS) 580,580,380
C       START STEADY STATE LOOP
  380 DO 550 IREP = 1,NREPSS
C       OUTPUT DECREMENTS FOR SS CALCULATION
  390 DO 420 N=1,NR
      N1=IABS (JRE(N,1))
      N2=IABS (JRE(N,2))
      IF (N2) 400,400,410
  400 D(N)=AK(N)*C(N1)
      GO TO 420
  410 D(N)=AK(N)*C(N1)*C(N2)
  420 CONTINUE
      ITEST = 0
  430 DO 530 IS=1,NSS
      IST = ISS(IS)
      XNUM=0.
      DEN = 0.
  440 DO 470 JS=1,IST
  445 KS=JSS(IS,JS)
  446 IF (KS) 460,470,450
  450 XNUM = XNUM + D(KS)
  452 GO TO 470
  460 KS=-KS
  465 DEN = DEN + D(KS)
  470 CONTINUE
      IF (DEN) 472,475,472
  472 F=XNUM/DEN
```

```
      IF (F) 477,475,477
  475 F=1.
      GO TO 488
  477 IF (F-1.) 480,488,484
  480 F=DAMP/F+1.-DAMP
      F=1./F
      GO TO 488
  484 F=F*DAMP + 1. -DAMP
  488 C(IS) = C(IS)*F
      FX = F-1.
  490 IF (IWRITE) 510,510,500
  500 WRITE (6,9100) IP,IT,IREP,XNUM,DEN,FW,
     1(CPDNAM(I),C(I),I=1,NSS)
 9100 FORMAT (' ',' PRINT INTERVAL',I3,2X,'ITERATION',I3,2X,
     1'SS REPEAT',I3,2X,'NUMERATOR',1PE12.5,2X,'DENOMINATOR',
     2E12.5,2X,'PER CENT CURRN.',2PF10.3,/,1X,6HCONCS.,1X,
     3 A4,1PE12.5,2X, A4,E12.5,2X, A4,E12.5,2X, A4,E12.5,2X, A4,E12.5,/
     4 A4,1PE12.5,2X, A4,E12.5,2X, A4,E12.5,2X, A4,E12.5)
  510 IF (ABS(FW) - .C05) 530,530,520
  520 ITEST = 1
  530 CONTINUE
  531 IF (CSSTOT) 540,540,532
  532 CS=0.
      DO 533 I=1,NSS
  533 CS=CS+C(I)
      F = CSSTOT/CS
      DO 537 I=1,NSS
  537 C(I) = C(I)*F
  540 IF (ITEST) 550,560,550
  550 CONTINUE
  553 WRITE (6,9110) NREPSS
 9110 FORMAT (' ',' STEADY STATE CALCULATION DID NOT CONVERGE',
     1' IN',I2,1X,'ITERATIONS')
  555 WRITE (6,9100) IP,IT,IREP,XNUM,DEN,FW,
     1(CPDNAM(I),C(I),I=1,NCPDS)
      GO TO 900
  560 IF (IP*(IT-1) 580,570,580
  570 DO 575 I=1,NTENT
  572 J=JTENTY(I)
  575 TBLCPD(I)=C(J)
  576 WRITE (6,9090) T,(TBLCPD(I),I=1,NTENT)
  580 CONTINUE
C
C     END OF STEADY STATE CALCULATIONS
C     MAKE REACTION DECREMENT CALCULATIONS
  585 DO 620 N=1,NR
      N1=IABS(JRE(N,1))
      N2=IABS(JRE(N,2))
  590 IF (N2) 600,600,610
  600 D(N)=AK(N)*C(N1)
      GO TO 620
  610 D(N)=AK(N)*C(N1)*C(N2)
  620 CONTINUE
C     IF REACTION NRCAT IS CATALYZED
  625 IF (NCPCAT*NRCAT) 630,630,627
  627 D(NRCAT) = D(NRCAT)*C(NCPCAT)
C     MAKE TRAPEZOIDAL CALCULATION
  630 DO 638 N=1,NR
  631 IF (DL(N)) 636,636,632
  632 DLAST = D(N)
  633 D(N) = 1.5*D(N) - 0.5*DL(N)
  634 DL(N) = DLAST
  635 GO TO 638
  636 DL(N) = D(N)
  638 CONTINUE
C     DECREMENT REACTANTS, INCREMENT PRODUCTS, LEAVE SS ALONE
C     IF JRE IS -, CPD IS SS.
  640 DO 680 N = 1,NR
  642 DO 680 I = 1,4
  644 IF (JRE(N,I)) 680,680,645
  645 II = JRE(N,I)
  650 IF (I-3) 655,665,665
  655 C(II) = C(II) - D(N)
  660 GO TO 680
  665 C(II) = C(II)+D(N)
  680 CONTINUE
  681 NGCHK=0
  682 DO 685 I=1,NCPDS
  683 IF (C(I)) 684,685,685
  684 NGCHK = NGCHK + 1
  685 CONTINUE
  690 IF (NGCHK) 750,750,700
  700 WRITE (6,9120) IT,(C(I),I=1,NCPDS)
 9120 FORMAT (' ',' NEGATIVE CONCS.-(INTERVAL',I3,1X,' ) C-ARRAY',
```

```
     1 1P6E14.5,/,40X,6E14.5)
  710 WRITE (6,9130) (D(I),I=1,NR)
 9130 FORMAT (' ',33X,'D-ARRAY',1PE14.5,/,40X,6E14.5)
  720 GO TO 900
  750 T=T+DT
  800 CONTINUE
C       800 STARTS AT 370
  805 DO 807 I=1,NTENT
  806 J=JTENTY(I)
  807 TBLCPD(I) = C(J)*91.2E6
  810 WRITE (6,9090) T,(TBLCPD(I),I=1,NTENT)
  850 CONTINUE
C       850 STARTS AT 360
  900 CONTINUE
C       900 STARTS AT 260
      END
```

REFERENCES

1. J. G. Roof and F. Daniels, "The Photolysis of Acetaldehyde and Ethyl Bromide Mixtures at 310°," J. Am. Chem. Soc., 62, 2912 (1940).

2. H. L. Friedman, R. B. Bernstein and H. E. Gunning, "C^{13} Isotope Effect in the Photolysis of Ethyl Bromide," J. Chem. Phys., 26, 528 (1957).

3. R. Barker and A. Maccoll, "Gas Phase Photolysis of Ethyl Bromide," J. Chem. Soc., 2839 (1963).

4. N. N. Semenov, "Some Problems of Chemical Kinetics and Reactivity," Vol. 2, Pergamon Press, New York, 1958, p. 236.

5. S. W. Benson and H. E. O'Neal, "Kinetic Data on Gas Phase Unimolecular Reactions," NSRDS-NBS 21, National Bureau of Standards, 1970.

6. V. S. Gurman, V. Z. Dubinskii and G. N. Kovalev, "Photolysis of Liquid Ethyl Bromide," Russ. J. Phys. Chem., 46, 1643 (1972).

7. R. J. Donovan and D. Husain, "Electronically Excited Bromine Atoms $Br(4^2P_{1/2})$," Trans. Faraday Soc., 62, 2643 (1966).

8. R. H. Schuler and W. H. Hamill, "The Fast Electron and X-Ray Decomposition of the Alkyl Halides," J. Am. Chem. Soc., 74, 6171 (1952).

9. R. J. Neddenriep and J. E. Willard, "The Radiolysis of n-Propyl Bromide," J. Phys. Chem., 65, 1206 (1961).

10. R. N. Schindler, "The Gas Phase Radiolysis of Ethyl Chloride," Radiochim. Acta, 2, 62 (1963).

11. T. O. Tiernan and B. M. Hughes, "Ionic Reactions in Ethyl Chloride," in Advances in Chemistry Series, 82, American Chemical Society, Washington, D.C., 1968.

12. R. N. Schindler and M. H. J. Wijnen, "The Gas Phase Radiolysis of Ethyl Iodide," Z. Physik Chem. Neue Folge, 38, 285 (1963).

13. A. P. Irsa, "Electron Impact Studies on C_2H_5Cl, C_2H_5Br and C_2H_5I," J. Chem. Phys., 26, 18 (1955).

14. S. Tsuda and W. H. Hamill, "Structure in Ionization-Efficiency Curves Near Threshold from Alkanes and Alkyl Halides," J. Chem. Phys., 41, 2713 (1964).

15. R. F. Pottie and W. H. Hamill, "Persistent Ion-Molecule Collision Complexes of Alkyl Halides," J. Phys. Chem., 63, 877 (1959).

16. L. P. Theard and W. H. Hamill, "The Energy Dependence of Some Ion-Molecule Reactions," J. Am. Chem. Soc., 84, 1134 (1962).

17. J. L. Beauchamp, D. Holtz, S. D. Woodgate and S. L. Patt, "Thermochemical Properties and Ion-Molecule Reactions of the Alkyl Halides in the Gas Phase by Ion Cyclotron Resonance Spectroscopy," J. Am. Chem. Soc., 94, 2798 (1972).

18. L. W. Sieck and R. Gorden, Jr., "Formation of Association Ions in the Photoionization of Alkyl Halides," Int. J. of Chem. Kinetics, 5, 445 (1973).

19. A. A. Christodoulides and L. G. Christophorou, "Electron Attachment to Brominated Aliphatic Hydrocarbons of the Form n-C_NH_{2N+1} (N = 1-6,8 and 10). I. An Electron Swarm Study," J. Chem. Phys., 54, 4691 (1971).

20. L. G. Christophorou, J. G. Carter, P. M. Collins and A. A. Christodoulides, "Electron Attachment to Aliphatic Hydrocarbons of the Form n-$C_NH_{2N+1}Br$ (N = 2-6 and 8). II. A Swarm Beam Study," J. Chem. Phys., 54, 4706 (1971).

21. K. M. Bansal and R. W. Fessenden, "Electron Disappearance in Pulse Irradiated CH_3Cl, C_2H_5Cl, CH_3Br and C_2H_5Br," Chem. Phys. Lett., 15, 21 (1972).

22. R. J. Hanrahan, "A Co^{60} Gamma Irradiator for Chemical Research," Intern. J. Appl. Radiation Isotopes, 13, 254 (1962).

23. M. C. Sauer, Jr. and L. M. Dorfman, "The Radiolysis of Ethylene: Details of the Formation of Decomposition Products," J. Phys. Chem., 66, 322 (1962).

24. G. G. Meisels, "Gas-Phase Dosimetry by Use of Ionization Measurements," J. Chem. Phys., 41, 51 (1964).

25. W. H. Bragg, "Studies in Radioactivity," Macmillan and Co., London, 1912, p. 94.

26. L. H. Gray, "An Ionization Method for the Absolute Measurement of X-Ray Energy," Proc. Roy. Soc., A156, 578 (1936).

27. G. J. Hine and G. L. Brownell, "Radiation Dosimetry," Academic Press Inc., New York, 1956, p. 25.

28. C. Chang, Ph.D. Dissertation, "The Radiation Chemistry of Hexafluoroacetone in the Gas Phase," Univ. of Florida, 1970, Appendix I.

29. E. C. Y. Inn and Y. Tanaka, "Ozone Chemistry and Technology," in Advances in Chemistry Series, 12, American Chemical Society, Washington, D.C., 1959, p. 263.

30. D. Porret and C. F. Goodeve, "The Continuous Absorption Spectra of Alkyl Iodides and Alkyl Bromides and Their Quantal Interpretation," Proc. Roy. Soc. (London), A125, 31 (1938).

31. C. F. Goodeve and A. W. C. Taylor, "The Continuous Absorption Spectrum of Hydrogen Bromide," Proc. Roy. Soc. A, 152, 221 (1953).

32. J. G. Calvert and J. N. Pitts, Jr., "Photochemistry," John Wiley and Sons, Inc., New York, 1966, p. 782.

33. G. S. Forbes, J. E. Cline, and B. C. Bradshaw, "The Photolysis of Gaseous Hydrogen Sulfide," J. Am. Chem. Soc., 60, 1431 (1938).

34. E. Heckel and R. J. Hanrahan, " The X-Radiolysis of Perfluorocyclobutane and Mixtures of Perfluorocyclobutane and Methane in the Gas Phase," in Advances in Chemistry Series, 82, American Chemical Society, Washington, D.C., 1968.

35. J. M. Donovan, M.S. Thesis, "The Radiation Chemistry of Methyl Iodide in the Gas Phase," Univ. of Florida, 1969.

36. R. Marcotte, Ph.D. Dissertation, "The Radiation Chemistry of Carbon Tetrachloride-Carbon Tetrafluoride Mixtures in the Gas Phase," Univ. of Florida, 1968.

37. J. W. Buchanan, Ph.D. Dissertation, "Radiation Chemistry of Systems Containing Phosphine," Univ. of Florida, 1968.

38. W. O. McReynolds, "Characterization of Some Liquid Phases," J. Chromatogr. Science, 8, 685 (1970).

39. G. A. Kennedy, Ph.D. Dissertation, "Effects of Free Radical Scavengers in the Radiolysis of Systems Containing Perfluorocyclohexane," Univ. of Florida, 1969.

40. R. Ryhage, "Efficiency of Molecular Separators Used in GC-MS Application," Ark. Kemi, 26, 305 (1967).

41. M. B. Fallgatter and R. J. Hanrahan, "SPC-12 Mass Spectrometer Routines: Real-Time Data Acquisition and Data Reduction for Bendix Time-of-Flight Instrument," Univ. of Florida, Radiation Chemistry, Gainesville, Fla., March, 1970. ORO-3106-33 available from COSMIC, Barrow Hall, University of Georgia, Athens, Ga. 30601 under library number COS--2260.

42. M. B. Fallgatter and R. J. Hanrahan, "High Pressure Mass Spectrometry of Simple Hydrocarbon and Alkyl Halide Systems Using Pulsed and Continuous Ionization," Paper No. 145, Am. Chem. Soc. Division of Physical Chemistry, 158th ACS National Meeting, New York, New York, September 8-12, 1969.

43. J. H. Futrell, T. O. Tiernan, F. P. Abramson and C. D. Miller, "Modification of a Time-of-Flight Mass Spectrometer for Investigation of Ion-Molecule Reactions at Elevated Pressures," Rev. Sci. Inst., 39, 340 (1968).

44. F. H. Field, "Chemical Ionization Mass Spectrometry," Accounts Chem. Res., 1, 42 (1968).

45. L. G. Christophorou, "Atomic and Molecular Radiation Physics," Wiley-Interscience, New York, 1971, p. 614.

46. A. A. Passchier, J. D. Gregory and N. W. Gregory, "The Ultraviolet-Visible Absorption Spectrum of Bromine between Room Temperature and 440°," J. Phys. Chem., 71, 937 (1967).

47. F. J. Welcher, "Organic Analytical Reagents," Vol. III, D. Van Nostrand Co., New York, 1947, p. 544.

48. F. J. Welcher, "Organic Analytical Reagents," Vol. IV, D. Van Nostrand Co., New York, 1948, p. 488.

49. N. A. Lange, ed., "Handbook of Chemistry and Physics," 10th ed., McGraw-Hill Book Co., Inc., New York, 1961.

50. Dictionary of Organic Compounds, Vol. 2, 4th ed., Oxford University Press, New York, 1965, p. 923.

51. Ibid. Vol. 1, p. 20.

52. D. R. Stull, E. F. Westrum, Jr, and G. C. Sinke, "The Chemical Thermodynamics of Organic Compounds," John Wiley and Sons, Inc., New York, 1969, p. 545.

53. "Physical Properties of Chemical Compounds-II," Advances in Chemistry Series, 22, American Chemical Society, Washington, D.C., 1959, p. 209.

54. J. Roboz, "Introduction to Mass Spectrometry," Interscience Publishers, New York, 1968, p. 290.

55. J. R. Majer and J. P. Simons, "Photochemical Processes in Halogenated Compounds," in Advances in Photochemistry, Vol. 2, W. A. Noyes, Jr., G. S. Hammond, J. N. Pitts, Jr., eds., Interscience Publishers, New York, 1964, p. 137.

56. T. L. Cottrell, "The Strengths of Chemical Bonds," Academic Press, Inc., New York, 1958, p. 277.

57. E. W. R. Steacie, "Atomic and Free Radical Reactions," Vol. 2, Reinhold Publishing Co., New York, 1954.

58. A. F. Trotman-Dickenson and G. S. Milne, "Tables of Bimolecular Gas Reactions," NSRDS-NBS9, National Bureau of Standards, 1967.

59. R. H. Luebbe, Jr. and J. E. Willard, "Temperature and Phase Effects on the Photolysis of Ethyl Iodide," J. Am. Chem. Soc., 81, 761 (1959).

60. H. A. Gillis, R. R. Williams, Jr, and W. H. Hamill, "Ionic and Free Radical Processes in the Radiolysis of Liquid Methyl and Ethyl Iodides," J. Am. Chem. Soc., 83, 17 (1961).

61. S. W. Benson, "Thermochemical Kinetics," John Wiley and Sons, Inc., New York, 1968, pp. 195-215.

62. D. A. Armstrong and J. W. T. Spinks, "Radiation-Induced Addition of HBr to C_2H_4 in the Gaseous State," Can. J. Chem., 37, 1210 (1959).

63. S. W. Benson, op. cit., pp. 142-3.

64. N. N. Semenov, "Some Problems of Chemical Kinetics and Reactivity," Vol. 2, Pergamon Press, New York, 1958, p. 236.

65. J. W. T. Spinks and R. J. Woods, "An Introduction to Radiation Chemistry," John Wiley and Sons, Inc., New York, 1964, p. 349.

66. D. Husain and R. J. Donovan, "Electronically Excited Halogen Atoms," in Advances in Photochemistry, Vol. 8, J. N. Pitts, Jr., G. S. Hammond and W. A. Noyes, Jr., eds., Wiley-Interscience, New York, 1971, p. 4.

67. N. N. Semenov, "Modern Concepts of the Mechanism of Hydrocarbon Oxidations in the Gas Phase," in Photochemistry and Reaction Kinetics, P. G. Ashmore, F. S. Dainton and T. M. Sugden, eds., The University Press, Cambridge, 1967, p. 229.

68. D. E. Hoare and G. S. Pearson, "Gaseous Photoxidation Reactions," in Advances in Photochemistry, Vol. 3, W. A. Noyes, Jr., G. S. Hammond and J. N. Pitts, Jr., eds., Interscience Publishers, New York, 1964, pp. 140-143.

69. L. C. Leitch and A. T. Morse, "Synthesis of Organic Deuterium Compounds III. 1,2-Dibromoethane-d_4 and Its Derivatives," Can. J. Chem., 30, 924 (1952).

70. G. L. Pratt, "Gas Kinetics," John Wiley and Sons, Ltd., London, 1969, p. 158.

71. D. H. Etzler and G. K. Rollefson, "Photolysis of Acetyl Bromide," J. Am. Chem. Soc., 61, 800 (1939).

72. A. E. Goldberg and F. Daniels, "Kinetics of the Pyrolysis of Ethyl Bromide," J. Am. Chem. Soc., 79, 1314 (1957).

73. D. F. DeTar, "A Computer Program for Making Steady-State Calculations," J. Chem. Ed., 44, 193 (1967).

74. N. N. Semenov, reference 64, p. 153.

75. American Petroleum Institute Project 44 Catalog of Mass Spectra Data Serial No. 607.

76. H. Okabe and J. R. McNesby, "Vacuum Ultraviolet Photochemistry. II. Photolysis of Ethylene," J. Chem. Phys., 36, 601 (1962).

77. T. J. Hardwick, "The Reactivity of Hydrogen Atoms in the Liquid Phase. IV. The Reaction with Some Halogenated Compounds," J. Phys. Chem., 66, 2246 (1962).

78. Private communication, R. N. Schindler, Institut für Physickalische Chemie, Julich, W. Germany.

BIOGRAPHICAL SKETCH

Arthur Jesse Frank was born in Cincinnati, Ohio, on January 17, 1945. He was graduated from Cheshire Academy, Cheshire, Connecticut, in 1963. In January, 1968, he received the Bachelor of Arts degree with a distributed major in chemistry, mathematics and psychology from the University of Colorado. From March, 1968, to December, 1969, he was enrolled in the post baccalaureate pre-professional program at the University of Florida. He entered Graduate School at the University of Florida in January, 1970. During his work toward the Doctor of Philosophy degree, he has held graduate teaching and research assistantships in the Department of Chemistry and was awarded a Proctor and Gamble Fellowship in 1973-1974.

Arthur Jesse Frank is married to the former Abbey Gail Hamilton. He is affiliated with the Society of Phi Kappa Phi and the American Chemical Society.

I certify that I have read this study and that in my opinion it conforms to acceptable standards of scholarly presentation and is fully adequate, in scope and quality, as a dissertation for the degree of Doctor of Philosophy.

Robert J. Hanrahan, Chairman
Professor of Chemistry

I certify that I have read this study and that in my opinion it conforms to acceptable standards of scholarly presentation and is fully adequate, in scope and quality, as a dissertation for the degree of Doctor of Philosophy.

Marvin L. Muga
Associate Professor of Chemistry

I certify that I have read this study and that in my opinion it conforms to acceptable standards of scholarly presentation and is fully adequate, in scope and quality, as a dissertation for the degree of Doctor of Philosophy.

Phillip M. Achey
Assistant Professor of Radiation Biology

This dissertation was submitted to the Graduate Faculty of the Department of Chemistry in the College of Arts and Sciences and to the Graduate Council, and was accepted as partial fulfillment of the requirements for the degree of Doctor of Philosophy.

March, 1975

Dean, Graduate School